



## **LOCAL SCOUR NEAR STRUCTURES**

by Leo C. van Rijn, [www.leovanrijn-sediment.com](http://www.leovanrijn-sediment.com)

- 1. Introduction**
- 2. Scour downstream of sills, weirs and barrages in steady currents (rivers)**
  - 2.1 Scour downstream of structure**
  - 2.2 Scour near tip of structure normal to bank**
- 3. Scour near seawalls due to waves and currents**
  - 3.1 Review of scour data**
  - 3.2 Wave-related scour near toe of seawall**
- 4. Scour near toe of wall-type breakwaters due to waves and currents**
- 5. Scour near toe of rubble-type breakwaters due to waves and currents**
- 6. Scour near tip of breakwaters and groynes due to waves and currents**
  - 6.1 Wave-dominated scour near tip of vertical wall-type breakwater**
  - 6.2 Wave-dominated scour near tip of rubble-mound breakwater**
  - 6.3 Current-dominated scour near tip of rubble-mound breakwaters and groynes**
- 7. Scour near vertical pipes, piles and piers due waves and currents**
  - 7.1 Definitions**
  - 7.2 Current-related scour near vertical pipes and piles**
  - 7.2 Wave-related scour near vertical pipes and piles**
  - 7.4 Wave and current-related scour near vertical pipes and piles**
  - 7.5 SEDSCOUR-model**
- 8. Scour near horizontal pipes due waves and currents**
  - 8.1 Current-related scour**
  - 8.2 Wave-related scour near horizontal pipes**
  - 8.3 Wave and current-related scour near horizontal pipes**
- 9. Scour near gravity-based structures**
  - 9.1 Introduction**
  - 9.2 Scour near wide structures**
  - 9.3 Scour mitigation measures**
- 10. Scour near bed due to ship propeller**
- 11. Scour near ship wrecks**
- 12. References**



## 1. Introduction

Local scour is herein considered to be the lowering of the bed in the direct vicinity of a structure due to local accelerations and decelerations of the near-bed velocities and the associated turbulence (vortices) leading to an increase of the local sand transport capacity. Once a scour hole is formed, flow separation will take at the edge of the hole and a mixing layer will develop increasing the turbulence intensities and stimulating further scour of the bed (self-intensifying process). Excessive scour close to the structure may ultimately lead to instability/failure of the structure.

A dramatic example of failure due to scouring processes is the sinking of submerged coastal structures on the sandy seabed at Santa Maria del Mar (SMM) Beach in Southwest Spain (Munoz-Peres et al. 2015). The mesotidal range has a medium neap to spring variation of 1.20 to 3.80 m. Wave incidence to SMM Beach consisting of 0.25 mm sand generally occurs from the west to southwest directions, having a significant wave height range of 0.5 to 2.0 m and a mean wave period range of 5.0 to 12.0 s. The structure consisted of precast modular concrete elements placed at a depth of about -2.5 m below Chart Datum without scour protection measures and were monitored during six months after installation, starting in November of 2005. The sinking of the concrete modules in a near-shore sandy seafloor started immediately after placement and ended 3 weeks later. The sinking speed was 1.5 m/month until the modules reached the rocky bottom. The average sinking speed was extremely rapid at approximately 3 to 6 cm/day due to scouring processes; 50% of the height of the elements was reached in three to six weeks. The total sinking was of the order of 1.2 to 1.5 m. Big scour pits with cross-shore length scales of 15 m were present on both sides of the structure. Wave-structure interaction due to the placement of modules close to the breaking zone (at LLWL) resulted in extensive scour and sinking. The scouring depth (approximately 1.2–1.5 m) was similar to the sinking depth. In this paper, scour by currents, waves and combined waves and currents is considered. The scour is generally referred to as clear water scour if the ambient bed-shear stress is smaller than that for initiation of motion and to as live-bed scour otherwise. The EXCEL-file **SCOUR.xls** can be used for determination of scour depth and length estimates (Van Rijn, 2006, 2012).

Bed scour problems near walls and breakwaters generally occur near the outer toe of the trunk section of the structure and near the tip of the structure and is predominantly related to the height of spilling and plunging breaking waves during storm events, but wave reflection (and standing wave patterns) may also be important for (nearly) vertical structures. Since, the breaking wave height is depth-limited (roughly between 0.5 h for an almost flat bottom and 1 h for a steep bottom), it is most logic to assume that the maximum scour depth is related to the water depth near the toe/tip of the structure.

The scouring processes with fluid accelerations, decelerations and vortex generation are rather complex and three-dimensional. Often, physical scale modelling is required, which is based on the downscaling of prototype (field) conditions to laboratory conditions using dimensionless parameters such as the Reynold, number, the Froude number, KC-number and the Shields number. The basic principle is that the hydrodynamics and sediment dynamics in nature and in the laboratory are similar as long as the dimensionless numbers are equal at both scales. Scale relationships are available for upscaling of measured results from the laboratory to prototype conditions. A basic problem of scale modelling is that not all parameters can be scaled down. The most problematic parameter is the sediment diameter. Cohesionless sand with size of 200  $\mu\text{m}$  can be scaled to about 50  $\mu\text{m}$ . Further downscaling to below 50  $\mu\text{m}$  leads to sediment with different (cohesive) properties and thus to scale errors.

Various mitigating measures are available to reduce or prevent local scour processes, such as: bottom/bank protection by means of rip-rap material (stones) dumped on geotextile filter material, by flexible mats or mattresses filled with gravel/sand, by sand bags, by artificial mats, by concrete slabs and by grout injections.

Reviews of bed scour near structures are given by **Powell (1987)**, **Kraus (1988)**, **Fowler (1992)**, **Kraus and McDougal (1996)**, **Herbich (1991)**, **Silvester (1991)**, **Oumeraci (1994 a,b)**, **Hoffmans and Verheij (1997)**, **Whitehouse (1998)**, **Sumer et al. (2001)** and **Sumer and Fredsøe (2002)**.



## 2. Scour downstream of sills, weirs and barrages in steady currents (rivers)

### 2.1 Scour downstream of structure

Two-dimensional vertical scour downstream of a structure such as a weir or a barrage in a unidirectional current (see Figure 2.1) has been studied by many researchers (see **Hoffmans and Verheij, 1997**). The maximum scour depth in the equilibrium situation as well as the development in time of the scour depth have been studied.

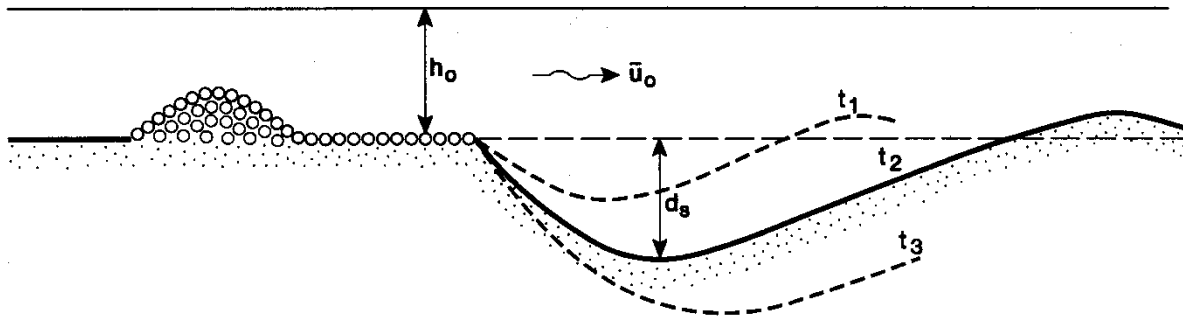


**Figure 2.1** Two-dimensional scour downstream of structure

**Delft Hydraulics (Breusers, 1967)** studied the time-dependent behaviour of scour holes (in sandy beds) related to closure works in tidal channels.

Based on experimental research in flumes, the time-dependent development of the scour depth in clear water flows was found to be:

$$d_s(t)/h_0 = (t/T_s)^{0.38} \quad (2.1)$$

with:  $d_s(t)$  = maximum scour depth at time  $t$  below original bed, see Fig. 2.1,  $h_0$ =upstream water depth,  
 $T_s$ = time (in hours) at which  $d_s = h_0$ .

Equation (2.1) is not valid close to the equilibrium situation.

A more general expression is:  $d_s(t)/d_{s,max} = 1 - \exp(-t/T_s)^p$  with  $p$ =calibration coefficient.

The time-scale  $T_s$  (in hours) was found to be:

$$T_s = 330 (s-1)^{1.7} (h_0)^2 / (\alpha U_0 - U_{cr})^{4.3} \quad (2.2)$$

with:  $U_0$  = depth-averaged velocity just upstream ( $x = 0$ ) of scour hole,  $U_{cr}$ =critical depth-averaged velocity (initiation of motion),  $s$  = specific density ( $\rho_s/\rho_w$ ),  $\alpha$ = coefficient depending on flow and turbulence structure at the upstream end of scour hole ( $\alpha = 1.7$  for two-dimensional flow without structure,  $\alpha = 3$  for very violent three-dimensional flow, **Van der Meulen and Vinjé, 1975**).

The  $\alpha$ -factor is related to the relative turbulence intensity  $r_0 = \sigma_u/U$  directly upstream of the scour hole ( $\sigma_u$ = standard deviation of local velocity field). For hydraulic rough flow it was found that  $\alpha = 1.5 + 5r_0$ . The value of  $r_0$  depends on the type of structure and the length of the bed protection downstream of the structure. If this length is larger than  $30h_0$ , additional turbulence produced by the structure has decayed and the  $r_0$ -value for uniform flow without a structure can be taken, yielding:  $r_0 = 0.1$  to  $0.15$ .



Generally-accepted formulae for the maximum scour depth in the equilibrium situation are not available. A rough estimate can be obtained from (Dietz, 1969; Schoppman, 1972):

$$d_{s,max}/h_{obs} = (\alpha_w)^{0.25} (\alpha_d U_0 - U_{cr})/U_{cr} \quad (2.3)$$

$$L_{s,max} = 10 d_{s,max}$$

with:  $d_{s,max}$  = maximum scour depth,  $L_{s,max}$  = maximum scour length,  $h_{obs}$  = obstacle height,  $\alpha_d = 1+3r_0$ ,  $\alpha_w = 1+U_m/U_{cr}$  = wave effect,  $U_m$  = peak orbital velocity near bed,  $U_{cr}$  = critical velocity initiation of motion,  $\alpha_w = 1$  if  $U_m < U_{cr}$ .

Usually, the river bed downstream of a weir or barrage is protected over a certain distance to reduce the maximum scour depth which is strongly dependent on the  $\alpha$ -factor ( $\alpha$  decreases with distance due to the decay of turbulence). The bed protection length generally is of the order of 10 to 20  $h_0$ . The surface of the protection layer should be as rough as possible to reduce the near-bed velocities and hence scour rates.

The maximum scour depth will be reduced, if there is a supply of sediment from the upstream river section (or from the flood and ebb direction in tidal flow). In the case of tidal flow the current velocity can be schematized by an effective current velocity  $U_{max,eff} = 0.9U_{max, mean\ tide}$  to represent the velocity variation over the daily cycle and the neap-spring cycle. The bottom slope at the beginning of the scour hole may become quite steep; slopes of 1 to 2 and 1 to 3 have been observed for  $r_0 = 0.2$  to 0.4. Undermining of the bed protection at this location should be prevented. Model studies are recommended for complicated geometries.

Scour data observed near the storm surge barrier in the Eastern Scheldt, The Netherlands show scour depths of  $d_{s,max} = 0.4$  to 1  $h_0$  (Hoffmans and Verheij, 1997). The observed scour depths are considerably smaller than those predicted by Eq. (2.3), because sediments supplied by the bidirectional tidal flow are partly trapped in the scour hole (reduction of scour depth due to upstream supply). This latter effect is not taken into account by Equation (2.3).

Dudill et al. (2018) summarized the experimental results from the literature and performed additional experiments. Experiments were undertaken in the laboratory flume at NHC, Vancouver, Canada. The experiments utilised crushed walnut shell to form the sediment bed. The walnut shell has a specific gravity of 1.3 and  $d_{50}$  of 0.2 mm. The flume is equipped with an acoustic doppler velocimeter (ADV) and a laser-bed scanner. The ADV is positioned at the channel centre line, 2 m from the upstream boundary, and was run with a sampling rate of 25 Hz and a sampling height of 7 mm. The critical depth-averaged flow of crushed walnut grains was found to be 0.116 m/s.

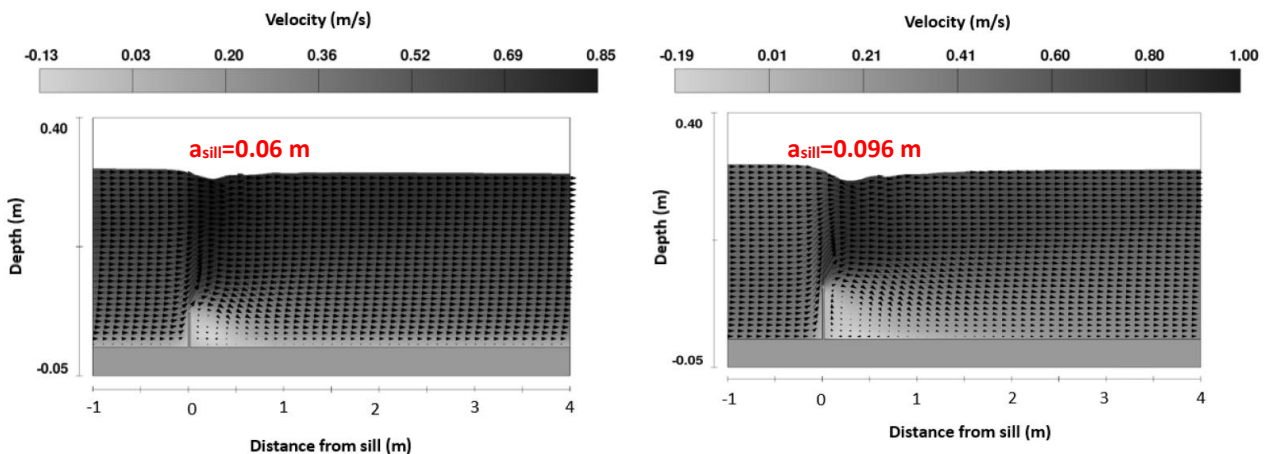


Figure 2.2 Computed flow (CDF-model) around vertical sill structure (upstream velocity=0.47 m/s)



Ten experiments were undertaken with a range of velocities and two different sill heights ( $a_{sill}$ ): 0.06 m and 0.096 m. The sill was a vertical structure (0.02 mm wide; **Figure 2.2**), made of plexi-glass, and spanned the width of the flume orientated perpendicular to the flow. In all the experiments the flow depth ( $h$ ) was 0.3 m and thus  $a_{sill}/h=0.2$  and 0.32. The initial condition for the experiments was a flat bed. To prevent plunging flows over the sill at the start of the tests, the flume was slowly filled with water from both the upstream and downstream boundaries. Once the flow depth reached 0.3 m, the pump valve and the flume tailgate were varied until the velocity reached the desired value and the flow depth was at 0.3 m. The experiments were run until the bed reached equilibrium, which was determined by monitoring the bed profile through a plexi-glass sidewall.

**Figure 2.2** shows the computed flow field (approaching flow velocity=0.47 m/s) with back eddy based 3D CFD-model.

**Figure 2.3** shows the experimental results of Dudill et al. (2018) as well some results from the Literature (Guan et al. 2015, 2016). The maximum scour depth is about 1 to 1.2 times the water depth ( $h$ ) and about 3 to 4 times the sill height ( $a_{sill}$ ) for  $V/V_c=3$  to 4. The maximum scour length is of the order of 40 to 70 times the sill height.

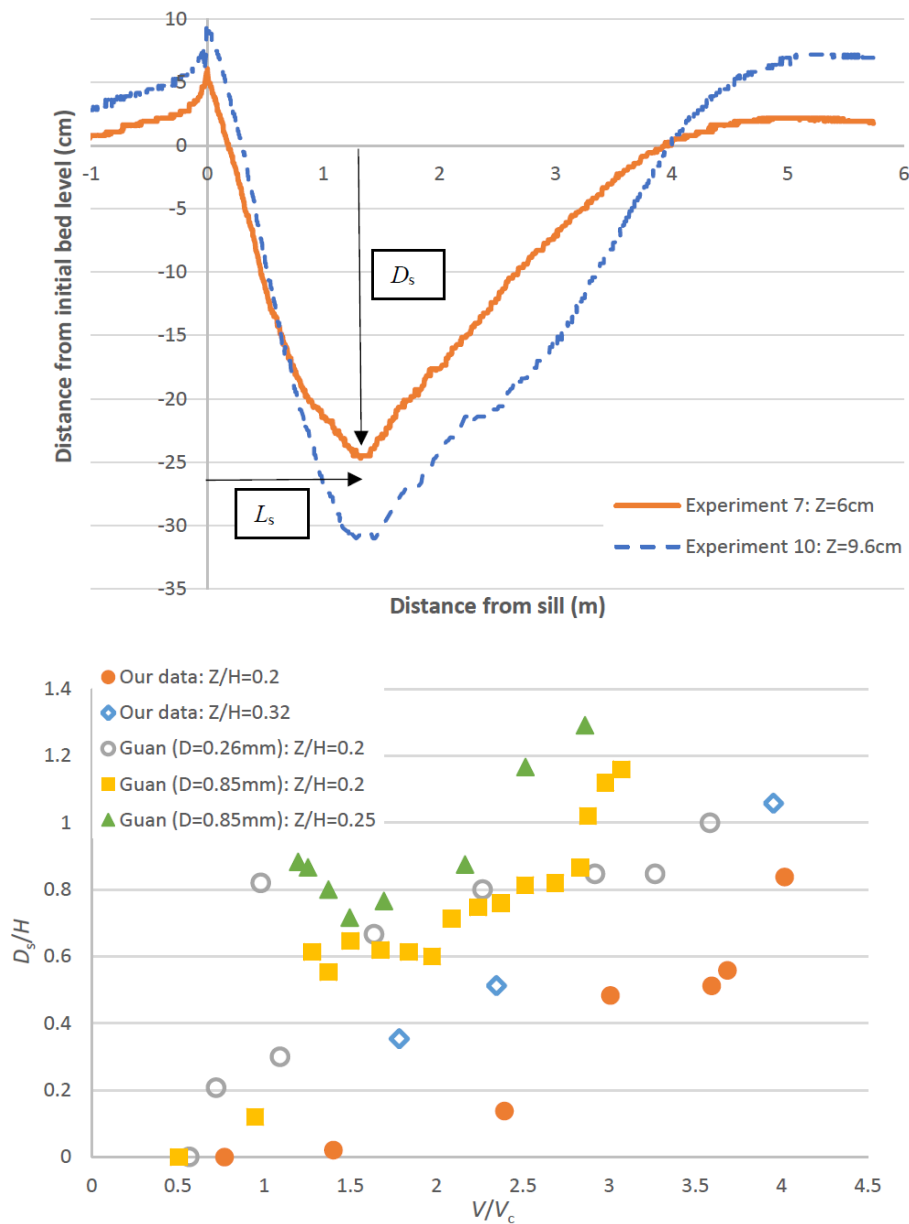


**Figure 2.3** Scour depth as function of relative flow velocity (Dudill et al., 2018)  
( $D_s$ = maximum scour depth;  $H$ = upstream flow depth;  $Z$ =sill height)  
( $V$ = depth-averaged flow velocity;  $V_c$ = critical flow velocity)



**Hoffmans (1990)** studied the scour of a sand bed (with length of about 10 m; thickness=0.25 m) downstream of a horizontal bed protection of gravel in a laboratory flume (width=0.8 m) with water flow. The approaching flow was free of sand (no initial sediment load). The bed protection of gravel was horizontal over a length of 10 m without any structure. The development of the scour hole was measured over nearly 30 hours, see **Figure 2.4**. The basic data of Test C60 are given in **Table 2.1**.

Parameter	Value
Water depth above bed protection (m)	0.2
Bed level of sand bed (m)	-0.015 m below bed protection
Depth-averaged flow velocity above bed protection (m/s)	0.583
Bed protection $d_{50}$ , $d_{90}$ (mm)	6; 8
Bed material $d_{50}$ ; $d_{90}$ (mm)	0.163; 0.21
Fall velocity (m/s)	0.015 to 0.019
Bed roughness (m)	0.01
Fluid and sand density (kg/m <sup>3</sup> )	1000; 2650
Kinematic viscosity (m <sup>2</sup> /s); Te=20 °C	0.000001
Bed porosity (-)	0.4
Stream tube width (m)	1 (constant)
Suspended load transport (kg/m/s) at x=0	0
Calibration factor sand transport (-)	1 (default)
Turbulence enhancement factor ( $r_{tf}$ )	0.3 to 0.5
Grid size (m)	0.1
Time step (hours)	0.1

**Table 2.1** Basic parameters of scour downstream of bed protection (Test C60); input parameters of SEDTUBE-model

The 2D SEDTUBE-model of LVRS has been used to simulate the scour downstream of the bed protection. This model computes the depth-averaged flow velocity and suspended plus bed load transport in a stream tube. The gradual adjustment of the suspended sand transport to the local flow conditions is represented by an empirical function. The suspended sand transport at the beginning of the sand bed is set to zero (no initial load). The effect of additional turbulence in the downstream deceleration zone is taken into account by an empirical coefficient acting on the mean current velocity as follows:  $u = \alpha_{tf} Q/(bh)$  with:  $\alpha_{tf} = [1+r_{tf} \exp(-x/40h_o)]$ ,  $Q$ = flow discharge,  $b$ = stream tube width;  $h$ =local water depth,  $h_o$ = upstream water depth,  $x$ = distance downstream of structure (where bed consists of sand),  $r_{tf}$ = turbulence enhancement factor (0.1 to 0.5 depending on type and height of structure), see **Figure 2.5**. The  $\alpha_{tf}$ -coefficient decays exponentially in downstream direction ( $\alpha_{tf}=1$  for  $r_{tf}=0$  no extra turbulence).

**Figure 2.4** shows measured and computed bed levels of the scour hole in the sand bed ( $x>0$ ) downstream of the bed protection for Test C60 for 2 values of the  $r$ -parameter (turbulence enhancement parameter  $r=0.3$  and  $r=0.5$ ). The value  $r=0.3$  produces the best agreement between measured and computed bed levels at  $t=3.7$  hours, while  $r=0.5$  produces the best agreement at  $t=29.5$  hours. As the scour depth increases, the flow deceleration is more violent resulting in higher turbulence levels (higher  $r$ -value).

The slope of the computed scour hole just downstream of the bed protection is about 1 to 1 and much steeper than the measured slope of about 1 to 5.

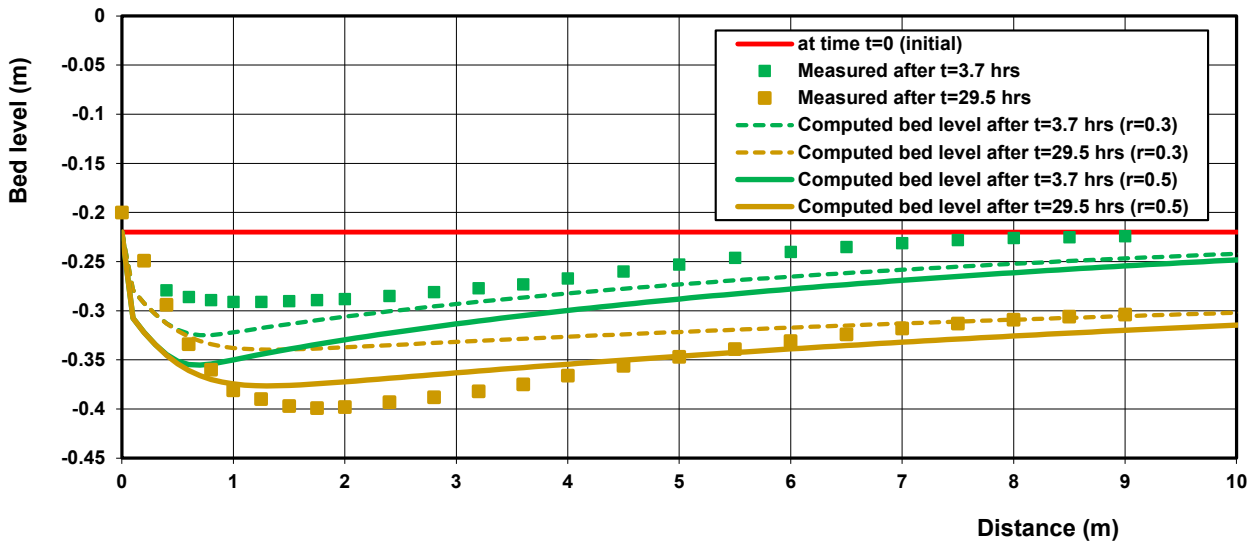


Figure 2.4 Measured and computed bed levels of scour hole in flume after 3.7 and 29.5 hours; SEDTUBE-model

Üşenti (2019) described the scour downstream of a new culvert in the dike of the Tidal Eastern Scheldt (The Netherlands) to allow water to flow into a natural reserve area. The structure was completed in December 2014. A deep scour pit was generated within 12 days after opening of the new structure. Figure 2.5 shows the bathymetry after 12 days. The basic parameters are given in Table 2.2.

Parameter	Value
Bottom level of culvert (m)	-2.0
Bed level inside (m)	-2.5
Water level outside (m)	+1 to +1.5
Mean flow velocity during intake (m/s)	1 to 1.5
Bed material $d_{50}$ , $d_{90}$ (mm)	0.13; 0.3
Fall velocity (m/s)	0.013
Bed roughness (m)	0.02
Fluid and sand density ( $\text{kg/m}^3$ )	1000; 2650
Kinematic viscosity ( $\text{m}^2/\text{s}$ ); $T_e=20\text{ }^\circ\text{C}$	0.000001
Bed porosity (-)	0.4
Upstream water depth (m)	4
Stream tube width (m)	constant over 30 m and widening at 1 to 20 after $x=30$ m
Suspended load transport ( $\text{kg}/\text{m}/\text{s}$ ) at $x=0$	0
Calibration factor sand transport (-)	1 (default)
Turbulence enhancement factor ( $r_{tf}$ )	0.3
Grid size (m)	1
Time step (hours)	1

Table 2.2 Basic parameters of scour process downstream of culvert; input parameters of SEDTUBE-model

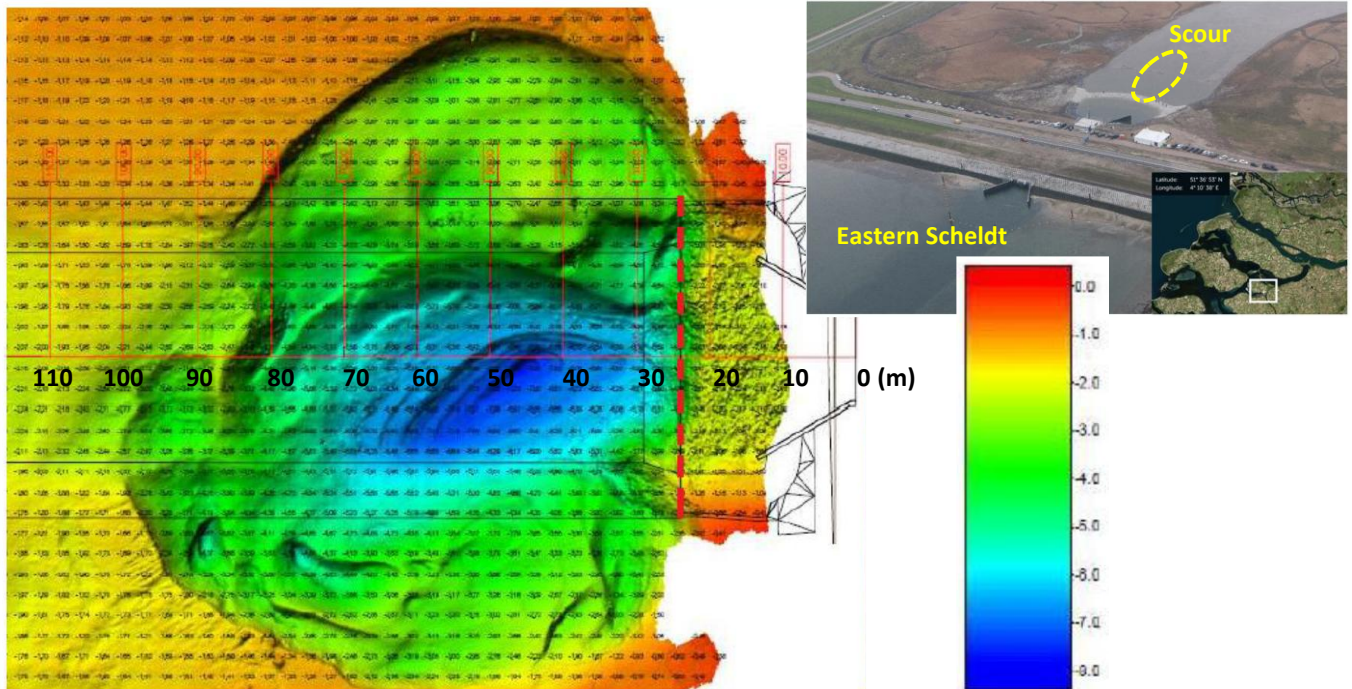


Figure 2.5 Bathymetry downstream of culvert in dike of Eastern Scheldt (NL)

The 2D SEDTUBE-model of LVRS has been used to simulate the scour downstream of the culvert. This model computes the depth-averaged flow velocity and suspended plus bed load transport in a stream tube. The gradual adjustment of the suspended sand transport to the local flow conditions is represented by an empirical function. The suspended sand transport at the beginning of the sand bed is set to zero (no initial load). The effect of additional turbulence in the downstream deceleration zone is taken into account by an empirical coefficient acting on the mean current velocity as follows:  $u = \alpha_{tf} Q/(bh)$  with:  $\alpha_{tf} = [1 + r_{tf} \exp(-x/40h_0)]$ ,  $Q$ = flow discharge,  $b$ = stream tube width;  $h$ =local water depth,  $h_0$ = upstream water depth,  $x$ = distance downstream of structure (where bed consists of sand),  $r_{tf}$ = turbulence enhancement factor (0.1 to 0.5 depending on type and height of structure), see **Figure 2.6**. The  $\alpha_{tf}$ -coefficient decays exponentially in downstream direction ( $\alpha_{tf}=1$  for  $r_{tf}=0$  no extra turbulence).

The computed bed levels along the scour pit are shown in **Figure 2.7** for three values of the depth-averaged flow velocity (1, 1.25 and 1.5 m/s). The precise current velocity during operation of the culvert is unknown, but is estimated to be in the range of 1 to 1.5 m/s. The turbulence enhancement factor is set to  $r_{tf}=0.3$ . The computed maximum scour depth after 12 days is of the right order of magnitude (scour depth of about 5 m below surrounding bed) for a mean current of 1.25 m/s in combination with  $r_{tf}=0.3$ . The eroded sand is deposited after 60 m in the area where the current velocity decreases and the extra turbulence has decayed.

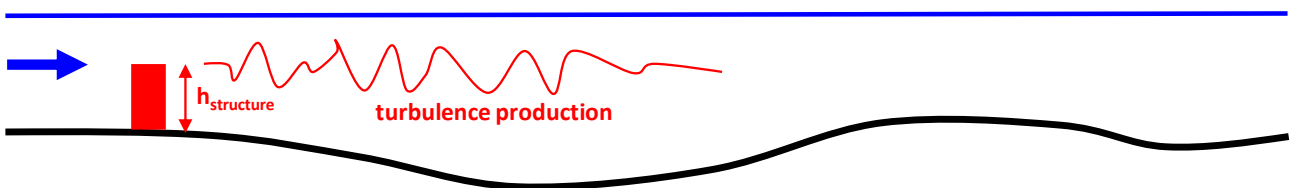


Figure 2.6 Effect of structure

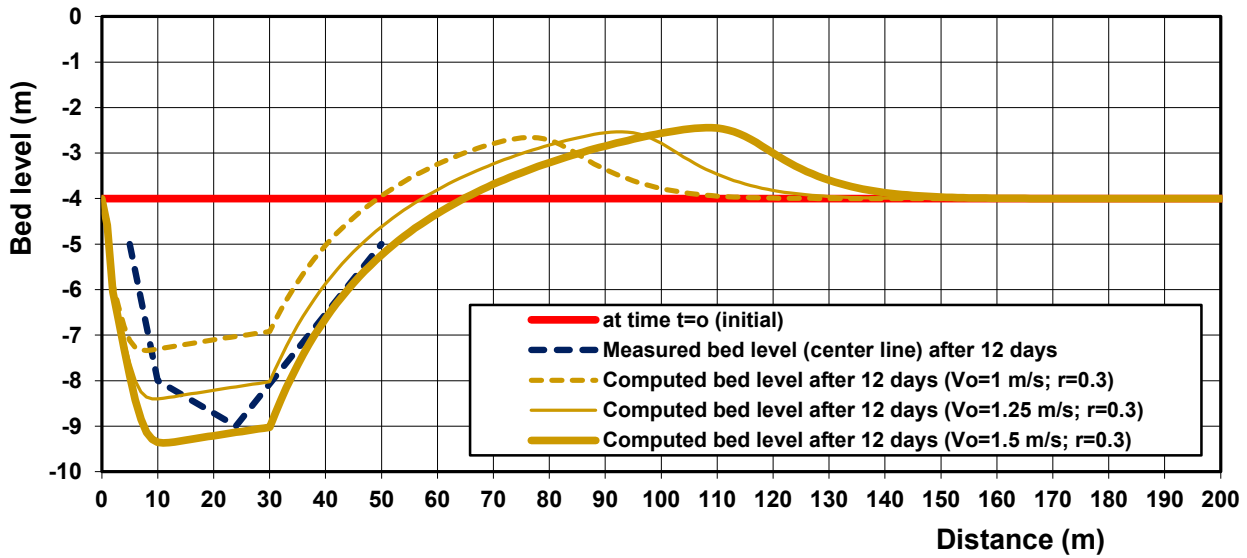


Figure 2.7 Measured and computed scour pit downstream of culvert; SEDTUBE-model

## 2.2 Scour near tip of structure normal to bank

The flow near the rounded tip of a vertical wall (groyne) normal to the bank in a steady current is characterized by the curvature of the streamlines resulting in a spiral type motion like flow in a river bend. The maximum velocity occurs near the tip of the groyne. The length  $L_1$  over which the flow field is disturbed in the contracted cross-section is approximately equal to the length of the groyne ( $L_1 \approx L$ ), if the total river width is larger than twice the groyne length (Figure 2.8).

Based on analysis of field data for unidirectional flow in rivers, the following scour depth expression for rivers has been proposed (Hoffmans and Verheij, 1997):

$$d_{s,max} = \alpha [q_o/(1-m)]^{2/3} - h_1 \quad (2.4a)$$

with:

- $d_{s,max}$  = maximum scour depth near head of structure,
- $h_1$  = mean water depth of contracted section before scour,
- $q_o$  = discharge per unit width upstream of contracted section (in  $m^2/s$ ),
- $m$  =  $L/B$ = blocking coefficient,
- $B$  = channel width,
- $\alpha$  = coefficient depending on geometry ( $\approx 1$  to 2 for straight channel and groyne normal to bank).

Lacey (1930) proposed a formula for the prediction of the maximum scour depth around abutment-type structures in rivers, as follows (see Rahman and Haque, 2003):

$$d_{s,max} = 0.47h_1K [Q/(f h_1^3)]^{1/3} - h_1 \quad (2.4b)$$

with:

- $d_{s,max}$  = maximum scour depth near head of structure,
- $h_1$  = mean water depth of contracted section before scour,
- $Q$  = regime discharge (in  $m^3/s$ ),
- $f$  =  $56(d_{50})^{0.5}$ = sediment factor,
- $d_{50}$  = sediment diameter (in m),



$K$  = coefficient depending on geometry ( $\approx 2$  for rounded head to 4 for steep sloping head).

**Rahman and Haque (2003)** taking the structure length into account, modified Equation (2.4b) for rivers into:

$$d_{s,max} = 0.47h_1 M^{1/3}[1+1.5L/h_1]^{1/3} - h_1 \quad (2.4c)$$

with:

- $d_{s,max}$  = maximum scour depth near head of structure,
- $h_1$  = mean water depth of contracted section before scour,
- $M$  =  $Q/(fh_1^3)$ = discharge coefficient,
- $f$  =  $56(d_{50})^{0.5}$ = sediment factor,
- $d_{50}$  = sediment diameter (in m).

**Rahman and Haque (2003)** also presented field data of scour depths near abutment-type structures along the Jamuna river in Bangladesh. The relative scour depth values ( $d_{s,max}/h_1$ ) are in the range of 0.5 to 2 for a length scale of about  $L/h_1=7$  to 12 and about 1 for  $L/h_1=40$ . This latter value is significantly overpredicted by Equations (2.4b and 2.4c).

**Coleman et al. (2003)** proposed for vertical wall bridge abutments in rivers of varying lengths the following expression:

$$d_{s,max} = K_{yL} K_d K_s K_\theta K_G K_i \quad (2.4d)$$

with:

- $U$  = depth-averaged approach velocity;
- $U_{cr}$  = critical depth-averaged velocity;  $h$ =approach water depth;
- $K_{yL}$  = factor related to abutment size= $10h$  for  $h/L=0.04$ ,
- $K_{yL} = 2(h_1L)^{0.5}$  for  $0.04 \leq h_1/L \leq 1$ ,  $K_{yL} = 2L$  for  $h_1/L > 1$ ;
- $K_d$  = sediment size factor= $1$  for  $L/d_{50} > 25$ ,
- $K_s$  = foundation type factor= $1$  for vertical wall;
- $K_\theta$  = alignment factor= $1$  for 90 degrees (normal to bank),
- $K_\theta = 0.95$  for 45 degrees,
- $K_\theta = 1.1$  for 150 degrees;
- $K_G$  = river channel factor= $1$  for rectangular channels;
- $K_i$  = flow intensity factor= $U/U_{cr}$ ;  $K_i=1$  for  $U/U_{cr} > 1$ .

Another method is to assume that the cross-sectional area of the contracted section ultimately will be equal to that without the groyne (see **Figure 2.4**). This means that the scoured area ( $A_s$ ) will be equal to the area blocked by the groyne. Thus:  $A_s = h_1L$ .

Assuming that  $A_s=1/3(d_{s,max}L_1)$  for a long groyne ( $L > 10 h_1$ ) and  $L_1=L$ , it follows that:

$$d_{s,max}/h_1 = 3 \quad \text{for } L > 10 h_1 \quad (2.5)$$

This is in good agreement with values observed by **Richardson et al. (1988)**, who found for rock dikes (with  $L/h_1 > 25$ ) in the Mississippi river:  $d_{s,max}/h_1 \leq 4$ .

The expression  $d_{s,max}/h_1=3$  is valid for a relatively long groyne ( $L/h_1 \geq 10$ ) resulting in a significant increase of the velocities in the contracted section. The channel bed is assumed to be composed of sandy material and the approach velocity is assumed to be larger than the critical velocity for initiation of motion ( $U/U_{cr} > 1$ ). Armouring which may occur in course bed material, will result in reduced scour depths.

The scour depth near a short groyne will be considerably smaller. The maximum scour depth is:

$$d_{s,max}/h_1 = 0.5 \text{ to } 1.5 \quad \text{for } L = 1 \text{ to } 3 h_1 \quad (2.6)$$



The shape of the groyne will also affect the scour depth. Scour is maximum near a vertical wall (rectangular cross-section). The scour depth may be reduced with about 30% in case of a rock-type groyne with a trapezoidal cross-section or with a rounded tip.

**Kothyari and Ranga Raju (2001)** discuss the scour around spur dikes and bridge abutments in alluvial rivers. The horse-shoe vortex and associated downflow are found to be the prime agents causing scour similar to scour around bridge piers (see Figures 6.1 and 7.1). They defined an analogous circular pier which has such a size that the scour around it is the same as that around the given abutment or spur dike under similar hydraulic conditions.

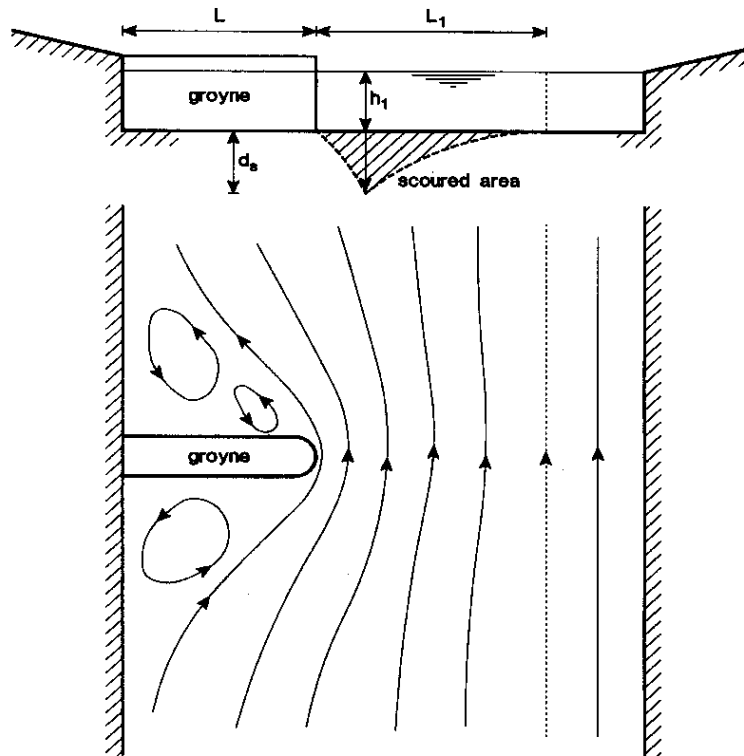


**Figure 2.8** Flow pattern and scour near a groyne



### 3. Scour near seawalls due to waves and currents

#### 3.1 Review of scour data

Seawalls are generally built on receding shorelines to protect the mainland against retreat and inundation. They are not built to maintain the beach (if present) in front of the seawall. Often, the recession of adjacent shorelines is continued and even accelerated by the interaction of the seawall with the morphological system. **Pilkey and Wright (1988)** distinguished between passive erosion and active erosion; the former being the natural erosion before construction of the wall (ultimately resulting in a more exposed position of the seawall) and the latter being the additional erosion caused by the presence of the wall.

Scour near seawalls can be classified as (see **Figure 3.1**):

- scour at the toe of the wall; the maximum scour depth ( $d_{s,max}$ ) is the depth below the position of the original sand surface (before the presence of the structure);
- scour of dune and beach on both ends of the wall (lee-side scour) resulting in a more exposed position of the wall and consequent narrowing of the beach in front of the wall by accelerating longshore currents around the protruding wall.

Seawalls contribute to erosion and scour by the following processes:

- interaction of incident and reflected waves and associated wave-induced drift velocities above the sand bed near the structure;
- enhancement of offshore-directed transport by waves breaking at or near the wall (generation of undertow and stirring of sediment);
- blocking (partly) of the updrift longshore transport in case of a protruding seawall; longshore currents in front of a protruding wall are accelerated resulting in bed erosion and general lowering/steepening of bed (and hence more intensive wave attack); increased turbulence and circulations generated at the downdrift end of the wall lead to scour and retreat of the shoreline;
- impoundment of sediment behind the wall, which would otherwise be released to the littoral drift system.

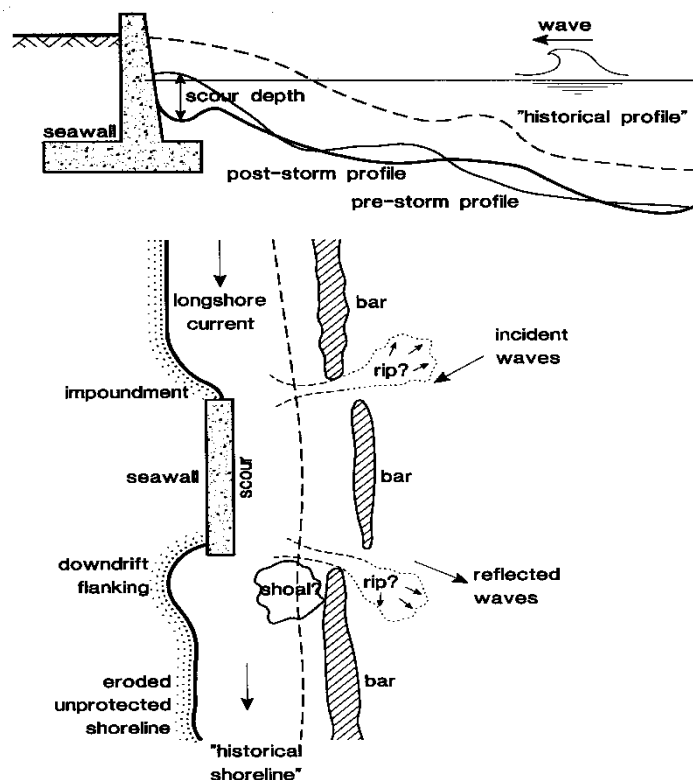


**Figure 3.1** *The effects of seawalls on the beach*  
Top: scour at toe of wall; Bottom: scour at end of wall



A review of the effects of seawalls on the beach has been given by **Kraus (1988)** and by **Kraus and McDougal (1996)**. Their main findings are:

#### **Based on laboratory studies**

- the primary force of wave action alone does not lead to severe toe scour; the scour depth increases strongly when currents are present;
- the maximum scour depth is approximately equal to 0.5 to 1 times the significant wave height in deeper water ( $d_{s,max}/H_{sig,0} = 0.5$  to 1) for an unbarred bottom profile (**Fowler, 1992**);
- an inclined wall produces less scour than a vertical wall;
- scour is reduced if the seawall is situated at the most landward position (not protruding in the surf zone);
- scour patterns due to (partial) standing waves in front of seawall depend on the mode of sediment transport: bed-load transport or dominant suspended load transport;
- beach recovery and reduction of scour depth during fairweather conditions is possible;
- formation of bar-trough system in front of seawall is not necessarily disturbed;
- increased beach erosion at downdrift end of seawall (lee-side erosion) may occur; the alongshore erosion length for an isolated seawall was found to be about  $L_e = 0.7 L_{wall}$ ; the maximum shoreline retreat at the end of the wall was  $y_{s,max} = 0.1 L_{wall}$  with  $L_{wall}$  = alongshore length of seawall (**Komar and McDougall, 1988**);

#### **Based on field studies**

- the impact of a seawall on a beach is a long-term phenomenon (decades); short-term observations do not give proper results; long-term scour in front of wall may be more serious than short-term scour due to storm event; scour trough may be filled rather quickly after storm event;
- quantitative data of toe scour depths are hardly available; some scattered data suggest values of  $d_{s,max}/h_{toe} = 0.5$  to 1, but other data show no scour at all (**Griggs et al., 1990, 1994**);
- the maximum scour depth at the toe is mostly assumed to be equal to the significant wave height at the edge of the surf zone (deeper water) during a storm event ( $d_{s,max}/H_{sig,storm} = 1$ ) for an unbarred bottom profile; this will give a rather conservative estimate for a barred profile and for less exposed seawalls at the backbeach;
- maximum scour is expected to occur when the water level is highest (peak surge level), because the higher water level can support larger waves;
- the additional scour in front of a seawall is approximately equal to the amount of sediment behind the wall that would erode in the absence of a seawall (**Dean, 1986**); this principle is difficult to apply, because it requires information of beach profiles without a seawall before and after a storm event;
- seawalls in the backshore with a beach in front give better performance than those without a beach; the impact of the wall is strongly dependent on its position with respect to the low water line; erosion is minimum if the seawall is built as far landward as possible (landward of level of maximum run-up during storm event); erosion is maximum if the seawall is built at a location seaward of the low water line so that waves will reflect and or break against the wall;
- reflective vertical or near-vertical seawalls cause relatively large scour depths at the toe; scour was found to be minimum in front of a dissipative rubble-mound seawall; reflection itself is not found to be a great contributor to scour in front of seawalls;
- erosion of berm and beach in front of seawall (located at the backshore) is of the same order of magnitude as that of adjacent beaches, but the erosion process proceeds faster if waves overtopping the beach/berm can reflect or break against the wall; narrow, steep beaches in front of seawalls are often severely eroded during storm events;
- rip currents enhance scour in front of wall; accelerating longshore currents around a protruding seawall enhance scour of the bed;
- the widths of dry beaches in front of natural shorelines (South and North Carolina and New Jersey, USA) were found to be consistently wider than those in front of hard structures; the higher the degree of stabilization, the narrower the beach (**Pilkey and Wright, 1988**);



- beach recovery in front of a seawall after a storm event proceeds in a similar way or somewhat slower than for a natural beach; the overall recovery often is partial for a narrow and steep beach;
- longshore bar-trough system in front of a wall need not to be destroyed and can develop in much the same way as at beaches without a wall;
- beach erosion at downdrift end of wall (lee-side erosion) is often increased.

### 3.2 Wave-related scour near toe of seawall

The basic shape of a toe scour hole (**Steetzel, 1988**) is shown in Figure 3.2. The proper determination of the water depth at the toe ( $h_{toe}$ ) of the structure may give problems in field conditions.

According to the **Shore Protection Manual (1984)**, the scour depth is given by the following simple rule:

$$d_{s,max} = \alpha_c H \quad (3.1)$$

with:  $H$  = height of maximum unbroken wave at toe of structure;  $\alpha_c = (1 + U_c/U_{cr})^{0.1}$  = current effect;  $U_c$  = longshore current velocity,  $U_{cr}$  = critical velocity for initiation of motion ( $\alpha_c = 1$  for  $U = 0$  m/s).

Many researchers have conducted two-dimensional movable-bed laboratory tests to determine the toe scour of wall-type breakwaters (see **Kraus, 1988**).

Hereafter, some examples of laboratory experiments are given.

**Herbich et al. (1965)** performed two-dimensional movable-bed tests in a laboratory flume with regular non-breaking waves (period of about 1.5 s) on walls made of plexiglas. The slope angle ( $\alpha$ ) of the wall was varied in the range of  $15^\circ$  to  $90^\circ$  ( $90^\circ$  = vertical). The bed material consisted of sand with a median diameter of 0.483 mm. The most important results are, as follows:

- slope angle of  $15^\circ$ : wave reflection was less than 20% and the equilibrium scour depth below the natural bed ( $d_{s,max}$ ) was about  $d_{s,max}/H = 0.4$  to  $0.45$  with  $H$  = incident wave height;
- slope angle of  $30^\circ$  to  $90^\circ$ : wave reflection was larger than 40% and the equilibrium scour depth was about  $d_{s,max}/H = 0.5$  to  $0.6$ ;
- primary scour was observed under the nodes of the wave envelope;
- (partial) standing waves were observed to give patterns of alternating scour and deposition in front of wall;
- more reflective conditions resulted in an increase of the scour depth,
- scouring always occurred within a distance of  $1/4 L$  ( $L$  = wave length) from the toe of the structure.

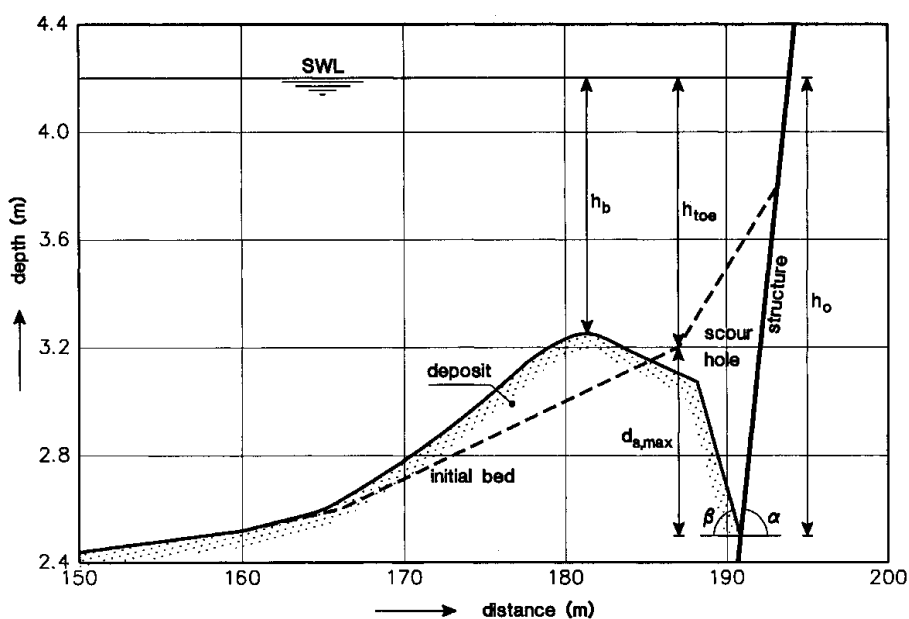


Figure 3.2 Basic shape of scour hole near toe of seawall (Steetzel, 1988)



**Steezel (1988)** analyzed toe scour near structures both in field conditions and in small-scale and large-scale laboratory experiments. His findings are:

- the scour depth is strongly related to the incident wave conditions, surge levels, beach slope and water depth near the toe;
- the maximum water depth including the scour depth was found to be  $h_0/h_b=1.7$  to  $1.8$  (see Figure 3.2) with  $h_0$ = maximum water depth in scour hole,  $h_b$ = minimum water depth above bar deposit; this is roughly equivalent with  $d_{s,max}/h_{toe}=0.75$  (see Figure 3.2);
- the maximum value of the landward slope of the scour hole was between 1 to 3 ( $\tan\beta=0.33$ ) and 1 to 5 ( $\tan\beta=0.2$ );
- the shape of the scour hole is related to the steepness of the seawall; the maximum scour depth is closer to the wall for a steeper slope of the wall.

**Fowler (1992)** analyzed laboratory test results and proposed an empirical method to determine the scour depth at the toe of vertical walls. Based on this approach, the maximum scour depth roughly is:

$$\begin{array}{ll} d_{s,max}/H_{s,0} = 0.6 & \text{for } h_{toe}/L_0 = 0.005 \\ d_{s,max}/H_{s,0} = 0.8 & \text{for } h_{toe}/L_0 = 0.02 \\ d_{s,max}/H_{s,0} = 1.0 & \text{for } h_{toe}/L_0 = 0.04 \end{array} \quad (3.2)$$

with:  $H_{s,0}$ = significant wave height in deep water,  $L_0$ = wave length in deep water,  $h_{toe}$ = water depth at toe of structure.

The scour depth increases with decreasing wave length, because shorter waves tend to break against or in front of the wall. Breaking waves produce a larger scour depth.

**Kraus and McDougal (1996)** reported about scour at the toe of a seawall due to breaking waves in large-scale tests conducted in the USA. Two-dimensional tests were conducted in a large-scale flume (Supertank at the Hinsdale Wave Research Laboratory, Oregon State, USA). The beach material consisted of uniform 0.22 mm-sand. The significant offshore wave heights ranged between 0.4 and 1.0 m and periods between 3 and 8 s. The vertical wall was placed at the end of the beach. A remarkable result was that the bed profiles in front of the wall did not show a large scour trench. A rather small scour trench was created at the toe of the wall, but the influence was highly localized in the immediate vicinity of the wall. The maximum scour depth was about 0.3 m after 10,000 waves in a (original) water depth of about  $h=0.5$  m. Thus,  $d_{s,max}=0.6h$ . Scouring of the bed was not observed outside a distance of 5 times the initial water depth at the toe. Reflection was found to be a relatively unimportant parameter in the scouring process.



#### 4. Scour near toe of wall-type breakwaters due to waves and currents

Emerged or submerged wall-type breakwaters are structures oblique or parallel (detached) to the shoreline; the seaward end section of the breakwater may run more or less parallel to the shoreline. Wall-type breakwaters may also be built as submerged structures parallel (detached) to the shoreline. Generally, the bed surface in front of a breakwater is relatively flat. For waves approaching normal to the structure, the scouring process is similar to that near a seawall.

The basic processes are:

- interaction of incident and reflected waves, yielding wave-induced drift velocities above the sand bed near the structure (relatively slow process);
- interaction of waves breaking in front of the structure and associated return currents (undertow) above the sand bed (relatively rapid process);
- seaward-directed currents generated along the structure in case of oblique (breaking) waves.

**Irie and Nadaoka (1984)** studied scour by reflecting non-breaking waves in two- and three-dimensional laboratory models with various sediments (sand of 0.2 mm and 0.33 mm; light-weight coal material of 0.33 mm). Their results are:

- deposition at the nodal locations and scour at the antinodal locations (N-type scour); this will occur when the bed-load transport is dominant because wave-induced drift velocities (under partial or full standing waves) near the bed cause the bed-load grains to move toward the nodes of the standing waves (see Figure 4.1);
- scour at the nodal locations (L-type scour) and deposition at the antinodal locations; this will occur when the suspended load transport is dominant due to the presence of drift velocities (above the wave boundary layer) in the direction from nodes to antinodes (see Figure 4.1); vortices generated in the scour hole enhance the movement of sediment to the nodes on both sides of the scour hole.

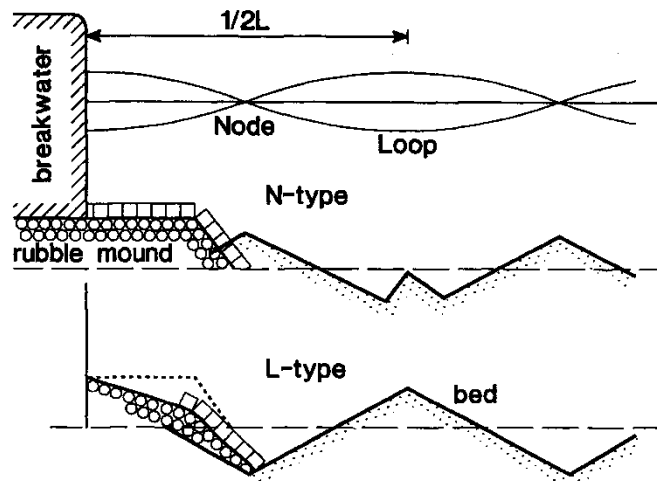


**Figure 4.1** Scour by standing waves  
Top: N-type scour for dominant bed-load transport conditions  
Bottom: L-type scour for dominant suspended transport conditions

L-type scour under suspended load conditions during storm events is most critical for the stability of the structure, because the scour hole develops close to the toe of the structure. This type of scour was found to be dominant for  $U_w/w_s > 10$  with  $U_w =$  near-bed peak orbital velocity and  $w_s =$  fall velocity of sediment. Toe protection should have a length equal to about  $0.25L_w$ .



A two-dimensional wave flume test with regular waves of 0.12 m (period of 1.4 s) in a depth of 0.3 m over a fine sand bed of 0.06 mm resulted in a scour hole with a maximum depth of  $d_{s,max}/h = 0.25$  with  $h =$  depth at the toe. Three-dimensional tests with irregular waves at 30° degrees (to a line normal to the breakwater) over a sand bed of 0.13 mm showed near-bed drift velocities parallel to the breakwater in the direction of the shoreline and scour at the nodal locations close to the toe in the case of dominant suspended load transport. Scour was found to be largest near the tip of the breakwater.

Table 4.1 shows scour depth values at the toe of detached vertical breakwaters given by **Sumer and Fredsøe (2000)** and by **Sumer et al. (2001)**. Regular and irregular waves were generated in a 2D wave flume with a sand bed (0.2 mm-sand) and a water depth of 0.3 m. Bed-load transport without much suspension was observed in the tests.

The toe scour data are in agreement with those of **Xie (1981)** for a breakwater with a vertical wall. The scour depths of Table 4.1 show an increasing trend with increasing wave length. This trend is opposite to the data of Fowler (1992). The scour depth strongly decreases with decreasing side slope angle of the breakwater.

Based on **Xie (1981)**:

$$\begin{aligned} d_{s,max}/H_{rms} &= 1.0 \quad \text{for } h/L_w=0.08 \\ d_{s,max}/H_{rms} &= 0.7 \quad \text{for } h/L_w=0.10 \\ d_{s,max}/H_{rms} &= 0.35 \quad \text{for } h/L_w=0.15 \end{aligned} \tag{4.1}$$

The scour depth was somewhat smaller in tests with irregular waves than in tests with regular waves. Deposition was observed at the location of the nodal points in front of the structure. The data of Table 4.1 in the bed-load transport regime are representative for normal daily wave conditions. The scour depth in the suspended transport regime are representative for storm events. These latter scour depths are roughly 20% to 40% larger than those in the bed-load transport regime. Toe protection against scour should have a length equal to about  $0.25L_w$ .

Field data of toe scour generally include the combined effect of currents and waves on the scouring process. Field results are given below.

Type	Fine sand (suspended transport mode) based on Xie (1981)	Coarse sand (bed load transport mode) based on Sumer and Fredsøe (2000)
Vertical wall	$d_{s,max}/H_{rms}=1.0$ for $h/L_w=0.08$ $d_{s,max}/H_{rms}=0.7$ for $h/L_w=0.10$ $d_{s,max}/H_{rms}=0.35$ for $h/L_w=0.15$	$d_{s,max}/H_{rms}=0.8$ for $h/L_w=0.08$ $d_{s,max}/H_{rms}=0.5$ for $h/L_w=0.10$ $d_{s,max}/H_{rms}=0.25$ for $h/L_w=0.15$
Rubble mound Slope angle=40° (1 to 1.2)	not tested	$d_{s,max}/H_{rms}=0.35$ for $h/L_w=0.08$ $d_{s,max}/H_{rms}=0.30$ for $h/L_w=0.10$ $d_{s,max}/H_{rms}=0.15$ for $h/L_w=0.15$
Rubble mound Slope angle=30° (1 to 1.75)	not tested	$d_{s,max}/H_{rms}=0.15$ for $h/L_w=0.08$ $d_{s,max}/H_{rms}=0.10$ for $h/L_w=0.10$ $d_{s,max}/H_{rms}=0.05$ for $h/L_w=0.15$

**Table 4.1** Scour depths at toe of breakwater ( $h =$  water depth in front of wall, but outside scour zone,  $H_{rms} =$  root-mean-square wave height in front of wall, outside of scour zone;  $L_w =$  wave length based on peak period in front of wall, outside scour zone; slope angle = angle of side slope with horizontal bottom)

**Sato et al. (1968)** studied toe scour near the vertical breakwater of Kashima Port and the east port of Niigata, Japan (see Fig. 4.2). Tidal currents are relatively small. The maximum scour depth near the breakwater of Kashima port was found to be 3 m, measured two weeks after a storm event. The maximum significant wave height was found to be 3 m at a depth of 12 m. Thus, the maximum scour depth is of the same order as the deep water wave height.

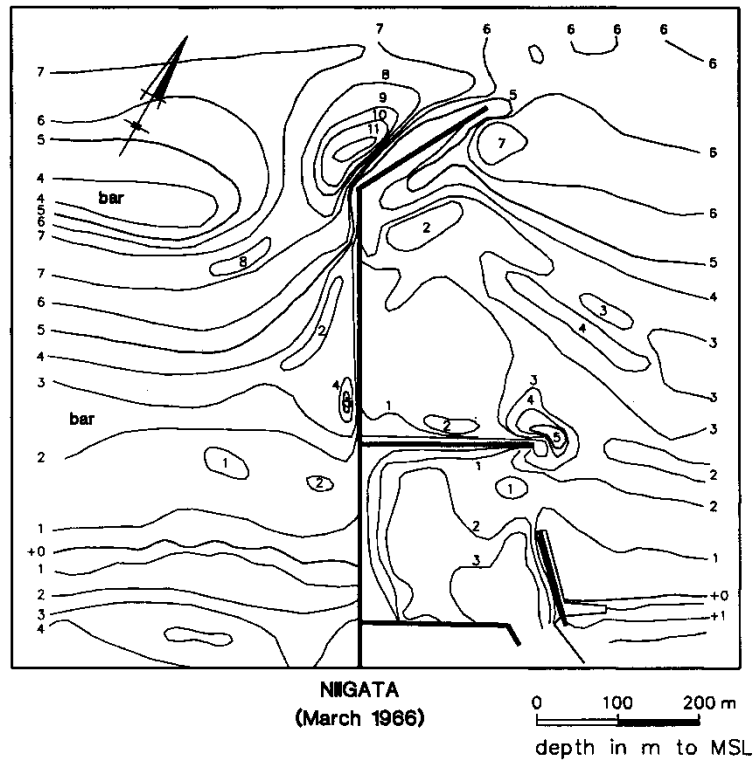


**Figure 4.2** Scour near breakwater of east port of Niigata, Japan (Sato et al., 1968)

In terms of the initial water depth at the toe of the structure, the following values can be derived from their data ( $h_{toe}$  = initial water depth prior to construction):

$$\begin{aligned}
 d_{s,max}/h_{toe} &= 1.5 && \text{for } h_{toe} < 2 \text{ m,} \\
 d_{s,max}/h_{toe} &= 0.5 && \text{for } h_{toe} = 4 \text{ m,} \\
 d_{s,max}/h_{toe} &= 0.3 && \text{for } h_{toe} = 7 \text{ m,} \\
 d_{s,max}/h_{toe} &= 0.1 && \text{for } h_{toe} = 9 \text{ m.}
 \end{aligned}
 \tag{4.2}$$

Scour was found to be maximum:

- in the zone where the breakwater crosses the longshore bar (see Figure 4.2),
- near the junction point (of different alignment angles) where seaward return currents are converging;
- near the tip of the breakwater due to relatively large gradients of wave energy and turbulence intensities.

The scour between the breakwater and the longshore bar at 4 m below MSL (see Figure 4.2) is of the order of the initial water depth ( $d_{s,max}/h_{toe,initial} = 1$ ). This relatively large value was believed to be related to the presence of seaward-directed rip currents, generated along the structure.

**Yokoyama et al. (2002)** have analysed field data and applied a numerical model to evaluate the scour depth near the toe of wall-type structures. From their graphs the following values can be obtained:

$$\begin{aligned}
 d_{s,max}/H_s &= 0.2 && \text{for } H_s/h_{toe} = 0.33 \\
 d_{s,max}/H_s &= 0.6 && \text{for } H_s/h_{toe} = 0.5 \\
 d_{s,max}/H_s &= 1.0 && \text{for } H_s/h_{toe} = 0.67 \\
 d_{s,max}/H_s &= 1.5 && \text{for } H_s/h_{toe} = 1.0
 \end{aligned}
 \tag{4.3}$$



## 5. Scour near toe of rubble-type breakwaters due to waves and currents

Emerged or submerged rubble-type breakwaters are the most common structures oblique or parallel (as detached breakwater) to the shore. Wave reflection tests on breakwaters of different armour units in flumes (**Losada and Gimenez, 1981**) show that the reflection coefficients can be as large as 70% for rubble mound or Dolos elements with  $\tan\alpha/(H/L_0)^{0.5}$  between 5 and 10.

**Irie et al (1986)** conducted three-dimensional tests in a laboratory basin with oblique regular and irregular waves on a rubble-mound breakwater. The bed material was uniform 0.14 mm-sand. The maximum scour depth was attained after 30,000 waves (10 hours) and found to be  $d_{s,max}/h_{toe} = 1$ . The scour depth was maximum within a distance of  $1/2 L$  from the toe of the breakwater.

**Delft Hydraulics (1985)** reported about two-dimensional large-scale laboratory tests on a rubble-mound breakwater related to the design of the breakwater of St. George Harbor, Alaska. The bed (slope of 1 to 30) consisted of rather uniform 0.225 mm-sand. The breakwater consisted of a rubble-mound structure with a berm (berm width=2.5 m, outer slope of 1 to 1.5, crest about 0.3 m above MSL, see Figure 5.1). The design storm was represented in 8 steps (duration of 30 to 45 minutes) of different wave heights and periods, as given in Table 9.5.1. The water depth at the toe of the breakwater was 1.2 m. The relative wave height at the toe varied between 0.6 and 0.9. The maximum scour depth after step 7 was found to be  $d_{s,max}/h = 0.5$  with  $h$ = water depth at toe.

**Sumer and Fredsøe (2000)** and **Sumer et al. (2001)** present results of toe scour in front of rubble-mound breakwaters based on tests in a 2D wave flume, see Table 4.1. The scour depth is significantly smaller than that near the toe of a vertical breakwater. Toe protection against scour should have a length equal to about  $0.25L_w$ .

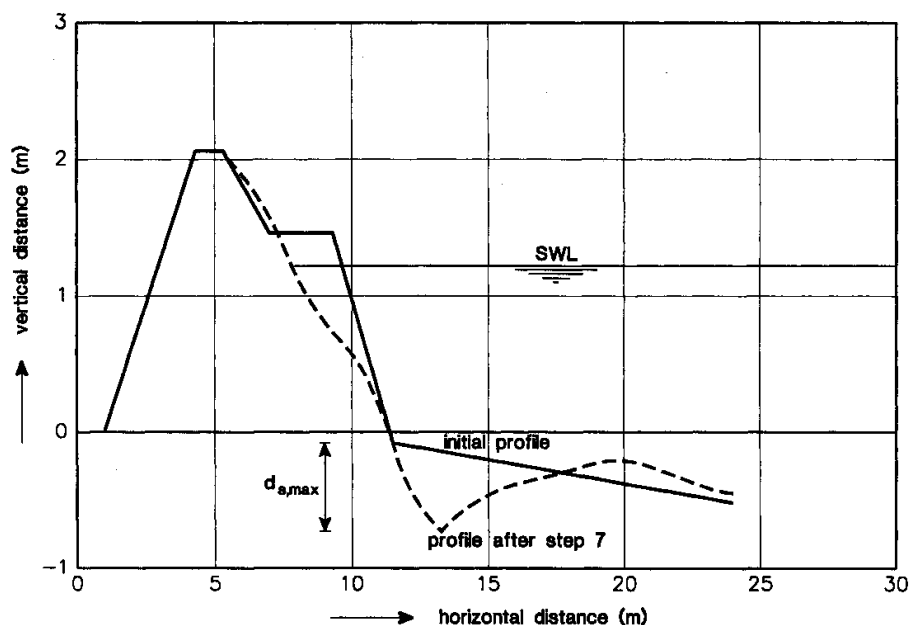


**Figure 5.1** Bed level profile at initial time and after step 7 for large-scale tests at Delft Hydraulics (1985)

**Katayama et al. (1974)** studied short-term scour at the toe and near the tip of an offshore breakwater (on the Niigata coast of Japan), which was temporarily submerged due to settlement and scour. The Niigata coast is exposed to severe wave action in winter season. The tidal range varies between 0.5 m and 1 m. The offshore breakwater was initially built as a partially submerged breakwater with a crest height of 1.1 m above low water (water depth of 4 m below low water level). The structure was heavily damaged due to scour beneath the structure and the crest height was raised to 3 m above LW.

The maximum scour depth was determined from the settlement of iron rings (free movable) along poles placed in the bed; the rings move downward if the bed is scoured. This technique has been used because it gives the



maximum scour depth, not affected by post-storm deposition in the scour hole. Two situations were studied: crest height at 1 m above LW and crest height at -2 m below LW (damaged submerged structure).

The results are:

- crest height at -2 m below LW,
  - maximum scour depth of 4 m in water depth of about 4 m ( $d_{s,max}/h_{toe}=1$ ) at the seaward side of the submerged structure; the maximum scour depth occurred at a distance of about 20 m from the toe of the structure; scour was negligible at a distance of 70 m from the toe;
  - maximum scour depth of 2.5 m at landward side of the structure due to wave overtopping;
- crest height at 1 m above LW,
  - maximum scour depth of 2 m in water depth of about 4 m ( $d_{s,max}/h_{toe}=0.5$ ) at the seaward side of the structure; the maximum scour depth occurred at a distance of about 20 m from the toe of the structure;
  - maximum scour depth of 0.8 m landward of breakwater due to longshore currents.

Thus, the scour near a submerged breakwater is considerably larger than that near a breakwater with its crest level above LW. This is caused by wave overtopping and overplunging.

**Ichikawa (1967), Silvester (1991) and Uda and Noguchi (1993)** present data of short-term (2 to 3 years) scour near breakwaters in micro-tidal regimes for some Japanese ports.

Based on the data, the following rough scour ranges are given:

$$\begin{aligned} d_{s,max}/h_{toe} &= 1 \text{ to } 0.5 && \text{for vertical caisson-type structures in depths of 5 to 10 m,} && (5.1) \\ d_{s,max}/h_{toe} &= 0.5 \text{ to } 0.2 && \text{for vertical caisson-type structures in depths of 10 to 30 m,} \\ d_{s,max}/h_{toe} &= 0.3 \text{ to } 0.2 && \text{for breakwaters with armour units in depths of 10 to 20 m.} \end{aligned}$$

**Sumer et al. 2005** have studied the scour at the toe of detached low-crested rubblemound breakwaters. Based on their results, the following approximate expression is given:

$$d_{s,max} = 0.25 \alpha_c (1 + F/h_{toe}) H_{s,toe} \quad ; \text{upper limit } d_{s,max}=0.5 \alpha_c H_{s,toe}; \text{lower limit } d_{s,max}=0.15 \alpha_c H_{s,toe} \quad (5.2)$$

with:  $F$  = height of breakwater crest above or below water level (+ for emerged and – for submerged structures),  $h_{toe}$  = water depth at toe,  $H_{s,toe}$  = significant wave height at toe of structure .  $\alpha_c = (1+U_c/U_{cr})^{0.1}$  = current effect factor,  $U_c$  = current velocity,  $U_{cr}$  = critical velocity for initiation of motion.

Geotextiles and filter layer foundations are extremely important to prevent or reduce the effects of scour, which may endanger the entire rubblemound structure.

**Munoz-Peres et al. (2015)** have studied the scour behaviour of various submerged coastal structures on the sandy seabed at a beach in southwest Spain. The structures with length of 8 to 12 m consisted of precast concrete square elements in the middle and triangular elements at both sides. The horizontal sizes of each element is  $2 \times 2 \text{ m}^2$  and the height is about 2 to 2.5 m. The cross-section of the structures has a trapezoidal shape. The structures were deployed at a depth -3 m below LLWL (Tidal range between 1.5 and 3.5 m) at the edge of the surf zone. The bed consists of a layer of sand ( $330 \mu\text{m}$ ) with a thickness of 2 to 3 m on top of a rock bottom. One structure was placed on a gravel foundation layer with thickness of 0.15 m. The other structures were placed directly on the seabed. Geotextiles were not used. The three structures began sinking into the sandy bottom due to strong scour processes immediately after placement and continued until they reached the rocky bottom within 2 months. The average sinking speed was extremely rapid at approximately 3–6 cm/day; 50% of the height of the element was reached in three to six weeks. A foundation of gravel only had a very small effect reducing the sinking speed slightly. The elements located in the middle of the structures sunk nearly vertically into the sand with minor tilting.

When scouring was nearly concluded, backfilling began to fill the scour hole due to a natural sand transport process. Backfilling occurred more rapidly than scouring, and the seabed reached its former profile within 2 weeks.



## 6. Scour near tip of breakwaters and groynes due to waves and currents

Scour near the tip of breakwaters can be classified as *current-dominated* scour or *wave-dominated* scour. Scour is considerably enhanced, if tide-, wind- and wave-induced longshore currents with velocities exceeding 0.5 m/s are present. Wave-related scour generally is dominant in micro-tidal conditions.

### 6.1 Wave-dominated scour near tip of vertical wall-type breakwater

**Sumer and Fredsøe (1997)** studied wave-dominated scour near the tip of a vertical wall-type (rounded tip) breakwater in laboratory conditions.

Based on flow visualization measurements, the scouring mechanisms were found to be:

- generation of vortices (see Fig. 6.1) in the lee-side zone of the wall for  $KC = 1$  to 12; vortices are not generated for  $KC < 1$ ;  $KC = U_w T / B =$  Keulegan-Carpenter number,  $U_w =$  peak orbital near-bed velocity,  $T =$  wave period and  $B =$  width of wall;
- generation of lee-side vortices and horse-shoe vortices for  $KC > 12$ ; horse-shoe vortices are vortices generated near the bed in front of and along the tip of the wall due to rotation of the approaching flow; in field conditions the  $KC$ -number is of the order of 1 and therefore horse-shoe vortices are not of practical relevance.

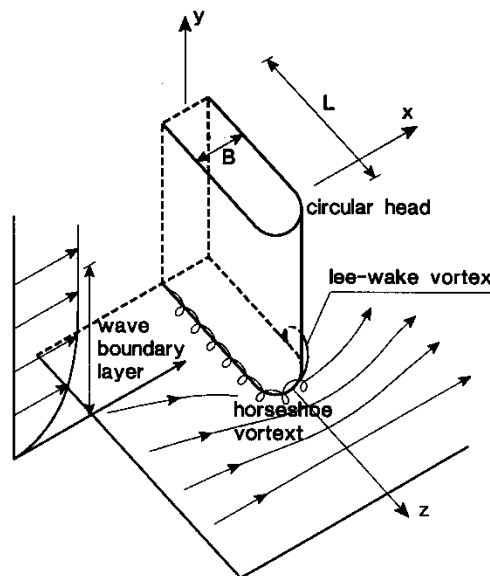


**Figure 6.1** Vortex patterns near tip of wall-type breakwater

Scour tests over a movable bed of 0.17 mm-sand were conducted in a depth of 0.4 m with regular non-breaking waves (periods between 1 and 4 s). The width of the structure was  $B = 0.14$  m and 0.40 m. Hence, the width-depth ratios were  $B/h = 0.35$  and 1. The observed maximum scour depths ( $d_{s,max}/B$ ) for normal incident waves ( $90^\circ$ ) were found to be related to the  $KC$ -number, see Table 6.1. The maximum scour depth was attained after about 1000 waves. The results are only valid for a vertical breakwater with a maximum width equal to the water depth ( $B/h = 1$ ).

The scour was maximum at the location of the tip (in the middle of the tip, see Fig. 6.2) of the breakwater. The observed scour length  $L_s$  (normal to wall) is also given in Table 6.1.

The maximum scour depth roughly increased by a factor 2 for a straight wall tip (sharp edge) in stead of a rounded tip.



The maximum scour depth increased by about 20% for oblique incident waves.  
The maximum scour increased considerably, when the waves were superimposed on a following current ( $U_c$ ).  
For example,  $KC=2$  and  $U_c/(U_c+U_w)=0.5$  resulted in  $d_{s,max}/B=1$ .  
The data of **Table 6.1** can be approximated by:  $d_{s,max}=0.05 (KC) (B)$

NON-BREAKING WAVES		
SCOUR DEPTH $d_{s,max}/B$	SCOUR LENGTH $L_s/B$	KC-number
0.02	0.5	1
0.1	1.5	2
0.2	2.5	4
0.3	3.5*	7
0.4	-	10

**Table 6.1** Scour depth for normal incident non-breaking regular waves over a sand bed of 0.17 mm in a laboratory flume (Sumer and Fredsøe, 1997)

The scour can be eliminated by means of a protection layer on the bed. The length  $L$  normal to the structure should be about  $L/B=2$  for  $KC=2$ . In that case the maximum scour depth is reduced by a factor 3. In case of  $L/B=1$ , the maximum scour depth is reduced by about 30%

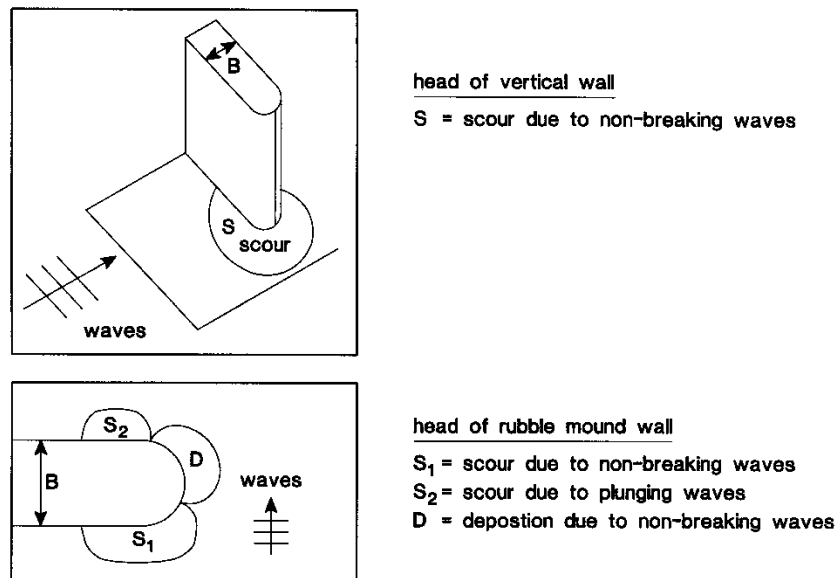


**Figure 6.2** Scour and deposition locations near vertical and rubble-mound breakwaters  
Top: Vertical wall      Bottom: Rubble-mound breakwater

## 6.2 Wave-dominated scour near tip of rubble-mound breakwater

**Fredsøe and Sumer (1997)** studied wave-dominated scour near the tip of a rubble-mound breakwater in laboratory conditions. The basic scouring mechanisms were found to be:

- non-breaking waves; wave-induced steady streaming near the bed due to non-uniformity of the wave boundary layer and contraction of flow upstream and around the tip of the breakwater (see Fig. 6.2);
- breaking waves; relatively high waves ( $H_s/h=0.5$  to 1 depending on bottom slope of foreshore) arriving near the toe of the breakwater may break locally by plunging on the sloping part of the tip; a three-dimensional jet is generated, attacking the sand bed in the lee of the sloping breakwater tip resulting in lee-side scour at the junction between the tip and the trunk section, see Fig. 6.2.



Scour tests over a movable bed of 0.19 mm-sand were conducted in a depth of 0.4 m with irregular (non) breaking waves (periods between 2 and 6 s). The relative wave heights were in the range  $H_s/h = 0.4$  to 0.5. The slope of the breakwater was 1 to 1.5. The bottom width of the breakwaer was about 2.25 m at the sand bed level (width-depth ratio of  $B/h=5.6$ ).

The observed maximum scour depth ( $d_{s,max}/B$ ) for normal incident **non-breaking** waves ( $90^\circ$ ) was found to be related to the KC-number, see Table 6.2. The maximum scour depth was attained after 20,000 waves. The scour was maximum at a short distance upwave of the tip of the breakwater. The observed scour length  $L_s$  was about  $L_s/B=1$  normal to the structure and about 1.5 parallel to the structure, see Fig. 6.2.

The data of table 6.2 can be approximated by:  $d_{s,max} = 0.03 [T_p (g H_{s,toe})^{0.5} / h_{toe}] H_{s,toe}$

The observed maximum scour depth ( $d_{s,max}/H_s$ ) for normal incident **breaking** waves ( $90^\circ$ ) was found to be related to the parameter  $T_p(gH_s)^{0.5}/h$ , see Table 6.2. The maximum scour depth was attained after 20,000 waves. The scour was maximum in the lee-side zone of the tip of the breakwater. The observed scour length  $L_s$  was about  $L_s/H_s=2$  to 3 normal to the structure and about 5 to 10 parallel to the structure, see Figure 6.2.

Based on laboratory data of **Fredsøe and Sumer**, the maximum scour depth for breaking wave conditions is:

$$d_{s,max}/h_{toe} = 0.25 \text{ to } 0.5 \text{ for } H_s/h = 0.5-1.0 \quad (6.1)$$

The scour depth decreased by factor 2 when the slope of the structure was decreased from  $45^\circ$  to  $30^\circ$ .

Scour can be eliminated by means of a protection layer. The length of the protection layer should be about  $L/B=0.5$  (normal to structure) for  $KC=0.4$  and  $L/B=1$  for  $KC=1$ . In that case the maximum scour depth is reduced by a factor 3. In case of  $L/B=0.3$ , the maximum scour depth is reduced by a factor 2.

NON-BREAKING WAVES		PLUNGING BREAKING WAVES	
SCOUR DEPTH $d_{s,max}/B$	KC-number	SCOUR DEPTH $d_{s,max}/H_s$	$T_p(gH_s)^{0.5}/h$
0.01	0.1	0.1	4
0.02	0.2	0.2	8
0.04	0.5	0.5	14

**Table 6.2** Scour depth for normal incident (non) breaking irregular waves over a sand bed of 0.19 mm in a laboratory flume (Fredsoe and Sumer, 1997)

**Fredsøe and Sumer (1997)** also present some scour depth values of rubble-mound breakwaters in field conditions in the USA (based on data of **Lillycrop and Hughes, 1993**), see Table 6.3.

Based on this dataset, the maximum scour depth is about:

$$d_{s,max}/h = 0.4-0.5 \quad \text{for } H_s/h = 0.8-0.9 \quad (6.2)$$

**Katayama et al. (1974)** present information of scour near the tip of an offshore breakwater on the Niigata coast in Japan. Scour depths between 2 and 4 m in water depth of about 4 m were observed (based on soundings made after the stormy season). All available field data of scour near the tip of rubble-mound breakwaters (weak currents) in Japan show:

$$d_{s,max}/h_{toe} = 0.3 \text{ to } 0.2 \quad \text{for depths between 10 and 20 m} \quad (6.3a)$$

$$d_{s,max}/h_{toe} = 0.5 \text{ to } 1 \quad \text{for depths smaller than 4 m} \quad (6.3b)$$



LOCATION	TYPE	DEPTH AT TOE <b>h (m)</b>	WAVE HEIGHT <b>H<sub>s</sub> (m)</b>	PEAK PERIOD <b>T<sub>p</sub> (s)</b>	MAX. SCOUR DEPTH <b>d<sub>s,max</sub> (m)</b>	
					front-side	lee-side
Morro Bay California	slope 1:2 base B=76 m	6	5.3	10-15	-	3
Cattaraugus Harbour New York	slope 1:2 base B=50 m	3	2.4	8.3	0.6	1.2

**Table 6.3** Maximum scour depth of sand and gravel bed near the tip of rubble-mound breakwaters due to wave motion (Fredsoe-Sumer, 1997)

The data of **Sumer et al. 2005** for a low-crested rubblemound structure (weak currents) can be approximated by:

$$\text{Front side: } d_{s,max} = \alpha_c [0.01(F/h_{toe}) + 0.02] B \quad (6.4a)$$

$$\begin{aligned} \text{Backside: } d_{s,max} &= 0.75 \alpha_c (1 + F/h_{toe}) H_{s,toe} && \text{for } F/h_{toe} < 0 \\ d_{s,max} &= 0.50 \alpha_c (1 - F/h_{toe}) H_{s,toe} && \text{for } F/h_{toe} > 0 \end{aligned} \quad (6.4b)$$

with:

F = height of breakwater crest above or below water level (+ for emerged and – for submerged structures),  $H_{s,toe}$  = significant wave height at toe of structure, B = width of structure normal to waves,  $\alpha_c = (1 + U/U_{cr})^{0.1}$  = current effect; U = longshore current velocity,  $U_{cr}$  = critical velocity for initiation of motion ( $\alpha_c = 1$  for  $U = 0$  m/s).

### 6.3 Current-dominated scour near tip of rubble-mound breakwaters and groynes

Scour near the tip of a groyne (normal or slightly oblique to the bank or shore) or breakwater is considerably enhanced, if wind-, wave- and tide-induced longshore currents with velocities exceeding 0.5 m/s are present. The key scouring mechanisms are:

- flow contraction near tip increasing with the protrusion length of the groyne/breakwater (Figure 6.1);
- large-scale vortices generated at the tip of the groyne/breakwater increasing the transport capacity of the flow.

The sediments are mobilized by the near-bed velocities and by the stirring action of the waves (if present) and carried away by the currents, but currents alone are also capable of mobilizing the sediments.

Laboratory experiments for combined wave-current scour near coastal structures parallel to the coast have been performed by **Hughes and Kamphuis (1996)** and by **Sumer and Fredsoe (1997)**.

The latter give some values for scour depth along the rounded tip of a vertical wall breakwater parallel to the coast:

$$\begin{aligned} d_{s,max} &= 0.2B && \text{for } U_c/(U_c+U_w)=0.2 \text{ and } KC=2 \\ d_{s,max} &= 0.7B && \text{for } U_c/(U_c+U_w)=0.2 \text{ and } KC=7 \end{aligned} \quad (6.5a)$$

$$\begin{aligned} d_{s,max} &= 0.7B && \text{for } U_c/(U_c+U_w)=0.4 \text{ and } KC=2 \\ d_{s,max} &= 1.5B && \text{for } U_c/(U_c+U_w)=0.4 \text{ and } KC=7 \end{aligned} \quad (6.5b)$$

with:  $U_c$  = depth-averaged current velocity and  $U_w$  = peak orbital velocity near bed,  $KC = U_w T_p/B$  with  $U_w$  = near-bed peak orbital velocity,  $T_p$  = peak wave period, B = width of wall.



The data can be roughly represented by:

$$d_{s,max} = 0.5 [U_c / (U_c + U_w)] KC B \quad (6.6)$$

These values do not represent the equilibrium values as the laboratory tests were only done for a relatively short time period (sand bed layer was not thick enough). As the maximum width of the structure in the model tests was about equal to the water depth, the maximum scour depth can also be related to the water depth yielding values in the range of  $d_{s,max} = 0.2$  to  $1.5 h$  for  $U_c / (U_c + U_w) = 0.2$  to  $0.4$  and  $KC=2$  to  $7$ . The equilibrium values may be 50% larger.

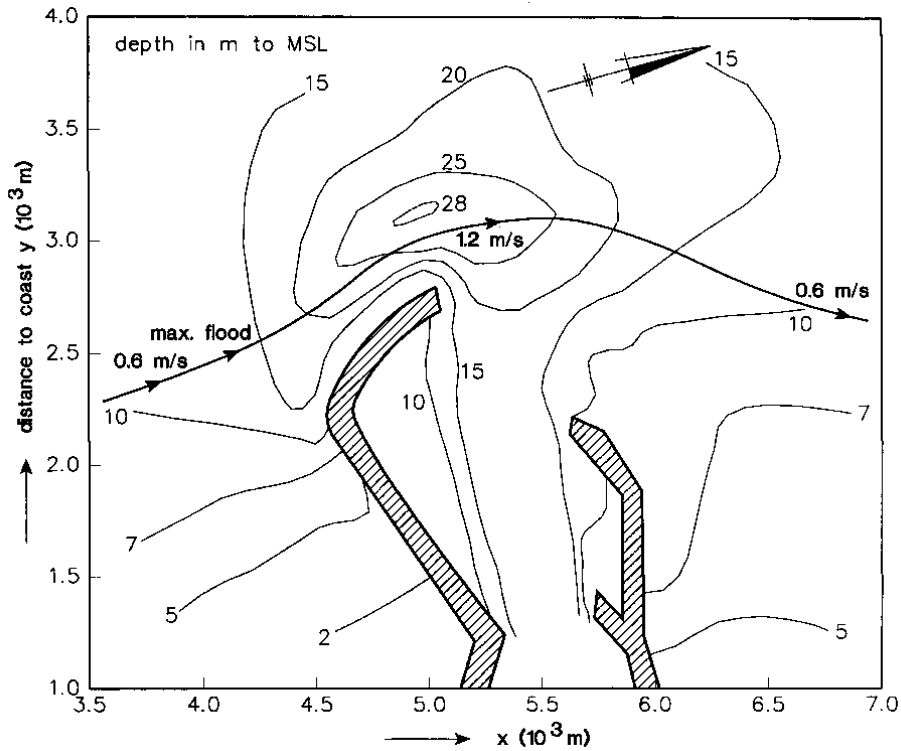


**Figure 6.3** Scour (in 1986) near tip of breakwater of IJmuiden on meso-tidal North Sea coast, The Netherlands (Delft Hydraulics, 1988)

**Delft Hydraulics (1988)** reported about a large scour hole (**Figure 6.3**), which was observed near the tip of the breakwater of IJmuiden harbour (approach to Port of Amsterdam), The Netherlands. The breakwater is built normal to the shore over about 2 km; the end section is situated at an angle of  $60^\circ$  to the shoreline over about 0.5 km. The bed consists of sand with  $d_{50}$  of 0.2 to 0.3 mm. The tide is meso-tidal; the maximum tidal current velocity in the original undisturbed situation was about 0.6 to 0.7 m/s during flood, which increased to about 1.2 m/s after construction of the breakwaters. The wind waves are oblique to the breakwater; swell is not of significant importance.

The maximum scour depth near the tip of the breakwater was found to be about 15 m below the original sea bed; the original water depth below MSL was about 15 m, see **Figure 6.3**.

Thus, the maximum scour depth is as large as the original water depth at the toe of the structure:

$$d_{s,max} / h_{toe} = 1 \quad \text{for original depth of 15 m} \quad (6.7)$$

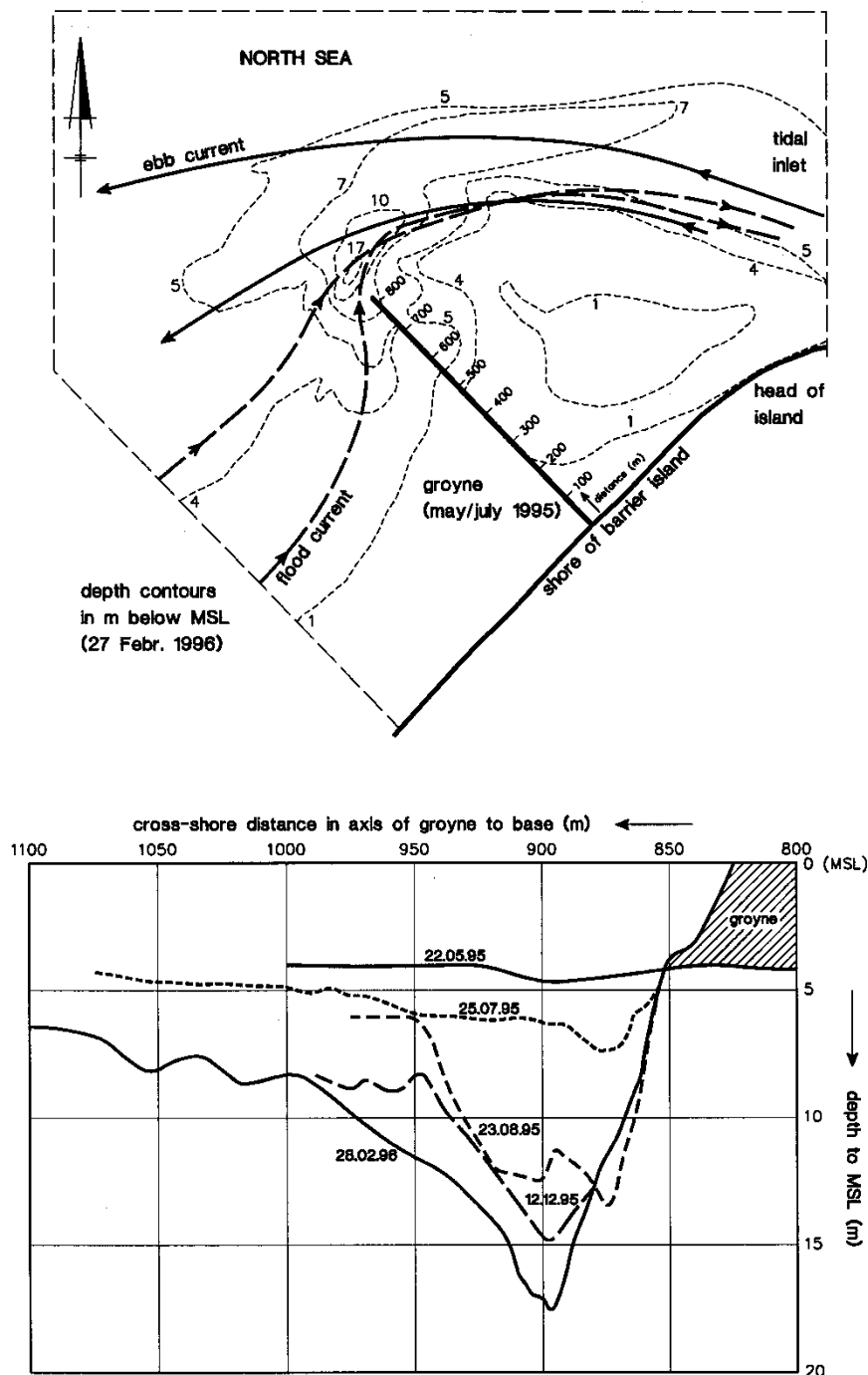


**Figure 6.4** Scour near tip of Eierland groyne on meso-tidal North Sea coast of barrier island, The Netherlands; Plan view (Upper) and Cross-sections in axis of groyne (Lower)

**Rijkswaterstaat (1996)** reported about a deep scour hole near a long groyne (Eierland dam; length of 800 m), which was built (in May-July 1995) normal to the North Sea coast of one of the West Frisian barrier islands of The Netherlands to protect the tip of the island against erosion by the tidal currents passing the inlet on the eastern side of the groyne, see **Figure 6.4**.

The bed consists of sand with  $d_{50}$  of about 0.3 mm.



The original water depth at the toe of the groyne was about 4 m below MSL.

The maximum current velocities (during flood) in the original situation were about 0.7 m/s, which increased to 1.2 m/s after construction of the dam based on flow computations.

The sand bed near the tip of the groyne was scoured away to a depth of 13 m below the original bed in a period of 9 months.

**Figure 6.4** shows a plan view of the scour hole after 9 months with respect to June 1, 1995 and **Figure 6.4** also shows cross-sections in the axis of the groyne at various times. The maximum scour depth is 13 m below the original bed (4 m below MSL). The width of the deepest section is about 150 m. The steepest slope close to the toe is about 1 to 1.5 and is protected by layers of stones. The maximum slope below -10 m is 1 to 2.5.

Thus, the ratio of the scour depth and the original water depth at the toe for a breakwater/groin normal to the coast is:

$$d_{s,max}/h_{toe} = 3 \quad \text{for original depth of 4 m} \quad (6.8)$$

Based on all available data, the ratio of the scour depth and original water depth (below MSL) at the toe roughly varies, as follows:

$$\begin{aligned} d_{s,max}/h_{toe} &= 4 \text{ to } 2 && \text{for depths } < 4 \text{ m,} && (6.9a) \\ d_{s,max}/h_{toe} &= 2 \text{ to } 1 && \text{for depths } = 4\text{-}10 \text{ m,} \\ d_{s,max}/h_{toe} &= 1 \text{ to } 0.5 && \text{for depths } > 10 \text{ m.} \end{aligned}$$

The field data can be roughly represented by:

$$d_{s,max} = 0.4 (B_{ref})^{0.7} (h_{toe})^{0.3} V_{par} \quad (6.9b)$$

with:

$h_{toe}$  = water depth to mean sea level at the toe,

$B_{ref}$  = reference crest width of the structure (= 5 m),

$V_{par} = [(U_c)^2 + (0.7U_w)^2]^{0.5} / U_{cr}$  = dimensionless velocity parameter,

$U_c$  = upstream velocity in the presence of the structure,

$U_w$  = near-bed peak orbital velocity at toe,

$U_{cr}$  = critical velocity for initiation of motion.

In current-dominated conditions the scour area can have large-scale dimensions. The slopes of the scour holes near the structure may be quite steep locally, which may lead to soil sliding due to grain-shear failure and liquefaction endangering the foundation of the structure. This should be prevented by construction of relatively large and flexible bottom protections (dumping of stone layers) over a length (normal to the structure) of 2 to 3 times the undisturbed water depth ( $L = 2 \text{ to } 3h$ ). Regular monitoring should be performed (after storms). Liquefaction can easily occur in loosely-packed sand layers (bore hole information and penetration resistance).



## 7. Scour near vertical pipes, piles and piers due waves and currents

### 7.1 Definitions

Various types of scour can be distinguished, as follows:

- local near-field scour near individual structures (monopiles; single pile of a group of piles);
- global scour, which is the near-field scour around the overall structure;
- edge scour which is the far-field scour at end of scour protection area around the structure.

In addition, local bed level changes may also occur due to migrating bed forms and sand waves.

Generally, free scour development without scour protection is the cheapest solution, but is only allowable for structures with a relatively long foundation length in conditions with weak currents, mild waves and fairly stable beds of coarse materials and/or non-erodible (cohesive) sediment layers.

Scour will lower the fixation length of the pile in the seabed requiring a longer penetration length (increase of embedded length). Generally, the allowable free scour depth in sandy soils is less than 5% of the pile penetration length, which is about  $5D_{pile}$ . Hence, the maximum scour depth allowed is  $0.05 \times 5D_{pile} = 0.25 D_{pile}$  resulting in values of 2 to 2.5 m.

In conditions with sandy soils and strong currents, bed protection against scour is necessary.

Scour protections may be placed, as follows:

- immediately after placement of the structure; first the thin filter layer of smaller/lighter materials is placed, then the pile is placed (driven into the sea bed) and after that the armour layer of larger materials is placed on top of the filter layer;
- later when a certain pre-defined scour level is exceeded (monitor and react); scour is allowed to take place up to a predefined level requiring intensive monitoring, after which scour protection material is placed (without filter layer; smaller sizes can be used as the material is more stable in the scour hole).

Edge scour may occur at end of scour protection area depending on type and length of the bed protection, the strength of tidal currents and seabed composition. Scour protection area should be flexible to be able to follow the bed lowering due to migrating sand waves (if present).

Migrating sand waves (if present) cause bed level variations over time which affect the foundation length of the structures (piles).

Structures with short foundation length should be placed in trough region of sand waves.

Structures with long foundation length (monopiles) should be placed in crest region of slowly migrating sand waves and in trough region of rapid migrating sand waves.

The necessity of scour protections is summarized in **Table 7.1.1** for various types of structures.

Type of structure	Loose bed of fine to medium fine sand		More stable bed of coarse materials and/or presence of non-erodible (cohesive) layers	
	weak current	strong current	weak current	strong current
Long, slender monopile (diameter up to 10 m)	free scour; scour protection may be placed later	scour protection	free scour	free scour; scour protection may be placed later
Jacket structure on long, slender piles (multiple piles with smaller diameter)	free scour	free scour	free scour	free scour
Jacket structure on short wide piles/cans/suction-buckets	free scour	not really suitable for these conditions	free scour	free scour
Wide gravity-based caisson-type structure	scour protection (limited)	scour protection (wider area)	free scour; scour protection may be placed later	scour protection (limited)

**Table 7.1.1** Types of scour and necessity of scour protections



Another distinction can be made between clear water scour and mobile-bed scour. The former is related to conditions with no upstream sediment transport ( $U < U_{cr}$  with  $U$ =depth-averaged velocity); the latter is related to conditions with sediment transport ( $U > U_{cr}$ ).

Literature reviews on scour along piles in currents have been given by **Breusers et al. (1977)**, **Melville (1988)**, **Melville-Sutherland (1988)**, **Kothyari et al. (1992)**, **Melville (1997)**, **Lim (1997)**, **Melville and Coleman (2000)**, **Zanke et al. (2011)**.

## 7.2 Current-related scour near vertical pipes and piles

The scouring process around vertical piles (bridge piers) is dominated by the following effects:

- local disturbance of the flow field (local scour);
- local reduction of cross-section (contraction of the flow due to the presence of the structure; contraction scour);  $h_1 = b_o h_o / b_1$  with  $h_1$ = mean depth of cross-section in contraction zone,  $b_1$ =effective flow width of cross-section in contraction zone,  $b_o$ = upstream flow width,  $h_o$ = upstream mean flow depth).

Other general scour effects which can be important are:

- general degradation effects (downstream of weirs, reservoir dams, etc);
- bend scour; deeper part of cross-section in outer bend area (variability in river planform); depth in bend may be 2 to 3 times larger than the mean depth of the cross-section;
- confluence scour; deeper parts of cross-section downstream of confluence;
- thalweg variations (deepest point of cross-section may shift in lateral direction);
- bed-form variations.

**Coleman and Melville (2001)** propose to determine the total scour depth near the foundation of a bridge pier on the basis of superposition of general scour and local scour at the foundation. They discuss the failure of bridges in New Zealand due to excessive scour at the piers. The Bulls Road bridge failure in 1973 during an annual flood event with a discharge of  $675 \text{ m}^3/\text{s}$  (not an extreme event; maximum recorded value is  $3800 \text{ m}^3/\text{s}$ ) can be attributed to a combination of general scour arising from gravel mining and local pier scour. The local scour was enhanced by: (i) the obliqueness of the flow to the pier, (ii) the flow constriction caused by the piling up of debris behind old timber piers immediately downstream of the bridge and (iii) the presence of fine sand substrata exposed during the scouring process and accelerating the scouring process. The maximum depth of scour measured below the armoured bed level adjacent to the collapsed pier was about 12 m.

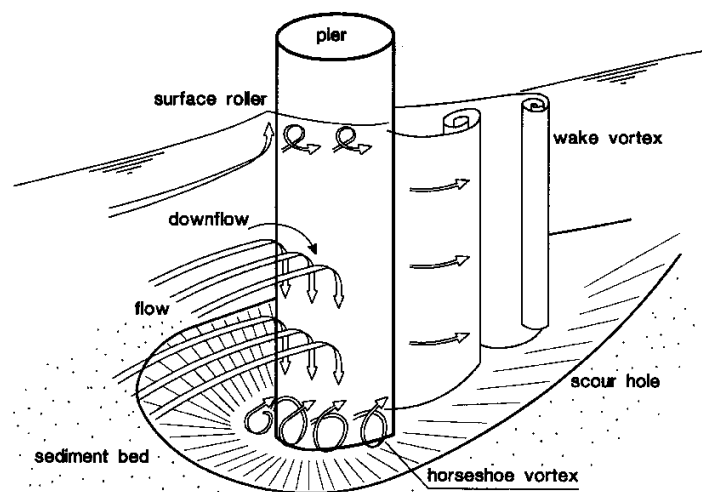


Figure 7.2.1 Flow pattern and scour near pipe (Melville, 1988)



The flow pattern around a cylindrical pipe is characterized by (see **Figure 7.2.1**):

- water surface roller in front of pipe;
- downflow in front of pipe;
- vortex-shedding in separation zone;
- wake flow downstream of pipe;
- generation of horseshoe-vortices in scourhole.

Based on analysis of field and flume data, **Breusers et al. (1977)** have found for a single pipe in uniform bed material:

$$d_{s,max}/D = \alpha_1 \alpha_2 \alpha_3 \alpha_4 \alpha_5 \alpha_6 \alpha_7 \quad (7.1)$$

with:

- $d_{s,max}$  = maximum scour depth below original bed,
- $D$  = width of pipe or pile cap (connecting several piles) normal to flow;  $D$ =diameter for circular pipe,
- $\alpha_1$  = coefficient related to  $U/U_{cr}$ ,
- $\alpha_2$  = coefficient related to  $h/D$ ,
- $\alpha_3$  = coefficient related to shape of pipe,
- $\alpha_4$  = coefficient related to angle of attacking flow,
- $U$  = depth-averaged flow velocity upstream of pipe,
- $U_{cr}$  = critical depth-averaged flow velocity (upstream),
- $U_w$  = near-bed orbital velocity,
- $h$  = flow depth (upstream),
- $\alpha_1 = 0$  for  $U/U_{cr} < 0.5$  (no upstream transport),
- $\alpha_1 = 2(U/U_{cr} - 0.5)$  for  $U/U_{cr} = 0.5$  to  $1.0$  (no upstream transport),
- $\alpha_1 = 1$  for  $U/U_{cr} \geq 1$ ,
- $\alpha_2 = 2 \tanh(h/D)$  yielding  $\alpha_2 = 2$  for  $h/D \geq 3$ ,
- $\alpha_2 = 1.5$  for  $h/D < 1$ ,
- $\alpha_3 = 1$  for circular pipes,
- $\alpha_3 = 0.75$  for streamlined pipes,
- $\alpha_3 = 1.3$  for rectangular pipes,
- $\alpha_4 = 1$  for flow normal to pipe,
- $\alpha_4 = 1.3$  for flow under angle of  $15^\circ$  and length-width ratio of 4,
- $\alpha_4 = 2$  for flow under angle of  $15^\circ$  and length-width ratio of 8,
- $\alpha_5 = 1+r$  = turbulence effect ( $r$ = input value),
- $\alpha_6 = (1+U_w/U_{cr})^{0.25}$  = effect of short surface waves,
- $\alpha_7 =$  group effect (see Scour.xls)

For a circular monopile with  $h/D = 3$ , this yields:  $d_{s,max}=1 D$  for  $U/U_{cr}=1$  and  $d_{s,max}=2 D$  for  $U/U_{cr}=3$ .

Xiang et al. (2020) found smaller values ( $h/d \approx 3.3$ ):

circular monopile:  $d_{s,max}=0.6 D$  for  $U/U_{cr} \approx 1$  in unidirectional flow and  $d_{s,max}=0.4 D$  for  $U/U_{cr} \approx 1$  in tidal flow.

square monopile:  $d_{s,max}=0.65 D$  for  $U/U_{cr} \approx 1$  in unidirectional flow and  $d_{s,max}=0.5 D$  for  $U/U_{cr} \approx 1$  in tidal flow.

diamond monopile (corner pointing into flow):  $d_{s,max}=0.4 D$  for  $U/U_{cr} \approx 1$  in unidirectional flow and in tidal flow.

The scour depth is smaller for tidal flow due to smaller upstream slopes on both sides (Xiang et al. 2020).

**Figure 7.2.2** shows the scour pit around a vertical structure on the beach due to wind flow ( $U_{wind} \approx 2 U_{wind,critical}$ ).

The depth of the scour pit is about equal to the diameter of the structure. The downwind length of the scour pit is 2 times the diameter. Undermining of the footplate can also be observed.

Often the piers of a bridge are connected by a pile cap under water (just above bed level). In that case the width of the pile cap should be taken to estimate the  $D$ -parameter. During flood events with relatively large water depths and oblique approaching flow (worst case scenario), the maximum scour will be of the order of  $d_{s,max} =$



4 to 5 D. If a pile cap (say width of 1.5 m) is present, the maximum local scour close to the pile cap can easily go up to values of 5 to 7 m. The piling up of debris at the bridge during flood events should be explicitly taken into account!

When bed forms are present, an extra foundation depth equal to 0.5 times the maximum dune height to be expected, should be taken into account.

The length of the scour hole is about 1D (D = diameter of pipe) upstream of the pipe and about 3 to 5D downstream of the pipe. The width of the scour hole is about 2D on each side of the pipe.

The time scale of the scouring process (time at which  $d_{s,max} = D$ ) depends primarily on the approach velocity, the sediment size and the width of the pipe.

A group of pipes yields a larger scour depth (factor 1.5 to 2) when the pipes are spaced closely (spacing < 5 to 10D). As the spacings between the piles decrease, a point is reached at which a cluster of piles would act as a single pile with a greater effective diameter.

**Zanke et al. (2011)** have proposed:

$$d_{s,max}/D = \alpha_3 \alpha_4 \alpha_6 \alpha_7 2.5(1-U_{cr}/U_c) \quad (7.2)$$

with:

$d_{s,max}$  = maximum scour depth below original bed,

D = width of pipe or pile cap (connecting several piles) normal to flow; D=diameter for circular pipe,

$U_c$  = depth-averaged flow velocity upstream of pipe,  $U_{cr}$ =critical depth-averaged flow velocity (upstream),

$\alpha_3$  = coefficient related to shape of pipe (see scour.xls),

$\alpha_4$  = coefficient related to angle of attacking flow (see scour.xls),

$\alpha_6$  =  $(1+U_w/U_{cr})^{0.25}$  = surface wave effect,

$\alpha_7$  = group effect (see Scour.xls),

$U_w$  = near-bed peak orbital velocity.



**Figure 7.2.2** Scour around structure due to wind flow ( $U_{wind}$  at 1 m  $\cong$  10 m/s;  $U_{critical} \cong$  5 m/s;  $d_{50} \cong$  0.25 mm)  
 (upper: side view; Lower: front view)



### 7.3 Wave-related scour near vertical pipes and piles

The near-bed flow around the pile generates horseshoe vortices generated at the upstream side of the pile and at the lee-side of the pile. The horseshoe vortices are insignificant if the wave boundary layer is thin ( $KC < 10$ ). Based on experimental data for regular waves, **Sumer et al. (1992)** have found for small circular piles with diameter  $D$  (see also **Figure 7.3.1**):

$$\begin{aligned} d_{s,max}/D &= 0.01 && \text{for } KC < 5 \\ d_{s,max}/D &= 0.1 && \text{for } KC = 10 \\ d_{s,max}/D &= 0.5 && \text{for } KC = 20 \\ d_{s,max}/D &= 1.0 && \text{for } KC = 100 \\ d_{s,max}/D &= 1.3 && \text{for } KC = 1000 \end{aligned} \quad (7.3)$$

The length of the scour hole with respect to the pile axis roughly is:  $L/D = 5$  to  $10$ .

**Sumer et al. (1993)** have tested piles with a square cross-section placed at different angles to the incident waves. The results are given in **Figure 7.3.1**.

**Hotta and Mauri (1976)** studied scour depths of piles in the surf zone of Ajigaura beach, Japan. The maximum scour depth was found to be  $d_{s,max}/D = 1$  to  $1.5$  and the maximum scour length with respect to the pipe axis was  $L/D = 7$  to  $10$ .

**Sumer et al. (2001)** state that wave-scour results from **Figure 7.3.1** are also valid in shallow depth with non-breaking waves on a sloping profile ( $1$  to  $20$ ). A pile landward of the breakerline is strongly affected by the position of the breaker bar. Scour depth will be relatively large in the trough zone of the bar.

**Sumer and Fredsøe (2001)** studied the scour near large circular cylinders under regular waves. The water depth was about  $0.4$  m. The cylinder diameters were  $D = 0.54, 1.0$  and  $1.53$  m. Rigid-bed and movable-bed experiments were performed. Detailed velocity measurements were carried out to determine the local flow field around the cylinder. The movable-bed experiments ( $0.2$  mm sand) were done to determine the maximum scour depth. Based on the velocity measurements, it is concluded that wave stirring in combination with wave-induced streaming are responsible for the scouring process. When a large vertical cylinder is subjected to a progressive wave, a complicated wave field is generated consisting of the incident waves, reflected waves and diffracted waves. A near-bed 3D steady streaming occurs in the vicinity of the cylinder. The streaming is directed toward (in wave direction) the cylinder in the region in front of the cylinder; the streaming is outward and opposite (to the wave direction) in the region adjacent to the cylinder. The maximum streaming is about  $25\%$  of the peak orbital velocity (undisturbed) near the bed. The scour depth increases with increasing  $KC$ -number and increasing  $D/L_w$  value. The maximum scour depth is about  $0.05 D$  for a  $KC$ -number of about  $1$  and  $D/L_w$  of about  $0.15$  with  $L_w =$  wave length.

The scour depth formula for waves alone reads as:

$$d_{s,max} = 1.3 D [1 - \exp\{-0.03(KC - 6)\}] \quad (7.4)$$

with:

- $D$  = pile diameter,
- $KC$  =  $U_w T_p / D$ ,
- $U_w$  = peak value of near-bed orbital velocity,
- $T_p$  = peak wave period.

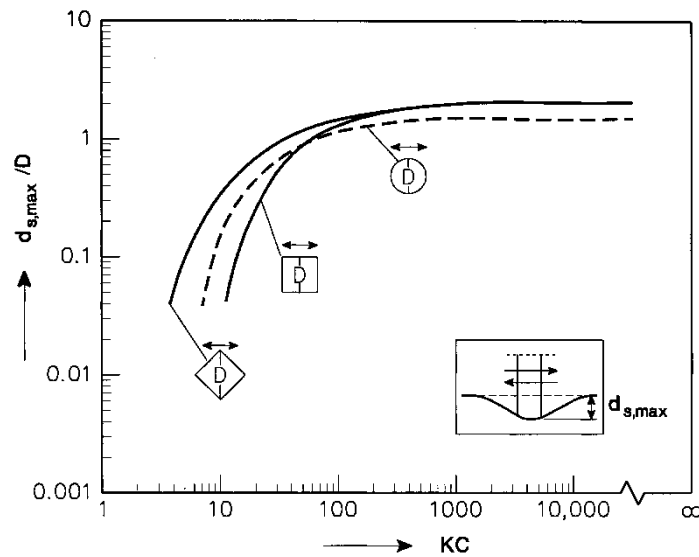


Figure 7.3.1 Wave-related scour near vertical piles (Sumer et al., 1993)

**Sumer and Fredsøe (1998)** studied the wave-induced scour around a group of vertical piles. Various configurations were tested. The water depth was 0.4 m above a sand bed (0.2 mm). The diameters of the single piles were  $D=32$  to 90 mm. Their conclusions are:

- the smaller the pile spacing, the larger the interference between the piles; the pile group behaves as a single body for very small spacings  $G/D < 0.1$ , with  $G$ = gap size between piles,  $D$ = pile diameter; the interference disappears for  $G/D > 1$  to 3, depending on pile arrangement;
- two-pile group: the scour depth increases by a factor of 3 for the side-by-side arrangement ( $G/D=0.4$  and  $KC=13$ ); the scour depth decreases by a factor of 2 for the in-line (tandem) arrangement ( $G/D=0.4$  and  $KC=13$ ); the angle of attack has a substantial effect on scour depth;
- three-pile group: the scour depth increases by about 30% for the side-by-side arrangement compared with the two-pile side-by-side arrangement; the scour depth for the in-line arrangement is the same as that for a two-pile group;
- four-pile square group; the scour depth decreases by a factor of 3 for  $KC=13$  compared with the scour around a single pile; the scour depth increases by a factor of 3 for  $KC=37$  compared with the scour around a single pile;
- given the pile spacing ( $G/D$ ), the scour depth is governed by the  $KC$ -number; the larger the  $KC$ -number, the larger the scour depth.

## 7.4 Wave and current-related scour near vertical pipes and piles

### 7.4.1 Near-field (local) scour

**De Bruyn (1988)** studied the scour process near a pipe in current and wave conditions. The bed material was sand with  $d_{50} = 0.2$  mm. The water depth (laboratory) was 0.3 m. The depth-averaged velocity upstream of the pipe was 0.4 m/s (mobile bed,  $U/U_{cr} > 1$ ). The maximum scour depth was found to be:

$$d_{s,max}/D = \alpha \quad (7.5)$$

with:

- $\alpha = 1.3$  for a current alone,
- $\alpha = 1$  for current and non-breaking waves,
- $\alpha = 1.9$  for current and breaking waves.



The length of the scour hole was 3D upstream and 5D downstream of the pipe for a current alone. For combined current and waves the scour length upstream was 4D and 6D downstream of the pipe.

**Eadie and Herbich (1986)** found  $\alpha=1.2$  for a current alone and  $\alpha= 1.4$  for irregular non-breaking waves plus current with  $H_s/h= 0.15$  and  $U_c= 0.15$  m/s over a fine sand bed.

**Rance (1980)** studied scour near large-diameter piles with  $D>0.1L_w$  ( $L_w$ =wave length) by waves and currents and found  $\alpha=0.04$  to 0.07 for circular and hexagonal piles and  $\alpha=0.13$  to 0.2 for square piles. The scour length was about 1D.

**Sumer and Fredsøe (2001)** studied the scour around a vertical pile in a sand bed (0.16 mm) with irregular non-breaking waves in combination with a current ( $U_c$ ). The water depth was 0.4 m. The depth-averaged current velocities ( $U_c$ ) were varied in the range between 0.1 and 0.5 m/s. The diameters of the single piles were  $D=30$  to 90 mm. They showed that the empirical expressions relating the scour depth to the KC-number in the case of regular-waves alone can also be used for the case of irregular waves alone, provided that the KC-number is computed as  $KC=U_w/(D f_p)$  with  $U_w=1.41\sigma_u$ = peak value of near-bed orbital velocity ,  $f_p$ =peak wave frequency ( $1/T_p$ ),  $\sigma_u$ =root-mean-square value of the near-bed orbital velocity. The maximum scour depth in conditions with a current alone was in the range between  $d_{s,max}/D= 1.2$  to 2. The observed maximum scour depths in relation to the KC-number and velocity ratio are given in **Table 7.4.1**.

The scour depth formula for waves plus currents reads as:

$$d_{s,max}= 1.3 D [1 - \exp\{-(0.03+0.75U_r^{2.6})(KC - 6 \exp(-4.7U_r))\}] \quad (7.6)$$

with:

D = pile diameter,

KC =  $U_w T_p/D$ ,

$U_w$  = peak value of near-bed orbital velocity (undisturbed),  $T_p$  = peak wave period.

$U_r$  =  $U_c/(U_c+U_w)$ ,  $U_c$  = upstream velocity (undisturbed).

KC-values	$U_c/(U_c+U_w)=0$ waves alone	$U_c/(U_c+U_w)=0.3$	$U_c/(U_c+U_w)=0.5$	$U_c/(U_c+U_w)=0.7$	$U_c/(U_c+U_w)=1.0$ current alone
KC=26	$d_{s,max}/D=0.8$	$d_{s,max}/D=1.3$	$d_{s,max}/D=1.5$	$d_{s,max}/D=1.6$	$d_{s,max}/D=1.2$ to 2.0
KC=8	$d_{s,max}/D=0.1$	$d_{s,max}/D=0.3$	$d_{s,max}/D=0.9$	$d_{s,max}/D=1.3$	$d_{s,max}/D=1.2$ to 2.0
KC=4	$d_{s,max}/D=0.06$	$d_{s,max}/D=0.1$	$d_{s,max}/D=0.6$	$d_{s,max}/D=1.0$	$d_{s,max}/D=1.2$ to 2.0

**Table 7.4.1** Scour depth in combined wave-current conditions

The data values show that for small KC-numbers a slight increase of the depth-averaged current velocity ( $U_c$ ) results in a significant increase of the scour depth. The scour depth approaches its steady-current value for a velocity ratio larger than about 0.7. The scour depth is practically independent of the angle between the wave and current direction; the scour depth was about the same for an angle of 0 and 90 degrees.

Usually, the bed near a pipe has to be protected by a layer of stones (rip-rap) on a filter layer or matt to prevent erosion of fine sediments through the protection layer of stones. The protection layer should be placed below the lowest bed level to prevent the creation of extra obstruction. The design velocity should be taken 2 times the average approach velocity to account for the local increase of the velocity near the pipe. Model tests are recommended for complicated situations.

**Deltares (2008)** has proposed:

$$d_{s,max}= 1.5 D [L_p/h_o]^{0.7} \tanh(h_o/D) [1-\exp\{-0.012KC - 0.57 KC^{1.8} U_r^4\}] \quad (7.7)$$

with:



- $U_r = U_c / (U_c + U_w)$ ,
- $U_c$  = upstream velocity (undisturbed).
- $h_o$  = water depth,
- $L_p$  = length of pile above bottom (if pile height is smaller than water depth  $L_p/h \leq 1$ ).

**Cefas (2006)** has studied the scour depth around the monopiles of an offshore wind farm within coastal waters, on Scroby Sands, off Great Yarmouth (east coast of England).

The site of Scroby Sands on the East Anglian coast is a particularly dynamic environment where significant quantities of material are frequently in suspension under fast tidal currents, and where numerous sand banks are in a state of continuous change.

The Scroby Sand wind farm (constructed in 2003-2004) consists of 30 monopiles of diameter 4.2 m driven up to 30 m into the seabed. The nearest monopile is located only 2.3 km from the shore. The minimum distance between monopiles is 320 m.

Three seabed landers (**Figure 7.4.2**) with a Seapoint OBS (optical backscatter sensor), an upward-looking ADCP and an acoustic current meter (ACM) near the seabed have been deployed to measure hydrodynamic data after construction of the monopiles in a transect normal to the coast (in depth of 20 m landward of Scroby Sands, in depth of 7 m at Scroby Sands and in depth of 19 m seaward of Scroby Sands). The deployment site on Scroby Sands was chosen in shallow depth of 7 m to measure conditions (exposed to NE storms) within the monopile array itself.

A grab survey was undertaken on the 24<sup>th</sup> April 2003 to collect surface samples of sediment. Most sediment samples have low proportions of very fine sands and are mainly comprised of medium sands in the range of 200 to 400  $\mu\text{m}$ . Various bathymetric and side scan sonar surveys were undertaken.

The deployment of the instruments after construction of the monopiles (2005) was timed to represent a winter season and coincided with a bathymetry survey.

The tidal elevation time-series shows a spring-neap signal (tidal range of about 2 m) typical of the southern North Sea and a surge event of approximately 0.7 m on 11th March 2005 (storm conditions).

The corresponding significant wave height data shows a series of wave events reaching a maximum  $H_s \cong 2.1$  m on a variety of occasions. Analysis shows that the wave height is modulated by the tidal elevation, decreasing at low tide and increasing at high tide during the period 23<sup>rd</sup> to 25<sup>th</sup> February 2005. This indicates that the waves were breaking over Scroby Bank.

The time series of current speed profiles from the upward looking ADP show the presence of tide and wind-driven currents up to 1.4 m/s during the spring-neap cycle.

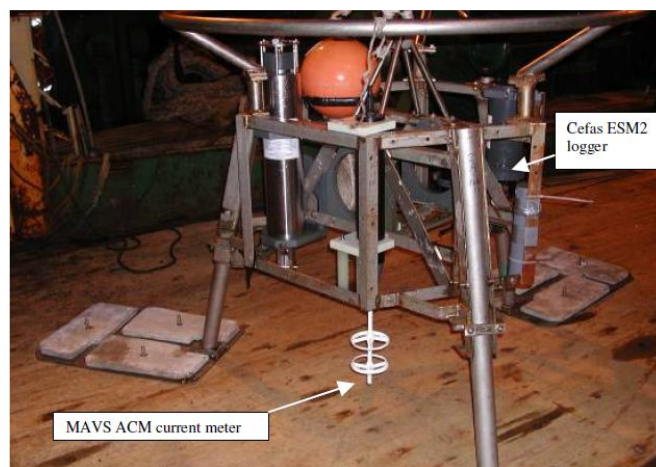


**Figure 7.4.1** Seabedlander with OBS (optical backscatter), upward-looking ADCP, acoustic current (ACM)

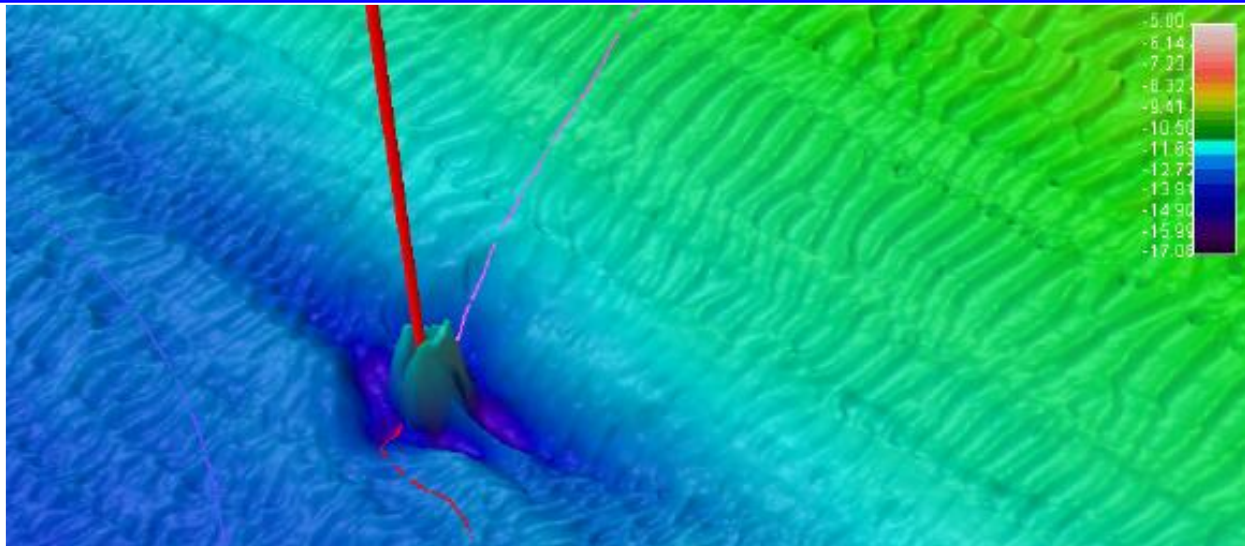


Figure 7.4.2 Top view of scour pit around monopile (red=pile=4.2 m; scour protection around pile; blue= scour pit); maximum scour depth= 5 m; horizontal scour distance= 60 m

The main features of the bathymetric surveys are (Figure 7.4.2):

- large ridge running north-south along the site; sandwave fields in the north-west corner of the site and megaripple fields across the site around and in between the monopiles.
- scour pits associated with monopiles (typical depths up to 5 m with a horizontal diameter of 60 m);
- scour wakes on the eastern monopiles extending from one monopile to the nearest downstream neighbour; scour wakes are orientated at approximately 30 degrees to the north-south tidal direction in line with the surge current direction;
- scour pans with a U-shaped profile in the north-westcorner within the sandwave field compared with the V-shaped scour pits in the remainder of the array;
- reduction in bed elevation along the inshore line of monopiles;
- secondary scour pits associated with the scour protection around the monopiles.

Whitehouse et al. (2010) have shown that the scour depth at a monopile depends on the water depth, see Figure 7.4.3.

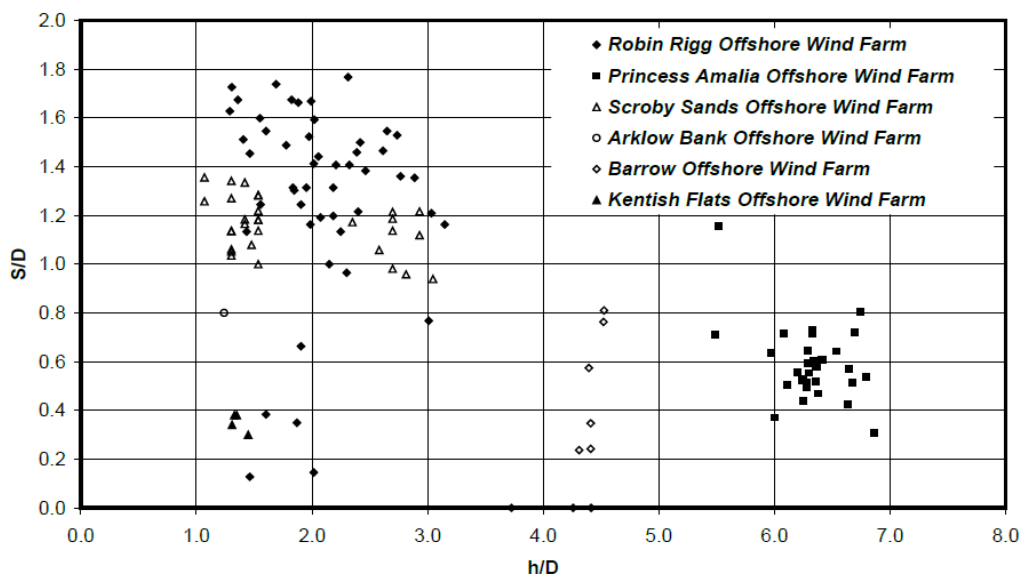


Figure 7.4.3 Scour near monopile as function of water depth (Whitehouse et al., 2010)



**Miles et al. (2017)** have studied the current and wave field around a monopile at a scale of 1 to 25 in a wave-current basin. The waves were normal to the current. Based on the measured data, it can be concluded that:

- the current-related wake region downstream of the pile has a length of  $5D$ ; the total length of disturbed velocities is about  $10D$ ; the maximum turbulent velocities do occur at a distance of  $2D$  downstream of the pile centre; the maximum standard deviation of the instantaneous velocities at that location is about  $\sigma_U = 0.7U_{c,o}$  with  $U_{c,o}$  = current velocity upstream of pile;
- the maximum velocity at both sides of the pile is about  $U_{c,local} = 1.35U_{c,o}$  at  $0.75D$  from the pile centre (normal to main current direction);
- the wave-related influence zone with disturbed orbital velocities is about  $3D$  on both sides of the pile (waves only); the maximum orbital velocity in the influence zone is about  $U_{w,local} = 1.85U_{w,o}$  with  $U_{w,o}$  = (undisturbed) near-bed orbital velocity outside influence zone.

**Nielsen (2011)** has studied the pickup of sediment particles from between the scour protection rocks/stones. Bathymetry survey results of the Horns Rev 1 wind farm located offshore of the Danish coast in 2005 showed that the scour protections adjacent to the monopiles had sunk by up to 1.5 m. The holes were filled by additional stones. The scouring of sediment from between the stones of the protection layer is caused by horseshoe-type vortices penetrating into the scour protection layer and mobilizing the sediment particles of the bed.

**Raaijmakers et al. (2013)** state that the scour protection can be omitted in conditions with weak currents, because the scour depth is relatively small ( $\cong 0.8 D$ , see **Table 7.4.1**) in conditions with weak currents plus waves. The pile diameter should be increased slightly as the effective windmill length above the seabed increases with maximum 5 m. The pile length beneath the seabed should be increased slightly (about 5 m) to obtain the same penetration length in the seabed. Increasing both the pile diameter and the pile length may be cheaper than the construction of a scour protection layer (costs: about 150.000 Euro per monopile).

**Garcia et al., 2025** have analyzed the scour depth around 460 monopiles at nine British wind farm sites situated in diverse marine regimes with current velocities from 0.54 to 1.77 m/s, significant wave heights from 1.5 to 2.7 m, water depths from 5 to 35 m, and grain sizes ranging from cohesive sediment (0.05 mm) to medium gravel (20 mm). The pile diameters are in the range of 4 to 7 m.

**Figure 7.4.4** shows the observed dimensionless maximum scour depth ( $S_{max}/D$ ) as function of the relative water depth ( $h/D$ ). It follows that:  $S_{max}/D \cong 1.5$  to 2 for  $h/D \cong 1$  to 3.

**Figure 7.4.5** the dimensionless maximum scour depth as function of the grain size. Most of the soil data are the range 100 to 500  $\mu\text{m}$ . The scour depth is maximum for grain size of about 150 to 300  $\mu\text{m}$ . It is clear that the scour depth decreases significantly for increasing grain size.

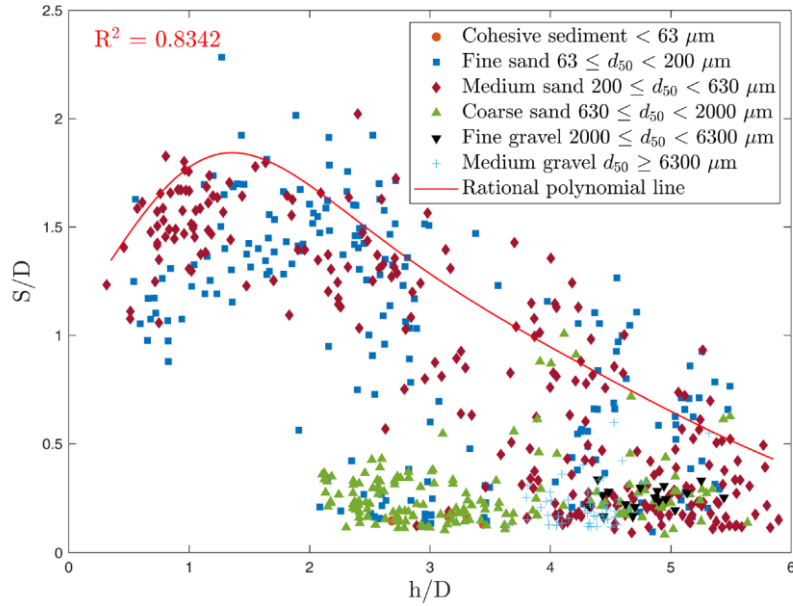


Figure 7.4.4 Relative scour depth ( $S/D$ ) as function of relative water depth ( $h/D$ )

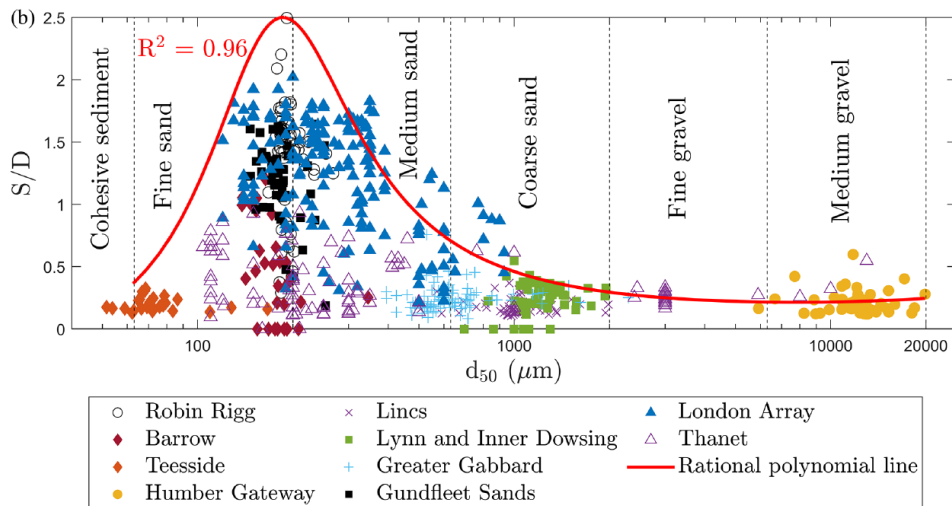


Figure 7.4.5 Relative scour depth ( $S/D$ ) as function of grain size

### Summary of field data

Table 7.4.2 shows the scour pit data around monopiles at various field sites. The maximum scour depths are in the range of  $d_{s,max}/D = 0.4$  to  $1.4$ .

Based on the data of Table 7.4.2, Van Rijn proposes for monopiles:

$$d_{s,max} = 0.8 D (D/h_o)^{0.2} (V_{par})^{0.5} \quad (7.8)$$

with:

- $D$  = pile diameter ( $D/h_o \leq 1$ ),  $h_o$  = water depth to mean sea level,
- $V_{par} = [(\alpha_s U_c)^2 + (0.7 U_w)^2]^{0.5} - U_{cr} / U_{cr}$  = dimensionless velocity parameter,
- $U_w$  = near-bed peak orbital velocity due to storm,
- $U_c$  = maximum flow velocity upstream due to tide+wind,
- $U_{cr}$  = critical velocity for initiation of motion,  
( $\cong 0.35$  m/s for  $100-300 \mu\text{m}$ ;  $0.4$  m/s for  $400 \mu\text{m}$  and  $0.5$  m/s for  $600 \mu\text{m}$ );
- $\alpha_s$  = velocity increase factor of streamline factor (1.1 to 1.2 for circular piles; 1.2 to 1.5 for rectangular piles).



Location	Sedi ment $d_{50}$  (mm)	Pile dia meter D  (m)	Water depths $h_o$  (m)	Tidal range  (m)	Peak tidal current  (m/s)	Sign. wave height and period (1x 50 yrs) (m and s)	Scour depth ( $d_{s,max}$ ) and length ( $L_{scour}$ ) in absence of scour protection (m)
Scroby Sands windpark, UK March 2004 (Whitehouse et al. 2008; Høgedal et al. 2005)	0.26	4.2	3-13	2	0.8-1.3	6; 8	scour depth= 5.9 m ( $d_{s,max}/D=1.4$ ) after 1 to 5 months
Q7 windpark 2005 at 20 km offshore Holland coast (Rudolph et al. 2008)	0.1- 0.3	4	20-25	2-3	0.6-0.8	7; 10	scour-depth= 1.5- 4.3 m ( $d_{s,max}/D=0.4$ - 1.1) after 3 months scour length= 20-30 m from pile
Barrow windpark North-East Irish Sea July 2005 (Whitehouse et al. 2008)	sand	4.75	12-18	4-6	$\cong 1$	3-5; 10	scour depth= 2.1 m ( $d_{s,max}/D=0.45$ ) after 9 weeks and 5.7 m ( $d_{s,max}/D=1.2$ ) after 1 year
Kentish Flats, UK (mouth of Thames) January 2005 (Whitehouse et al. 2008)	fine sand	5	4-5	4-5	$\cong 1$	3-4; 10	scour depth=2.3 m ( $d_{s,max}/D=0.45$ ) after 10 months
Arklow Bank, UK 2003; east coast ireland, south of Dublin (Whitehouse et al. 2008)	sand	5	4-5	3	$\cong 0.5$	3-4; 10	scour depth=2.3 m ( $d_{s,max}/D=0.8$ ) after 1 month due to tidal current
Field test tidal inlet Gulf of Mexico; NW Florida (Sheppard and Albada 1999)	sand 0.28	0.61 (square pile)	3.8	1	0.6-0.8	0	eq. scour depth=0.75 m after 160 hrs (80% after 100 hrs); ( $d_{s,max}/D=1.2$ )
Wind farm Luchterduinen, NL Raaijmakers et al., 2014)	0.2- 0.25	5 round	23	2.5	0.6-0.8	$H_{s,winter}= 2$ m; $T_p=10$ s $H_{s,summer}= 1.2$ m; $T_p=7$ s $H_{s,storm}= 5$ m; $T_p=15$ s; 10 storm events per year	Scour depth= 5 m ( $d_{s,max}/D=1$ ) after 12 months; 80% after 3 winter months Scour diameter=5 pile diameter (25 m); side slopes 1 to 2
Large scale flume test (Sheppard 2003)	sand 0.22	0.305	1.22	0	0.31	0	eq. scour depth=0.37 m ( $d_{s,max}/D=1.2$ ) after 130 hours (80% after 30 hrs)

Table 7.4.2 Scour pit data of monopiles at field sites



Example monopile:  $U_c = 1$  m/s;  $U_w = 0.15$  m/s ( $H_s = 1$  m;  $T_p = 7$  s);  $U_{cr} = 0.35$  m/s;  $\alpha_s = 1.2$ ;  $D = 5$  m;  $h_o = 20$  m (water depth); yields  $V_{par} = 2.45$  and or  $d_{s,max} = 4.7$  m;  $d_{s,max}/D \cong 0.95$ .

The time scale of erosion can be derived from the scour pit volume  $V_{scour}$  divided by the characteristic sand transport scale.

Using:  $V_{scour} \cong 0.5 d_{s,max} L_{scour} b_{scour} \cong 0.5 \times 1.5D \times 15D \times D \cong 10D^3$ ,  $q_{total}$  = total sand transport rate (in the range of 1 to 2 kg/m/s during conditions with storm waves and strong currents of 1-1.5 m/s),  $\rho_{bulk} = 1600$  kg/m<sup>3</sup> and  $\alpha$  = adjustment coefficient  $\cong 0.1$ , it follows that:

$$T_{scour,max} \cong 10\rho_{bulk}D^3 / (\alpha D q_{total}) \cong 10\rho_{bulk}D^2 / (\alpha q_{total}) \cong 100 \rho_{bulk}D^2 / q_{total}$$

The time evolution of scour follows from:  $d_s = d_{s,max} (t/T_{scour})^{0.4}$ ; see Equation (2.1).

If relatively strong currents over a sand bed (about 150 to 250  $\mu$ m) are present, the total depth-integrated sand transport rate is in the range of 1 to 2 kg/m/s and the maximum scour depth may be generated in about 30 days for a pile diameter of  $D = 5$  m.

Geotextiles and filter foundation layers are extremely important to prevent or reduce the effects of scour, which may endanger the entire protection layer.

#### 7.4.2 Far-field scour scour

**Petersen et al. (2015)** have studied the (edge) scour problem further away from monopiles. The bathymetry data around monopiles (see **Figure 7.4.6**) point to the generation of significant scour beyond the (protected) cover stone area. This is partly caused by the cover area itself, as the cover layer protrudes into the flow (due to the thickness of the cover layer of stones) resulting in a local increase of the velocities and bed-shear stresses, see **Figures 7.4.2; 7.4.6**.

Edge scour of the sea bed beyond the scour protection area may cause deformations and failure of the scour protection of monopiles. This can reduce the stability of the stone layer and cause exposure of cables.

The scour depth beyond the protected area is found (Petersen et al. 2015) to depend on the length of the protected area, as follows:

$$d_{s,max} = 0.6D \quad \text{for } L_{foundation,under} = L_{cover} = 3D \text{ and } \delta_{total}/L_{cover} = 0.05-0.1 \quad (7.9a)$$

$$d_{s,max} = 1.2D \quad \text{for } L_{foundation,under} = L_{cover} = 3D \text{ and } \delta_{total}/L_{cover} = 0.2-0.3 \quad (7.9b)$$

$$d_{s,max} = 0.1D \quad \text{for } L_{foundation,under} = 6D \quad (7.9c)$$

with:

$d_{s,max}$  = maximum scour depth in the direction of the main current,

$D$  = pile diameter,  $\delta_{total}$  = thickness of cover and foundation layer,

$L_{foundation,under}$  = length of foundation layer with respect to the pile centre (Figure 7.4.4).

$L_{cover}$  = length of cover armour layer with respect to the pile centre (Figure 7.4.4).

The scour depth is maximum (in the range of 0.6-1.2D) if the length of the foundation layer is equal to the length of the cover layer and depends on the current strength, the wave height, the local water depth and the thickness of the protection layer.

The scour depth can be substantially reduced by placing the protection layer in a trench around the monopile so that the top of the protection layer is flush with the surrounding seabed. This requires the dredging of a trench around the monopile.

The scour depth decreases for increasing length of the foundation layer.

The scour length in the direction of the main current is of the order of 5D.

The scour length normal to the main current direction is of the order of 3D.

The scour protection should be placed on a geotextile, otherwise the rocks/stones will partly sink into the bed ( $\cong 0.2-0.3D$ ) due to erosion of particles through the pores of the protection layer (Nielsen, 2011).

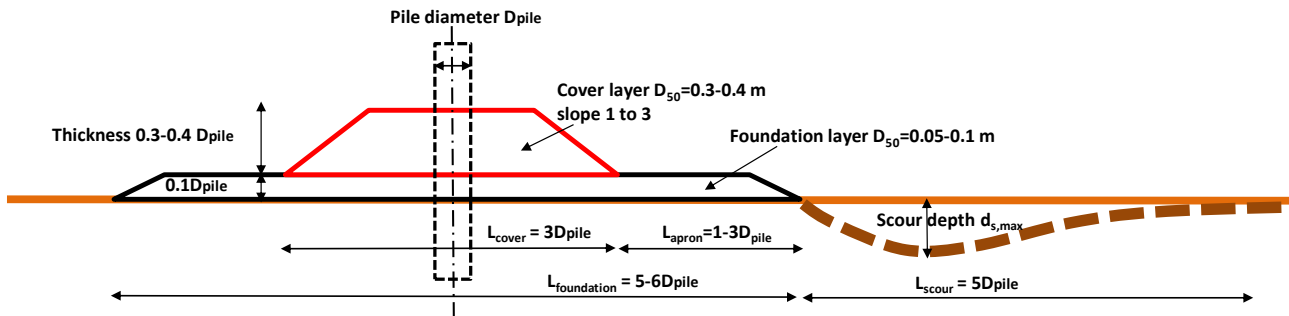


Figure 7.4.6 Edge scour pit near monopile

Figure 7.4.7 shows the edge scour around as monopile with scour protection (offshore wind farm Egmond aan Zee, The Netherlands; Deltares 2020) in conditions with peak tidal current velocities of about 0.7 to 0.8 m/s. The scour protection has a diameter of about  $5D_{pile}$ . The maximum edge scour depth below the seabed is about 1 m after 3 years to about 2 m after 7 years. The edge scour diameter is of the order of 4 to 5  $D_{pile}$ .

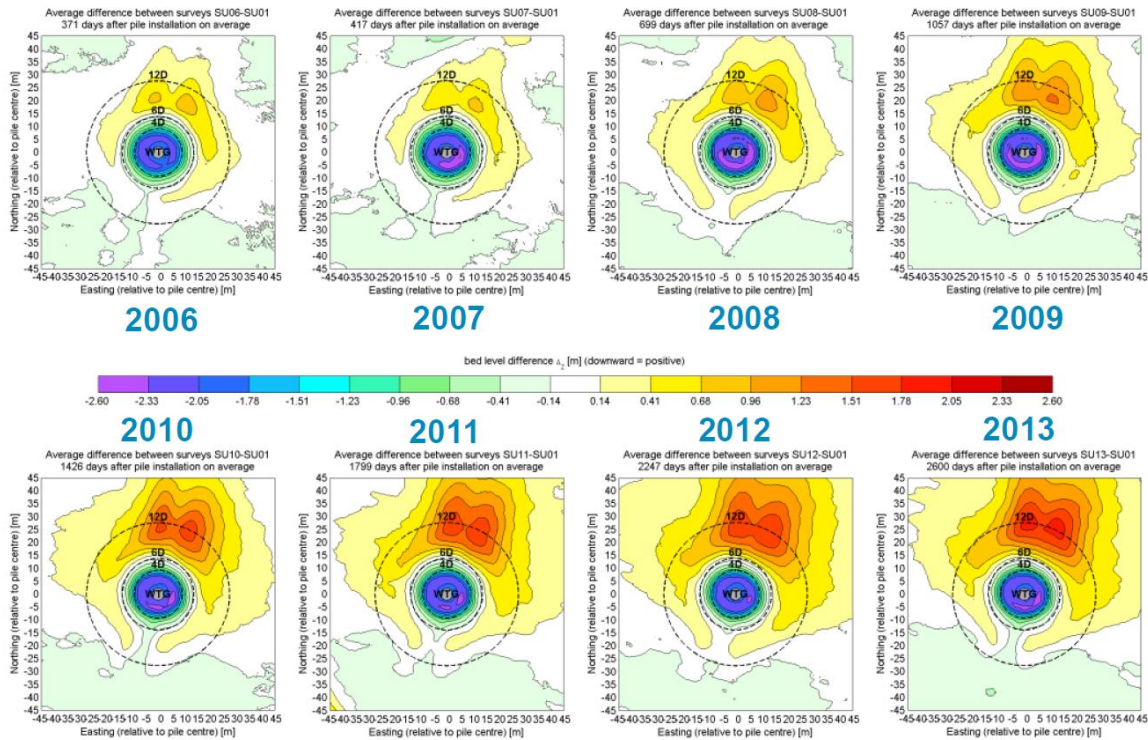


Figure 7.4.7 Edge scour over a time span of 7 years; monopile of offshore wind farm Egmond aan Zee, The Netherlands



## 7.5 SEDSCOUR-model

### 7.5.1 General

Pile-type foundation structures in offshore conditions with tidal currents and storm waves suffer from scour development around the structure, particularly when a proper scour protection is absent

Experimental data of free scour development around pile-type structures is abundantly available in the International Literature. Most early studies are related to the scour around bridge piers in rivers in conditions with clear-water scour and live-bed scour. Later on, the scour around monopiles in coastal seas was studied extensively related to the development of offshore wind turbine parks.

Based on the experimental results of scour depth around piles, various researchers have developed a range of empirical scour depth equations. As these types of empirical formulations have no general validity, each equation is only valid for a specific regime requiring a set of selection criteria to find the proper equation for a certain structure and hydro-dynamic conditions. Furthermore, the time scale to reach equilibrium scour depth is unknown.

Detailed 2DH/3D prediction models including the simulation of increased turbulence levels and sediment entrainment and transport are still in its infancy. Short term predictions for simple structure are possible, but long term predictions are not yet feasible.

Herein, a fairly simple 1D numerical model for sand transport and scour depth predictions near pile-type structures is explained and described. The model SED-SCOUR of LVRS-Consultancy can predict the time evolution of free scour depth around pile-type structures, as well as the edge scour further away from the pile in unidirectional and bidirectional tidal flows (weak and strong currents) in combination with waves over a sandy sediment bed with  $d_{50}$  in the range between 0.2 and 2 mm. Global scour under a jacket-type of foundation can also be simulated. The model is valid for cohesionless and for mud-sand mixtures with slight cohesive properties.

The model is most suitable for pile-type foundation structures with diameter smaller than the water depth and open jacket-type structures.

### 7.5.2 Scouring processes

Summarizing available information for pile scour in a fine sand bed (0.2 to 0.44 mm), the free scour pit around a monopile without scour protection consists of:

- near-field pit with maximum scour depths in the range of 1 to  $2D_{pile}$  over a horizontal distance (radius) within 3 to  $4 D_{pile}$ ;
- far-field scour pit with shallow scour depth of 0.3 to  $0.5 D_{pile}$  over a horizontal distance between 3 to  $30D_{pile}$ .

The side slopes in field situations are rather gentle (order of magnitude 1 to 10), which is very different from the steep side slopes often found in laboratory experiments (about 1 to 2 or 1 to 3).

When a scour protection around the monopile is placed, a shallow edge scour pit is generated with maximum scour depth of the order  $0.5$  to  $1 D_{pile}$  depending on the strength of the tidal current.

The scour depth can be substantially reduced by placing the protection layer in a trench around the monopile so that the top of the protection layer is flush with the surrounding seabed.



### 7.5.3 SEDSCOUR-model

#### Local scour around pile

The free scour hole/pit generated around a pile-type structure (without scour protection) is schematized into two separated scour pits on the upstream and downstream sides of the pile, as shown in **Figure 7.5.1**. The deepest scour pit is generated in the lee of the pile downstream of the highest peak tidal current velocity (assuming a slight velocity asymmetry;  $u_{\text{flood}} > u_{\text{ebb}}$ ). Both scour holes are similar in shape. Herein, it is assumed that the flood current is dominant with the highest peak current velocity.

Herein, only the deepest scour hole (with scour depth  $d_s$  and length  $L_s$ ) is considered (on the right in **Figure 7.5.1**). This scour pit consists of a deep scour pit near the pile ( $< 3$  to  $7D_{\text{pile}}$ ) and a shallow scour pit further away from the pile (3 to  $15 D_{\text{pile}}$ ).

Two tidal periods are used: flood period of about 6 hours with one flood-averaged and depth-averaged velocity  $u_{\text{flood}}$  (to right in **Figure 7.5.1**) and similarly an ebb period of about 6 hours with one ebb-averaged and depth-averaged velocity  $u_{\text{ebb}}$ . Thus, each tidal phase (flood/ebb) is represented by one representative velocity. The variation of the flow velocity over the tidal cycle is not represented. The neap-spring variation of the velocities is represented based on input values.

The scour hole erosion downstream of the pile over a tidal cycle of 12 hours is the net result of the following tide-averaged sand transport processes:

- flood: erosion of sand ( $E_{\text{flood}}$ ) from the bed in the lee of the pile due to flow accelerations and increased turbulence levels;
- flood: deposition of sand ( $D_{\text{flood}}$ ) from the incoming flood flow;
- ebb: deposition of sand ( $D_{\text{ebb}}$ ) from the incoming ebb flow (after reversal of the tidal current).

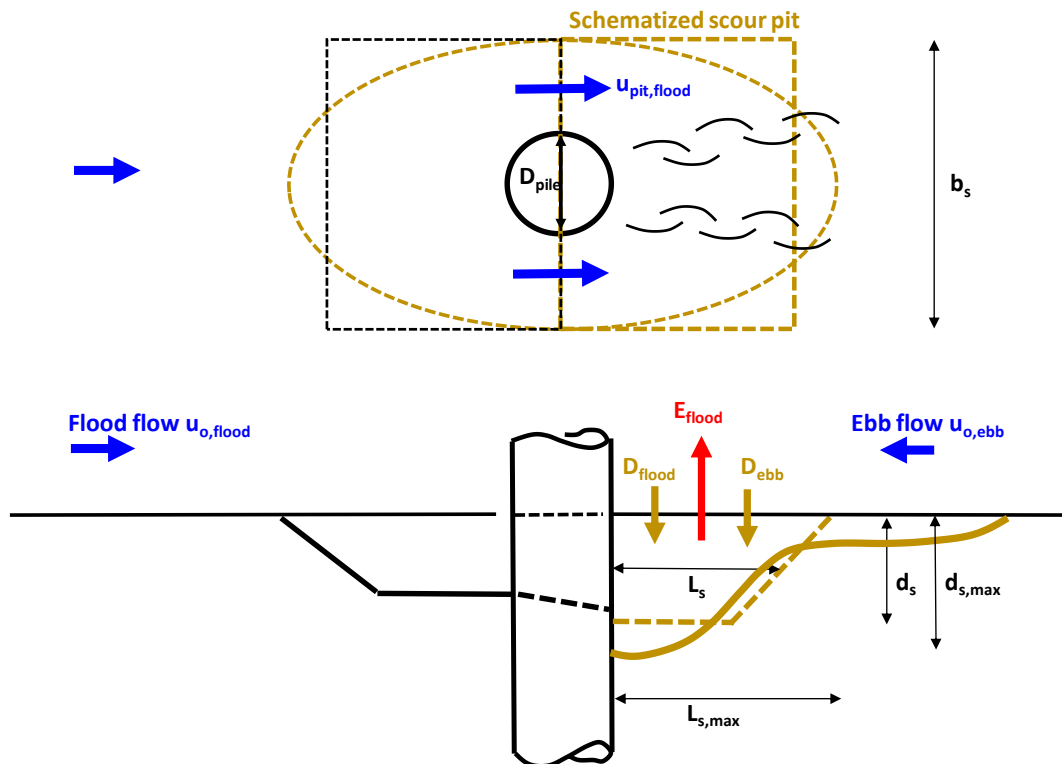


Figure 7.5.1 Plan view and cross-section of scour pit due to tidal flow



The deep part of scour pit is represented in the SEDSCOUR-model as a rectangular box with dimensions:  $d_s$ =mean scour depth,  $b_s$ =mean scour width and  $L_s$ =mean scour length. The shallow part of the scour pit is not represented by the SEDSCOUR-model

The mean scour depth is  $d_s$ ; the maximum scour depth is set to  $d_{s,max}=\alpha_s d_s$  with  $\alpha_s =1.3$  for laboratory cases (more triangular scour profile) and  $\alpha_s =1.2$  for field cases.

The scour width is assumed to be  $b_s=3D_{pile}$ . The scour width is  $b_s=1$  m (unit width) in the case of free scour downstream of a structure.

The mean scour length is assumed to be  $L_s=\alpha_L d_s$  with input value  $\alpha_L =3$  for laboratory scour pits and  $\alpha_L =7$  for field scour pits (see Section 2.2); the maximum scour length is  $L_{s,max}=L_s + 0.5 d_s/\tan\alpha$ . The scour is much longer in the case of scour downstream of a structure placed on the bed ( $L_s \cong 10$  to 100 obstacle height).

The scour volume is:  $V_s=d_s L_s b_s$ .

The scour volume over a complete tidal cycle (time step=12 hours) is:

$$V_s = \sum \Delta V_s = \sum (E_{flood} - D_{flood} - D_{ebb}) \Delta t / [(1-p)\rho_s]$$

The net volume change per time step is given by:  $\Delta V_s = (E_{flood} - D_{flood} - D_{ebb}) \Delta t / [(1-p)\rho_s]$

The scour depth at time t is given by:  $d_s = V_s / (b_s L_s)$

The erosion (E) and deposition (D) parameters during each time step of  $\Delta t=12$  hours are:

$$E_{flood} = b_s [(q_{b,flood,pit} - q_{b,flood,o}) + \alpha_E (q_{s,flood,pit} - q_{s,flood,o})];$$

$$D_{flood} = b_s (q_{b,flood,o} + \alpha_D q_{s,flood,o});$$

$$D_{ebb} = b_s (q_{b,ebb,o} + \alpha_D q_{s,ebb,o}).$$

with:

$q_{b,flood,o}$ =flood-averaged equilibrium bed load transport outside pit based on undisturbed velocity  $u_{flood,o}$ ;

$q_{s,flood,o}$ =flood-averaged equilibrium suspended load transport outside pit based on undisturbed  $u_{flood,o}$ ;

$q_{b,ebb,o}$ =ebb-averaged equilibrium bed load transport outside pit based on undisturbed velocity  $u_{ebb,o}$ ;

$q_{s,ebb,o}$ =ebb-averaged equilibrium suspended load transport outside pit based on undisturbed  $u_{ebb,o}$ ;

$q_{b,flood,p}$ =flood-averaged equilibrium bed load transport in scour pit area based on  $u_{flood,pit}$ ;

$q_{s,flood,p}$ =flood-averaged equilibrium suspended load transport in scour pit area on  $u_{flood,pit}$ ;

$\alpha_p$ = pickup coefficient of equilibrium suspended load transport ( $\alpha_E < 1$ ;  $\alpha_E = 1$  for bed load transport);

$\alpha_D$ = trapping coefficient of equilibrium suspended load transport ( $\alpha_D < 1$ ;  $\alpha_D = 1$  for bed load transport);

$\tan\alpha$ =downstream slope gradient of scour pit (1 to 7);

$\Delta t = \alpha_{tide} T_{tide}$ =effective time step;  $T_{tide}$ =duration of tidal cycle ( $\cong 12$  hours);  $\alpha_{tide}$ =efficiency coefficient (velocities around around slack tide are too small to cause substantial erosion;  $\alpha_{tide} \cong 0.4-0.6$ ).

It is noted that the that the pickup of sand particles in the scour pit is related to the excess sand transport rate which ensures that the pickup is zero for a plane bed without structure ( $\alpha_u = 1$  and  $r_o = 0$ ).

The equilibrium sand transport values are computed by the formulations proposed by Van Rijn (1984a,b,c; 1993; 2007a,b), which depend on the depth-averaged velocity, the depth-averaged critical velocity for initiation of motion, the water depth, wave height ( $H_s$ ), wave period ( $T_p$ ) and sediment parameters ( $d_{50}$ ).

The flood and ebb velocity outside ( $u_{flood,o}$  and  $u_{ebb,o}$ ) are input values.



The depth-averaged flow velocity inside the scour pit/hole during the flood period is computed as:

$$u_{\text{flood, pit}} = \alpha_u \alpha_r [h_{\text{flood,o}} / (h_{\text{flood,o}} + d_s)]^n u_{\text{flood,o}}$$

with:

$\alpha_u$  = velocity increase factor related to structure (range 1-1.3; input value);

$\alpha_r = 1 + r_o(1 - \alpha_s d_s / h_o)^{0.5}$  = turbulence factor related to structure;

$r_o$  = initial turbulence effect close to structure (input);  $r$  decreases weakly for increasing scour depth;

$n$  = exponent (range 0.5-1);  $\alpha_s$  = coefficient influencing turbulence factor (0 to 1; 0 = turbulence factor is constant).

The trapping coefficient is given by:

$$\alpha_D = 1 - \exp(-A L_{\text{eff}} d_s / h_{\text{pit}}^2)$$

with:

$A = \gamma_D [w_s / u_{*,\text{pit}}] [1 + 2w_s / u_{*,\text{pit}}]$  = coefficient,

$\gamma_D$  = calibration coefficient (input value 0.5 to 1.5; trapping  $\alpha_D = 0$  for  $\gamma_D = 1$ ; trapping  $\alpha_D$  is higher for higher  $\gamma_D$ );

$L_{\text{eff}}$  = effective settling length;  $L_{\text{eff}} = 0.5L_s + D_{\text{pile}}$  for flood and ebb flow,

$d_s$  = scour depth;

$h_{\text{pit}} = h_o + d_s +/\eta_{\text{max}}$  = water depth in pit during flood/ebb;  $\eta_{\text{max}}$  = tidal amplitude;

$u_{*,\text{pit}} = g^{0.5} u_{\text{pit}} / C$  = bed-shear velocity inside pit;

$C = 5.75 g^{0.5} \log(12h_{\text{pit}} / k_s)$  = Chézy-coefficient;

$k_s$  = bed roughness height;

$w_s$  = fall velocity of suspended sand

The pickup coefficient is given by:

$$\alpha_P = \alpha_{P,o} \exp[(-1/\gamma_P) w_s / u_{*,\text{pit}}]$$

with:

$\alpha_{P,o}$  = calibration coefficient (0.1 to 1);

$\gamma_P$  = calibration coefficient (input value range 0.5 to 1.5; pickup increases for higher value of  $\gamma_P$ ; pickup is constant and equal to for very high value of  $\gamma_P$ );

$w_s$  = fall velocity of suspended sand;

$u_{*,\text{pit}}$  = bed-shear velocity in pit.

In the case of a very long scour hole the pickup coefficient is approximately constant (range 0.5 to 1).

The sand transport capacity (equilibrium transport) on both sides and downstream of the structure in the flood period is much higher than the sand transport capacity upstream of the pile, which is caused by the velocity increase and extra turbulence generation in the lee zone of the pile (vortex shedding). The actual sand transport in the lee zone close to the pile is somewhat smaller than the local increased sand transport capacity due to the space lag effect (growing effect of suspended load by upward transport processes). This effect is represented by a pickup coefficient (<1), which depends on the fall velocity ( $w_s$ ) of the sand and the strength of the turbulence in the scour pit area ( $u_{*,\text{pit}}$ ). The pickup coefficient gradually decreases for increasing scour depth, because the pickup of sand is more difficult in a deep scour pit.

**Table 7.5.1** shows the input data of the SEDSCOUR-model.



Free scour/edge scour (1/2)		<b>1</b>	(integer)				
Pile diameter D <sub>pile</sub>		<b>5</b>	(m)				
Water depth outside h <sub>o</sub>		<b>23</b>	(m)				
Water depth near pile h <sub>p</sub>		<b>23</b>	(m)				
Tidal range		<b>2.5</b>	(m)				
Initial scour depth		<b>0</b>	(m)				
Innitial scour length		<b>0</b>	(m)				
Max depth-av. vel. mean tide outside		<b>0.7</b>	(m/s)				
Amplitude velocity neap-spring cycle		<b>0</b>	(m/s)			(=0 for constant velocity)	
Ratio max Flood and Ebb velocity		<b>0.9</b>	(-)			(<1 if flood velocity is higher; =1 if flood and ebb velocity are equal)	
Fluid density		<b>1020</b>	(kg/m <sup>3</sup> )				
Sand density		<b>2650</b>	(kg/m <sup>3</sup> )				
Kinematic viscosity		<b>0.000001</b>	(m <sup>2</sup> /s)				
sand diameter d <sub>50</sub>		<b>0.00022</b>	(m)		D*	<b>5.505509</b>	
sand diameter d <sub>90</sub>		<b>0.0005</b>	(m)				
Fall velocity sand w <sub>s</sub>		<b>0.02</b>	(m/s)				
Critical velocity sand U <sub>cr</sub>		<b>0.35</b>	(m/s)				
Bed roughness k <sub>s</sub>		<b>0.05</b>	(m)				
Porosity bed material p		<b>0.4</b>	(-)				
Percentage mud in bed		<b>5</b>	(%)				
Slope scour hole (ratio depth /length)		<b>0.15</b>	(-)				
Time step		<b>12</b>	(hrs)				
Alfa coefficient-velocity for velocity increase		<b>1.3</b>	(-)			(1.3 for free scour; 1.1 for edge scour)	
Turbulence factor R <sub>o</sub>		<b>0.3</b>	(-)			(0.2 for free scour; 0.1 for edge scour)	
Factor bed load transport upstream		<b>1</b>	(-)				
Factor suspended load transport		<b>1</b>	(-)				
Pickup coefficient sand transport upstream		<b>0.5</b>	(-)				
Trapping coefficient sand transport		<b>1</b>	(-)				
Alfa-coefficient pit length		<b>7</b>	(-)			(=3 for laboratory cases; 7 for field cases)	

**Table 7.5.1** Input data of SEDSCOUR-model for Local scour

### Edge scour and Global scour

The SEDSCOUR-model can also be used to compute the edge scour near a protected monopile and the global scour beneath an open tubular type of foundation structure (jacket-type structure).

In the case of a protected monopile, the scour processes develop at the edge of the scour protection and are similar to that of free scour, but the effects of velocity increase and extra turbulence production are much less (further away from the pile). A similar approach as for local scour can be used to compute the pickup and trapping of the sand particles.

In the case of a Jacket-type structure, the main (tidal) flow will go through the open structure with slightly increased velocities (say 10% to 15% depending on the blocking effect of the structure). The additional turbulence generated by the structure can be taken into account by a turbulence coefficient ( $r_o$ ).

A similar approach as for local scour can be used to compute the pickup and trapping of the sand particles. The mean scour depth ( $d_s$ ) follows from the net volume change per tide over the global scour area, which is defined as  $A_{global} = 1.5 b_{jacket} \times 1.5 L_{jacket}$ . The maximum scour depth ( $d_{s,max}$ ) is set to  $d_{s,max} = \alpha_s d_s$  with  $\alpha_s \cong 1.2$ .



### Free scour downstream of structures on seabed

The SEDSCOUR-model can also be used to compute the free scour downstream of a structure on the seabed such as a rock protection on a pipeline or a weir/sill on a river bed, see **Figure 7.5.2**.

The deep part of scour pit is represented in the SEDSCOUR-model as a rectangular box with dimensions:  $d_s$ =mean scour depth,  $b_s$ =mean scour width and  $L_s$ =mean scour length.

The mean scour depth is  $d_s$ ; the maximum scour depth is set to  $d_{s,max}=\alpha_s d_s$  with  $\alpha_s=1.5$  for field cases.

The tidal current is assumed to be perpendicular (normal) to the structure

The length of the structure in the direction normal to the tidal current is assumed to be very long so that the scour process is almost two-dimensional and can be represented as a process per unit width. Therefore, the scour width normal to the tidal current is set to  $b_s=1$  m (unit width).

The mean scour length in the direction of the tidal current is assumed to be  $L_s=\alpha_L h_s$  with  $h_s$ = upstream obstacle height;  $\alpha_L$ =input value in the range of 10 to 100. The scour is much longer in the case of scour downstream of a structure placed on the bed ( $L_s \approx 10$  to  $100 h_s$  with  $h_s$ =obstacle height).

The scour volume is:  $V_s=d_s L_s b_s$ .

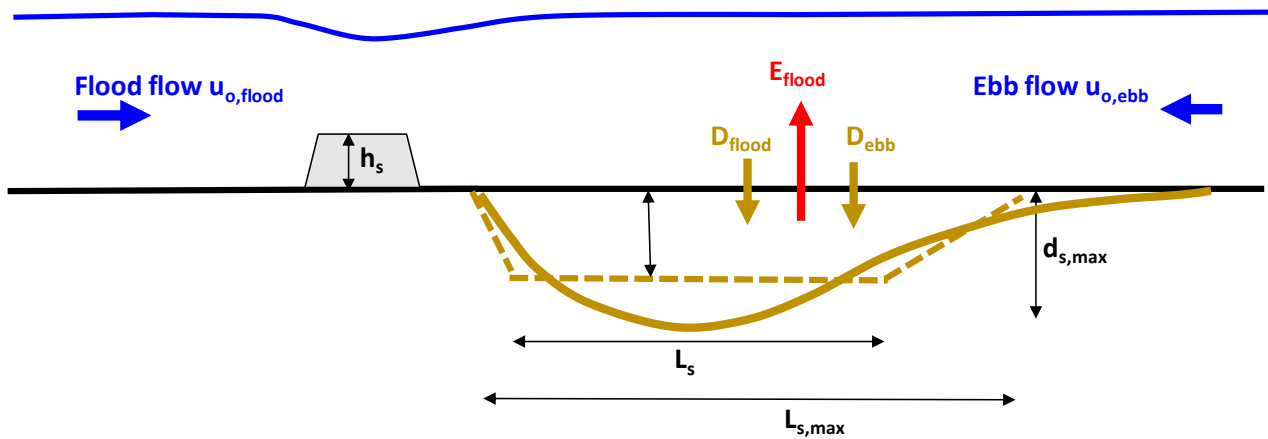


**Figure 7.5.2** Scour downstream of a hard structure on the sea bed

### Model calibration: Laboratory case

Sheppard and Miller (2006) measured the scour depth around a monopile in a laboratory flume with a sand bed ( $d_{50}=0.27$  mm, fall velocity= $0.03$  m/s;  $u_{cr}=0.27$  m/s, porosity= $0.4$ ; sediment density= $2650$  kg/m<sup>3</sup>). The water depth was about  $0.42$  m. The pile diameter was  $0.152$  m. The approach current velocity was varied in the range of  $0.17$  to  $1.64$  m/s, see **Table 7.5.2**.

The test with velocity of  $0.17$  m/s is a clear-water scour tests (no sediment load in upstream current); the other tests are live-bed scour tests with recirculation of the sediment load.

The basic data and model input coefficients are given in **Table 7.5.2**.

The velocity increase-coefficient is  $\alpha_u=1.4$  for all cases, the turbulence coefficient is in the range  $r_o=0.3$  to  $0.4$ .

The pickup and trapping coefficients are the same for all cases ( $\alpha_p=1$  and  $\alpha_D=0.5$ ).

The measured and computed dimensionless scour depths ( $d_{s,max}/D_{pile}$ ) are shown on the vertical axis of **Figure 7.5.3**. The horizontal axis refers to the ratio of the current velocity and critical velocity for initiation of motion ( $u/u_{cr}$ ). The computed values show rather good agreement (about 10% too small) with measured values for all live-bed scour test results, but the computed value is too high (20%) for the clear-water-scour test result. The time scale is 200 hours for the clear-water scour tests and less than 1 hour for most of the live-bed scour tests.

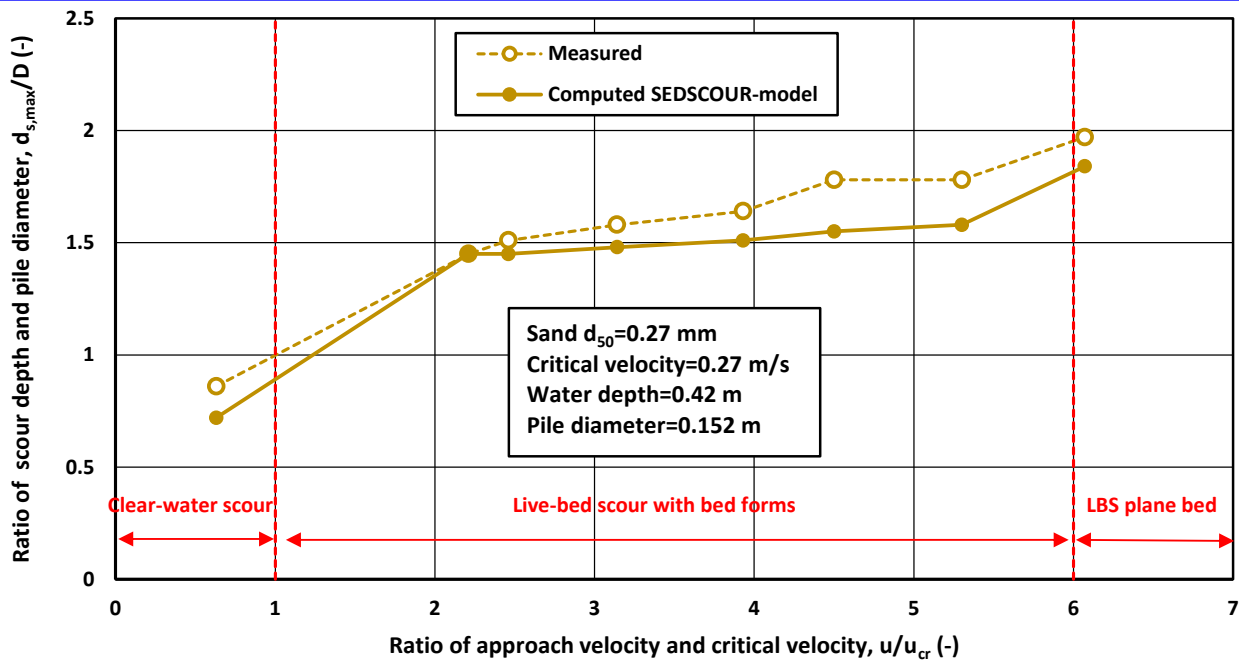


Figure 7.5.3 Scour depth as function of current velocity; test results of Sheppard and Miller (2006)

Test	Current (m/s)	Measured scour depth (m)	Computed scour depth (m)	Bed and suspended load coefficients	Bed roughness (m)	Turbulence coefficient $r_o$	Velocity increase coefficient $\alpha_u$	Pickup coefficient $\alpha_p$	Trapping coefficient $\alpha_D$	Scour length coefficient $\alpha_L$	Time scale (hours)
1	0.17	0.13	0.1	default	0.03	0.4	1.4	1	0.5	3	200
2	0.62	0.22	0.21	default	0.03	0.3	1.4	1	0.5	3	2
8	0.69	0.23	0.22	default	0.03	0.3	1.4	1	0.5	3	1
3	0.88	0.24	0.23	default	0.02	0.3	1.4	1	0.5	3	<1
4	1.10	0.25	0.255	default	0.01	0.3	1.4	1	0.5	3	<1
5A	1.26	0.27	0.26	default	0.005	0.3	1.4	1	0.5	3	<1
5B	1.43	0.27	0.275	default	0.003	0.3	1.4	1	0.5	3	<1
6	1.64	0.3	0.3	default	0.003	0.4	1.4	1	0.5	3	<1

Table 7.5.2 Measured and computed scour depth and model coefficients (water depth=0.42 m); test Sheppard-Miller (2006)

**Model calibration: Field case Free scour Monopiles Q7 wind park (NL)**

The offshore wind park Q7 Princess Amalia was built in 2006/2007 at about 20 km off the Dutch coast. The water depths are between 20 and 25 m. The bed consists of medium fine sand (0.2 to 0.3 mm). The monopiles (diameter of 4.0 m) were exposed to waves and currents for several months without scour protection. The tidal range is about 2 m. The main direction of the tidal current is SSW-NNE. The maximum tidal current during a spring tide is about 0.9 m/s (depth-averaged). The basic data are given by Rudolph et al. (2008).

The measured maximum scour depths of 29 monopiles (without scour protection for almost 1 year) were in the range 1.5 to 4.5 m ( $3 \pm 1.5$  m), see also Figure 7.5.4. The variation is most likely related to variations of the hydrodynamic conditions, which are not exactly the same among the piles.

The maximum scour depth occurred predominantly at the western side (10 of 29 data sets) and at the eastern side of the piles (10/29). The scour extent (radius of longest axis) was about 20 to 30 m.



The shape of the scour hole was oval with a length ratio of 1.8 between the main axis (averaged radius 27 m) and the short axis (average radius 15 m).

The side slopes in the Q7 field data were rather gentle (order of magnitude 1 to 10), which is very different from the steep side slopes often found in laboratory experiments (about 1 to 2 or 1 to 3).

Measured and computed scour depth are shown in **Figure 7.5.4**. The measured values are those of Pile 48. (Rudolph et al., 2008). The model input data are given in **Table 7.5.3**. The neap-spring tidal cycle is represented by a sinusoidal function with maximum (tide-averaged) velocity of 0.7 m/s during spring tide and 0.3 m/s during neap tide. The wave height is set to a value of 1 m (no storms).

The agreement between measured and computed scour depths is rather good.

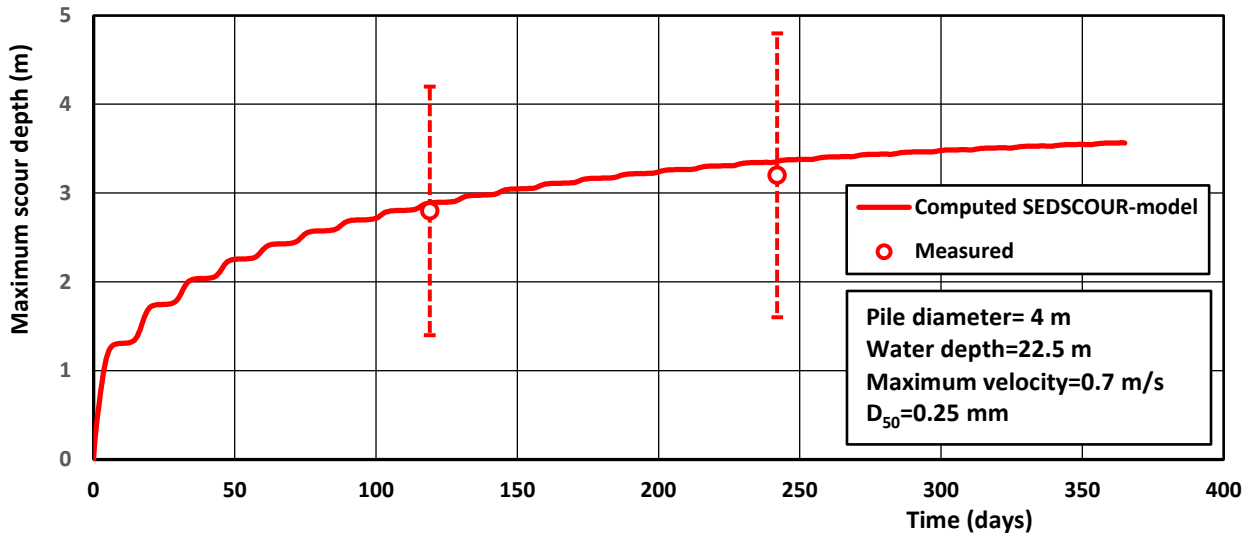


**Figure 7.5.4** Measured and computed free scour depth as function of time; Q7 windpark (NL)

Parameter	Q7 North Sea (NL)
Pile diameter (m)	4
Water depth to Mean Sea level (m)	22.5
Maximum tidal velocity Spring (m/s)	0.7
Maximum tidal velocity Neap (m/s)	0.3
Tidal range (m)	2
Significant wave height $H_s$ (m) and peak period $T_p$ (s)	1;7
Sand diameter $d_{50}$ (mm)	0.25
Percentage fines/mud < 63 $\mu\text{m}$ (%)	5
Fall velocity sand $w_s$ (m/s)	0.03
Critical velocity $u_{cr}$ (m/s)	0.4
Bed roughness $k_s$ (m)	0.03
Velocity increase coefficient $\alpha_u$ (-)	1.3
Turbulence coefficient $r_o$ (-)	0.3
Pickup coefficient $\alpha_P$ (-)	0.7
Trapping coefficient suspended sand transport $\alpha_D$ (-)	0.7
Pit length coefficient $\alpha_L$ (-)	10
calibration factor bed and suspended load $\gamma_b, \gamma_s$ (-)	1

**Table 7.5.3** Model input data of field calibration



## 8. Scour near horizontal pipes due waves and currents

### 8.1 Current-related scour

Scour near and under a pipeline is caused by changes of the local flow field due to the presence of the pipeline, see Fig. 8.1 and Fig. 8.2. Where there is a local increase in the transport capacity, erosion will take place. Sedimentation will take place where the transport capacity decreases. Usually, the velocity under the pipe will increase when there is a small local gap between the pipe and the sea bed. This will initiate and intensify the erosion process.

Experiments have shown that erosion will always take place if a pipeline is placed on an erodible seabed, and when there is transport of sediment upstream of the pipeline. The processes causing onset of scour will be briefly described hereafter.

The mechanisms can be divided into three groups:

- *flow induced pressure differences*  
In the case with flow perpendicular to the pipeline axis, there is a pressure difference between the upstream and the downstream part of the pipeline. This difference  $\Delta P$  is normally written as  $\Delta P = \rho C_p (U^2/2g)$  with  $U$  = the undisturbed near-bed velocity; the pressure coefficient is approximately  $C_p = 1$  in steady current and  $C_p = 3$  for waves; due to these pressure differences, ground water flow can take place and the sediment may be carried away.
- *vortices near the pipeline*  
Three types of vortices are observed near the pipeline, see Figure 8.1. The vortices can transport the sediment away; suspended as well as bed transport can occur. Vortex A and vortex C move the sand particles away from the pipe area, while vortex B moves the sand particles toward the pipe.
- *imperfections in the seabed near the pipeline*  
Variations/imperfections of the bed near the pipeline or of the pipeline itself may result in the presence of gaps between the pipeline and the bed and hence to flow under the pipeline.

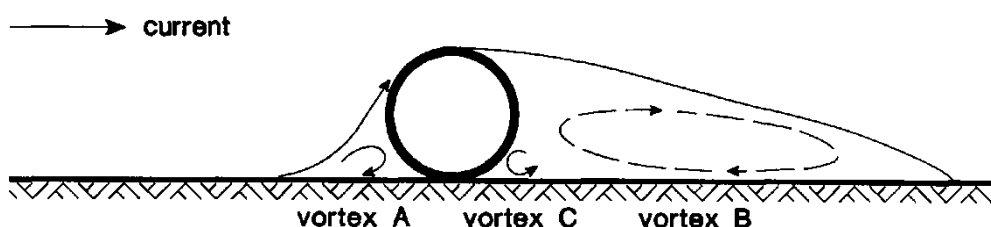


Figure 8.1 Vortices near the pipeline in unidirectional flow

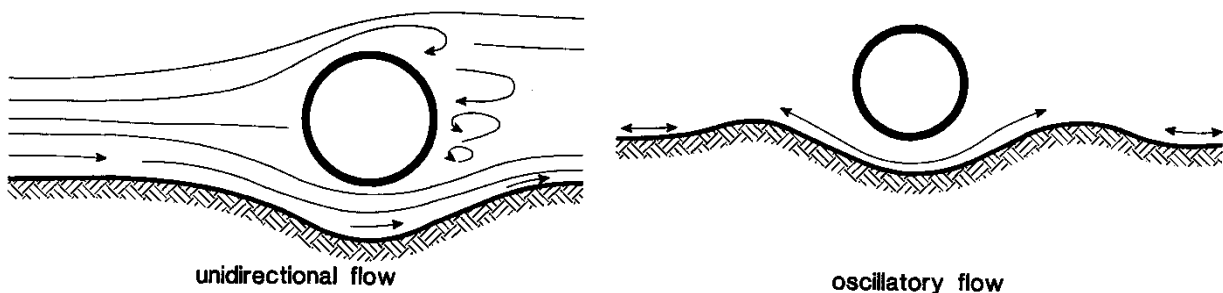


Figure 8.2 Scour in unidirectional and oscillatory flow



The development of scour in a current is governed by the velocity below the pipeline, the downstream wake and the vortex shedding downstream of the pipeline. From experimental results it appears that the near-bed velocity below the pipeline decreases with the depth of scour and increases with the width of scour.

If a pipeline is placed on a plane seabed in a current, a downstream wake will be developed. The length of this downstream wake is approximately six times the pipeline diameter.

If the pipeline is partly buried, the length of the downstream wake decreases. An analogy can be made with flow past a step.

In cases with a small gap below the pipeline (less than 0.3 times the diameter) no vortex shedding occurs.

If the current approaches the pipeline axis at a certain angle, the length of the downstream wake decreases. For flow angles below 30° no vortex shedding occurs.

**Kjeldsen et al. (1973)** performed flume experiments with pipelines resting on the bed. Based on dimensional analysis, they found ( $U$  = mean flow velocity,  $d_{s,max}$  = scour depth below bottom of pipe,  $D$  = diameter of the pipe,  $h$  = water depth,  $d_{50}$  = mean grain diameter,  $g$  = gravity) that the maximum scour depth can be expressed as:

$$d_{s,max} = 0.97 \alpha_w D^{0.8} (U_c^2/2g)^{0.2} \quad (8.1)$$

with:

$D$  = pipe diameter,

$U_c$  = upstream velocity (undisturbed),

$\alpha_w = (1+U_b/U_{cr})^{0.25}$  = surface wave effect (=1 if no waves),

$U_w$  = near-bed peak orbital velocity (undisturbed),

$U_{cr}$  = critical velocity for initiation of motion.

This formula should not be applied for conditions which do not represent the test conditions. For example, the formula can give erroneous results in the clear water case, i.e. where no sediment transportation takes place far from the pipeline.

All measurements of the scour development under a fixed pipeline in a current perpendicular to the pipe axis show that the maximum scour depth is obtained when the pipe is placed on the original seabed and the maximum scour depth (below the bottom of the pipe) is approximately one diameter.

Even, if there is no moving sediment upstream the pipeline (i.e. clear water case with small Shields parameters) scour may take place under the pipeline.

The bed-shear stress increases with the near-bed velocity. So even, if the far-field Shields parameter is less than the critical value of 0.05, the value near the pipe can be larger than 0.05, and erosion will take place.

The maximum scour depth will be highly dependent on the far-field Shields parameter. The maximum scour depth in the clear water case (no upstream sediment transport) is always observed to be smaller than that in case with active sediment transport.

The scour profile in unidirectional currents is characterized by a steep upstream slope and a more gentle downstream slope. In tidal flow the scour profile is symmetrical.

## 8.2 Wave-related scour near horizontal pipes

In flow with small Keulegan-Carpenter KC numbers, (KC is defined as  $KC = U_w T/D$  where  $U_w$  is the amplitude of the near-bed orbital velocity,  $T$  = wave period, and  $D$  = diameter of the pipeline), the downstream wake will not be fully developed. For low KC values ( $KC < 6$ ) no downstream wake will be developed and the flow field can be described by potential theory. This theory predicts relatively high velocities below the pipeline.

In comparison with the development of scour in stationary flow, different mechanisms are present in the wave-induced scour processes. The time scale for the scour development and the maximum scour depth can change significantly. For example, scour depths of two times the pipe diameter are observed in the case of waves alone, while scour depths are less than approximately one pipe diameter in the case of currents alone.



In unidirectional flow the scour hole is formed by the combined effect of upstream erosion due to increasing velocities under the pipeline and downstream erosion due to turbulent velocities in the wake zone behind the pipe. The downstream erosion zone is wider and has a more gentle slope than the upstream erosion zone.

In oscillatory flow the upstream and downstream effects are reversed every half cycle of the wave motion, yielding a larger erosion zone.

This explanation is valid when the wave motion is sufficiently long, so that lee-wake induced erosion can be effective in each half period of the wave motion. This will be the case for wave motion with a large Keulegan-Carpenter number ( $KC > 300$  with  $KC = U_w T / D$ , where  $U_w =$  maximum undisturbed near-bed orbital velocity).

**Sumer and Fredsøe (1990)** have given a simple empirical formula that expresses the maximum scour depth  $d_{s,max}$  under the pipe with diameter  $D$  for waves:

$$d_{s,max}/D = 0.1 \alpha_c (KC)^{0.5} \quad (8.2a)$$

with:  $KC = U_w T_p / D$ ,  $U_w =$  maximum undisturbed near-bed orbital velocity,  $T_p =$  wave period,  $\alpha_c = (1 + U_c / U_{cr})^{0.5} =$  current effect factor ( $\alpha_c = 1$  for  $U = 0$  m/s),  $U_c =$  current velocity,  $U_{cr} =$  critical velocity for initiation of motion.

The pipe is assumed to rest on the bed and to remain in that position (no vertical lowering of pipe). The stage at which the scour breaks out is the onset of the scouring process. The onset of scour is primarily caused by piping (groundwater flow). The scour depth was found to be sensitive for the presence of a gap (height  $e$ ) between the bottom of the pipe and the bed surface. This gap is often related to the presence or development of free spans. The  $e$ -parameter was varied. Scour did also occur for embedded pipes (negative  $e$ -values). The scour depth was maximum for  $e$  between  $e=0$  (pipe resting on bed) and  $e=-0.5 D$  (pipe buried over half its diameter). If the pipe is partly buried, the scour depth is given with respect to the bottom of the pipe. The scour depth decreases for increasing (positive) values of  $e/D$ , because the pipe is further away from the bed. The scour depth was found to be zero ( $d_{s,max}/D = 0$ ) for  $e/D = 1$  at  $KC < 10$ ; for  $e/D = 1-3$  at  $KC = 10-30$  and for  $e/D = 3-5$  at  $KC = 30-1000$ .

The roughness of the pipe was not found to have a significant effect on the scouring process.

The length of the scour hole (centerline to end of scour hole) can be estimated from (**Sumer and Fredsøe, 2002**):

$$L_{s,max}/D = 0.35 \alpha_c (KC)^{0.65} \quad (8.2b)$$

According to **Myrhaug and Rue (2003)**, the scour characteristics of horizontal piles in random waves should be based on  $H_{1/10}$  rather than on  $H_{rms}$  or  $H_{1/3}$ .

**Cevik and Yüksel (1999)** studied the scour under horizontal pipelines at a sloping bed (1 to 5 and 1 to 10). The pipeline was parallel to the shoreline. The scour depth on a sloping bottom is found to be about two to three times larger than that on a horizontal bottom for the same incident wave conditions.

**Sumer et al. (2001)** studied the onset of scour in steady currents and in regular waves and the self-burial of pipelines. The water depths were about 0.3 m. The bed consisted of sand with  $d_{50}$  of 0.18 mm and 1.25 mm. The pipe diameters were  $D=10$  and 5 cm. The onset of scour is defined as the stage when the bed is washed away underneath the pipe. This situation is basically related to the seepage flow in the sand beneath the pipeline, which is driven by pressure differences between the upstream (up wave) and downstream (downwave) sides of the pipeline.

Various modes of self-burial of the pipe may occur: (i) scour, sagging, backfilling and eventually self-burial of the pipeline between the span shoulders and (ii) sagging of the pipeline at the span shoulders due to general shear failure of the soil or failure of the soil supporting the pipeline due to liquefaction.

After the scour breaks out underneath the pipeline at certain locations, it will propagate along the length of the pipeline. A 3D-scour pattern will develop in which the scour holes are interrupted by stretches of soil (known as span shoulders, see Figure 8.3), where the pipeline obtains its support. As the process continues, the length



of the free span will be larger and larger at the expense of the span shoulder. More and more weight of the pipe will be exerted on the soil over a shorter and shorter length of the span shoulder. The soil will fail when the bearing capacity of the soil is exceeded (general shear failure or liquefaction). As the sand at the span shoulder fails progressively, the pipeline sinks into the sand and, at the same time, it sinks into the scour hole on both sides of the span shoulder. The scour process comes to an end when the pipeline reaches the bottom of the scour holes. At this moment the scour depth will be fairly close to that obtained for a fixed pipeline originally in contact with the bed. This scour depth is given by Eq. (8.2) for waves alone and by Eq. (8.1) for steady currents. Subsequently the space between the pipe and the scour hole is gradually backfilled with sand and the length of the span shoulder begins to increase due to backfilling process. When this process is completed, the pipeline is buried. The burial depth will be approximately equal to the scour depth.

A pipeline will be fully buried ( $e/D = -1$ ) for  $KC$  larger than about 100. The self-burial depth may reach values as large as  $e/D = -3$  for very large  $KC$ -numbers (say 1000), representing tidal flow. In the case of a steady current the self-burial depth will be about  $e/D = -0.7$ .

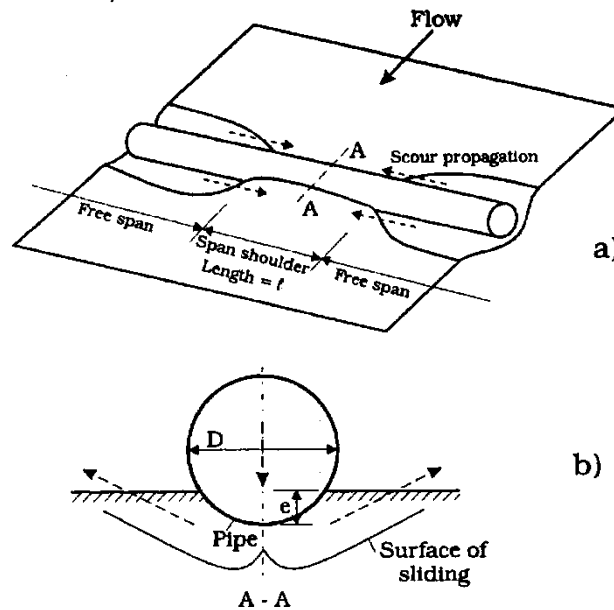


Figure 8.3 Pipeline resting on span shoulder (scour along pipeline creating free spans)

Kiziloz et al. 2013 have found for a pipe resting on the bed under irregular wave attack:

$$d_{s,max} = 0.05 \alpha_s \alpha_c D [H_s^3 L^2 / (h_o^3 D^2)]^{0.3} \quad (8.3)$$

with:

$D$  = pipe diameter,

$\alpha_s$  = streamline factor (shape effect),  $\alpha_c = (1 + U_c/U_{cr})^{0.5}$  = current effect factor,

$H_s$  = significant wave height,  $L$  = wave length,  $h_o$  = water depth,

$U_c$  = current velocity,  $U_{cr}$  = critical velocity for initiation of motion.

### 8.3 Wave and current-related scour near horizontal pipes

In combined wave and current motion it is advised to use the wave-related scour data, if the wave motion is dominant. The current-related scour data should be taken, if the current motion is dominant. The relative strength of both types of motions can be determined from the wave/current ratio  $\alpha = U_m/U_c$  where  $U_c$  is the current velocity at  $1/2$  to 1 pipe diameter above the bed and  $U_m$  is the amplitude of the near-bed oscillatory velocity.



## 9. Scour near wide gravity-based structures

### 9.1 Introduction

#### 9.1.1 Type of structure

Various types of foundation types of offshore wind turbines are used: monopiles, gravity-based structures and jacket/tripod structures (**Figure 9.1.1**). Offshore wind turbines in deeper water are mostly founded by jacket or tripod like structures. Jacket-type structures are open space tubular frames mounted on pile-type legs.

The monopile is the most applied foundation type in shallow waters with a sandy soil and often covered with migrating sand waves in European waters. Gravity-based structures are suitable for wind turbines in shallow water with sandy and rocky soils. The shape of the foundation structures may vary from very rectangular to conical and tapered shapes (**Figures 9.1.1, 9.1.2**).

The stability of gravity-based structures on sandy soils is easily threatened by deep scour holes/pits generated by currents and waves close to the structure. Due to the presence of the foundation structure, the flow around the structure is accelerated causing erosion of sediments (scour) near the foundation at the seabed. Deep and long scour holes/pits can develop. The depth of these scour holes depends on the current velocity, the wave height and length, the sediment size of the seabed and the structure dimensions. Often, it is necessary to install scour protection of rocks (rip rap) or protection mats. The structure may be placed in a dredged pit with depth of 2 to 3 m to reduce the scour depth. Steel skirts can be attached to the foundation structure to prevent undermining of the structure in conditions with strong flows.

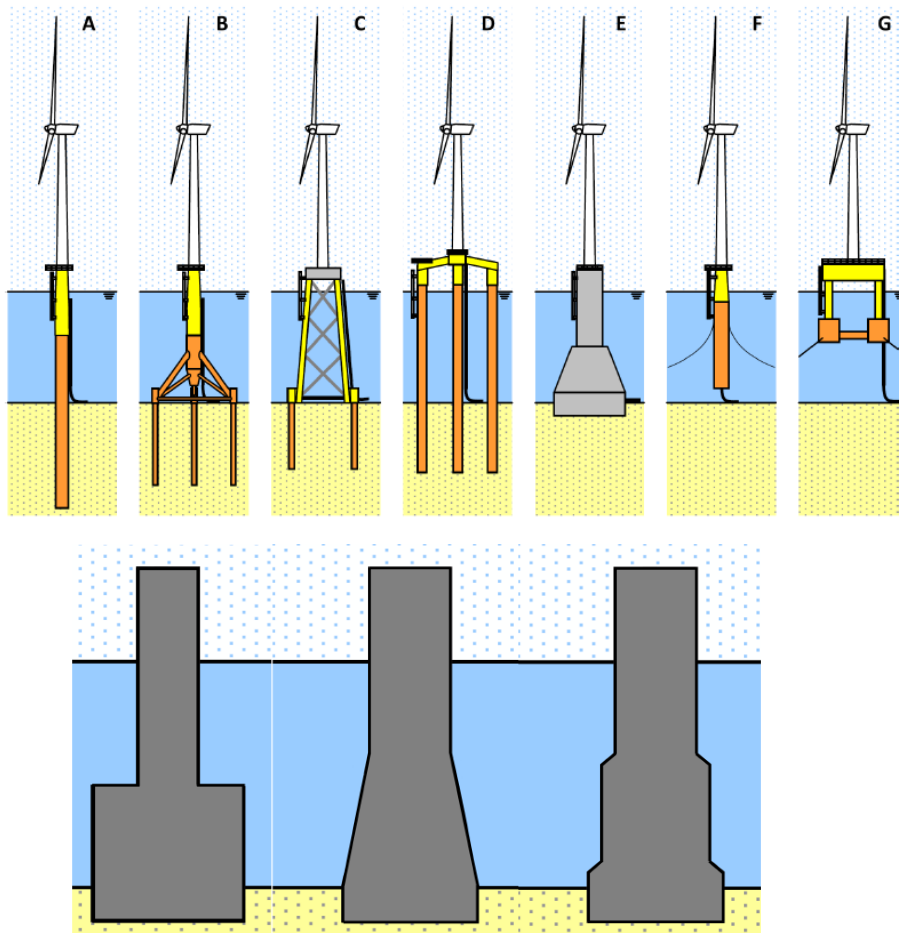


**Figure 9.1.1** Foundation structure of offshore windturbines (Van Eijk, 2016)

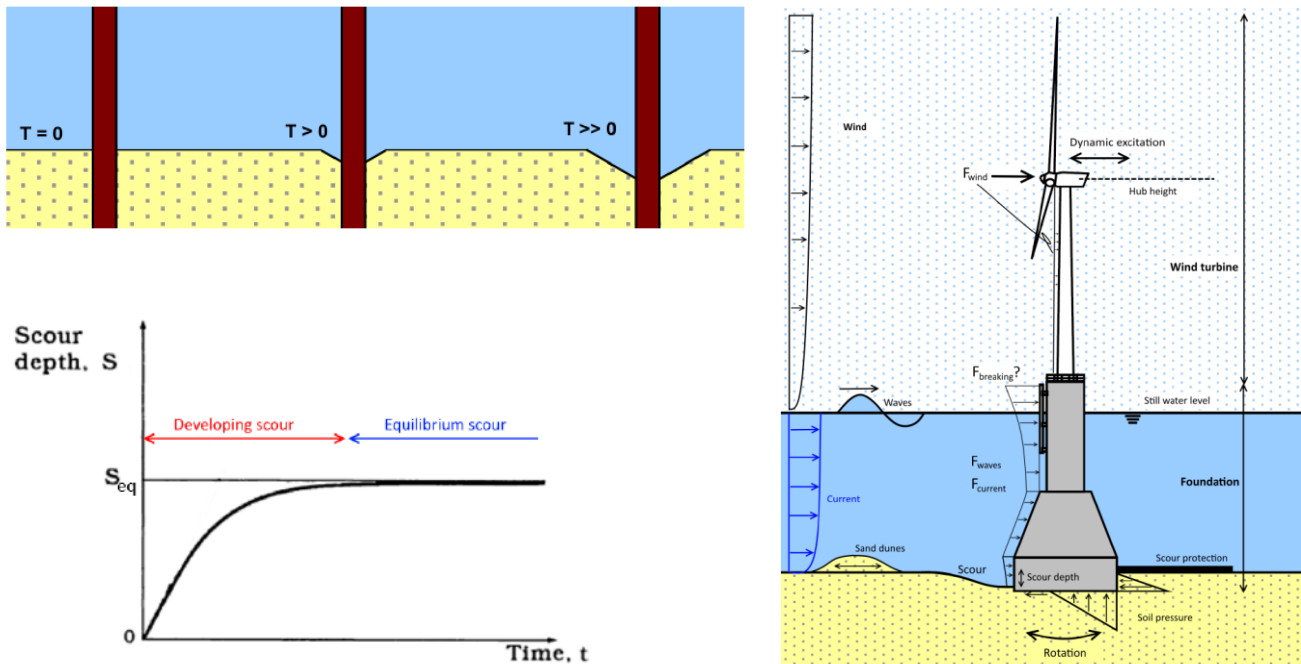


Figure 9.1.2 Local scour processes near gravity-based structure (Van Eijk, 2016)

### 9.1.2 Scour processes and definitions

Two types of scour can be distinguished :

- near-field or local scour around the structure and
- far-field scour (global scour) in the wake of the large-scale structures.

Scour is generally referred to as clear water scour if the ambient bed-shear stress is smaller than that for initiation of motion and to as live-bed scour otherwise.

Local scour is herein considered to be the lowering of the bed in the direct vicinity of a structure due to local accelerations and decelerations of the near-bed velocities and the associated turbulence (horseshoe and wake vortices) leading to an increase of the local bed-shear stress ( $\tau_{b,local} > \tau_{b,upstream}$ ) and hence the sand transport capacity. Once a scour hole/pit is formed, flow separation will take at the edge of the hole and a mixing layer will develop increasing the turbulence intensities and stimulating further scour of the bed (self-intensifying process). In the presence of waves, the generation of larger horseshoe vortices strongly depends on the length (stroke) of the orbital excursion and the length of the structure, which is expressed by the Keulegan-Carpenter number  $KC = U_w T / L_s$  with  $U_w =$  peak orbital velocity,  $T =$  wave period and  $L_s =$  length of structure normal to waves. Horseshoe vortices cannot really develop for  $KC < 5$  (small waves). Therefore, relative scour (scour depth /structure length) is less for larger structures. As the diameter  $D$  of round structures increases, the strength of the vortices weakens and for very large round structures the vortex motions have little effect on the scouring process. The relative scour depth for small diameter (slender) structures in water depth  $h$  with  $D/h < 0.3$  is about  $1D$ , whereas the scour depth for large diameter structures with  $D/h \cong 2$  is about  $0.35 D$  (Whitehouse et al., 2012). Using  $h=10$  m;  $D_{small}=5$  m and  $D_{large}=20$  m, the absolute scour depth is about 5 m for a small diameter structure and about  $0.35 \times 20 = 7$  m for a large diameter structure.

The scour develops in time to an equilibrium depth and length. Scour will gradually cease when (i) the local bed shear ( $\tau_b$ ) in the deepest part of the scour hole/pit is below the critical stress ( $\tau_{b,cr}$ ) for initiation of motion of sand particles or ii) when the supply of sand from upstream is equal to the local transport of sand ( $\tau_{b,local} \cong \tau_{b,upstream}$ ). An impression of the amplification ( $\alpha = (\tau_{b,local} / \tau_{b,upstream})$ ) of the bed-shear stress around a structure in comparison with the bed-shear stress in undisturbed conditions upstream of the structure can be obtained from



measurements and numerical modelling. Hjorth (1975) published amplification factor results for 8 experimental runs at small scale laboratory conditions with pile diameter of  $D = 0.05$  and  $0.075$  m, water depth of  $h = 0.1$  and  $0.2$  m; flow velocity of  $U = 0.15$  and  $0.30$  m/s. **Figure 9.1.3 right** shows measured amplification factors and computed factors based on numerical CDF-model for an experiment of Hjorth (1975) with  $U=0.3$  m/s,  $h=0.1$  m and  $D=0.05$  m. Measured amplification factors are rather high (up to 10) compared to those (up to 4) produced by the numerical model. The zone influenced by the structure extends to about  $0.5 D$  on both sides of the structure and about  $3D$  on the downstream side.

Scour is enhanced by wave stirring and wave reflection in the case of large-scale structures and by breaking/punging waves in shallow water. Excessive scour close to the structure may ultimately lead to instability/failure of the structure.

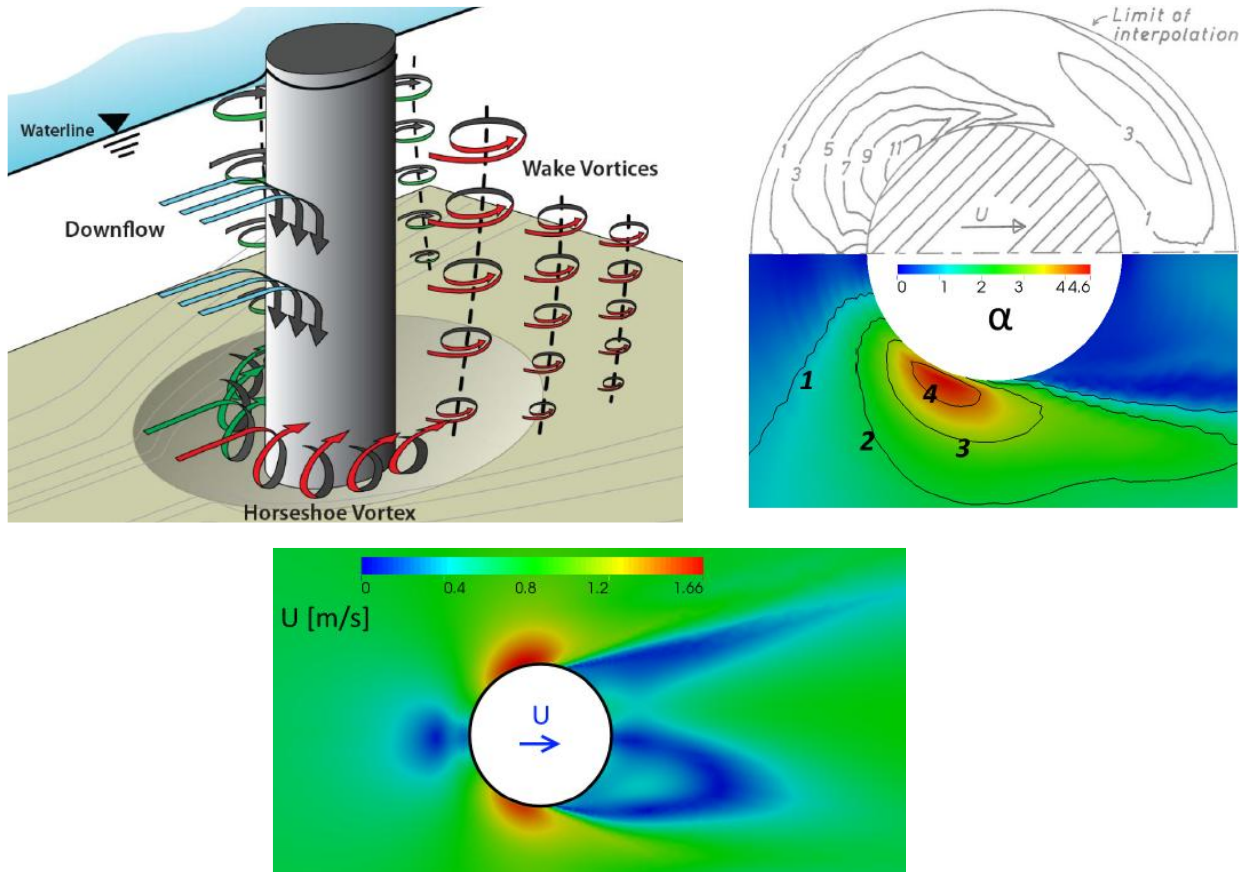


**Figure 9.1.3** Flow around a pile (Van Eijk, 2016)

- Left: vortices structure
- Right: Amplification of bed-shear stress
- Under: flow velocity around pile

A dramatic example of failure due to scouring processes is the sinking of submerged coastal structures on the sandy seabed ( $0.25$  mm sand) in the breaker zone at Santa Maria del Mar (SMM) Beach in Southwest Spain (Munoz-Peres et al. 2015) in mesotidal conditions (neap-spring range of  $1.20$  to  $3.80$  m). The structure consisted of precast modular concrete elements placed at a depth of about  $2.5$  m without scour protection. The sinking of the concrete modules in a near-shore sandy seafloor started immediately after placement and ended 3 weeks later when the modules reached the rocky subbottom. The total sinking was of the order of  $1.2$  to  $1.5$  m. Big scour pits with cross-shore length scales of  $15$  m were present on both sides of the structure.

The EXCEL-file **SCOUR.xls** can be used for determination of scour depth and length estimates (Van Rijn, 2006, 2012).



### 9.1.3 Estimate of global scour

A first order estimate of the global scour depth below or besides a wide massive structure can be derived from the blocking of the cross-sectional area. The flow through the blocked area is diverted around the structure. The region on both sides of the structure with increased velocities is of the order of half the structure width.

The global scour depth  $d_s$  for a caisson-type structure with height  $h_s$  and width  $b_s$  and an open jacket-type structure with height  $h_s$  and width  $b_s$ .

Caisson:  $d_s \times 2 \times 0.5b_s = \alpha_c \times b_s \times h_s$   
 $d_s = \alpha_c h_s$

Jacket:  $d_s \times 2b_s = \alpha_j \times b_s \times h_s$   
 $d_s = \alpha_j h_s$

with:  $\alpha_c$ =blocking coefficient for caisson-type structure ( $\cong 0.5-0.6$ );  $\alpha_j$ =blocking coefficient for jacket-type structure ( $\cong 0.1-0.2$ )

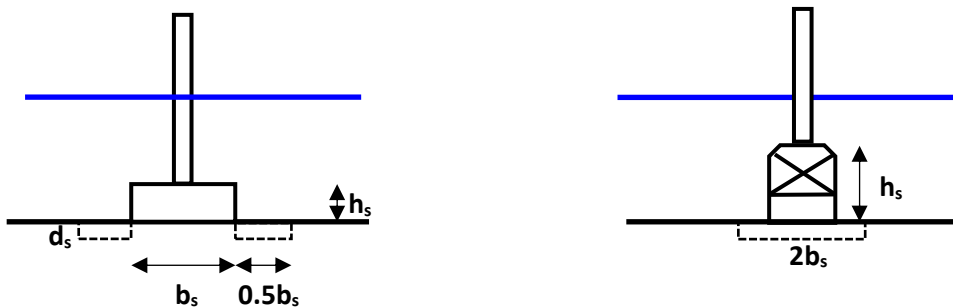


Figure 9.1.4 Global scour around caisson-type and jacket-type structures

## 9.2 Scour near wide structures

### 9.2.1 General

In offshore oil and gas engineering, wide sub-sea structures (GBS) such as subsea caissons, gravity anchors, manifolds, platform foundations etc. are commonly used as low vertical structures placed on the seabed. Often these structures are gravity-based structures resting on the seabed or in a small pre-dredged pit or trench. Wide structures can be subdivided in low (small-depth) or high (full-depth) structures. The plan shape of these massive structures may vary from circular to square and hexagonal with dimensions of the order of 10 to 100 m. Legs of jackup platforms with wide spudcans (diameters of 10 to 15 m; heights of 2 to 4 m) at the bottom end can also be seen as low structures placed on the seabed.

The construction of a wide gravity-based structure (platform) on the seabed may lead to considerable near-field and far-field scour (dishpan scour). Liquefaction can occur due to rocking of the base although this can be mitigated with skirts and drainage systems under the foundation.

The local scour depth mainly depends on the:

- shape and dimensions of the foundation structure creating flow accelerations and turbulence (horseshoe and wake vortices);
- structure mounted on top of the foundation structure creating downflow at the front side and additional turbulence (vortices) in the wake region;
- current and wave conditions and sediment characteristics.



Laboratory tests (Whitehouse et al. 2012) have shown that scour around a round caisson-type structure is not much affected if a much smaller pile is placed on top of the foundation structure. Much of the downflow in front of the pile is absorbed by the roof of the foundation structure not leading to additional scour. If the foundation structure has a conical transition section between the foundation structure and the upper structure (turbine tower unit), the scour may be more severe compared with a flat topped foundation, see **Figure 9.2.1**.

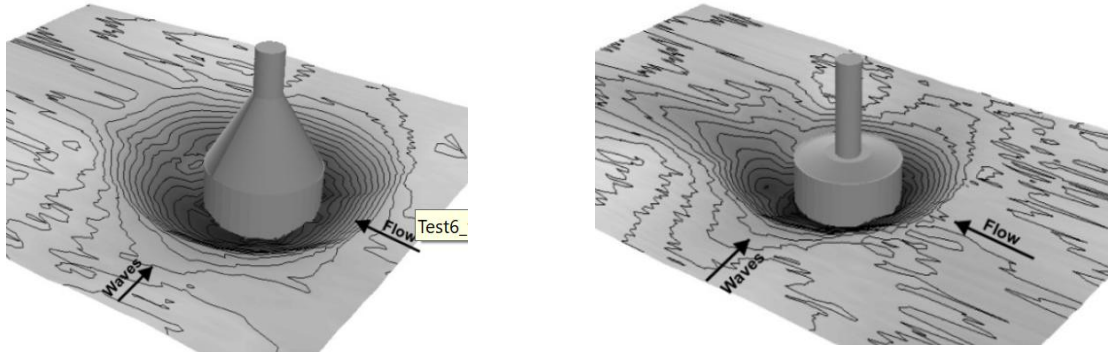


**Figure 9.2.1** Scour around foundation structures: conical (left); flat-topped (right); (Whitehouse et al. 2012)

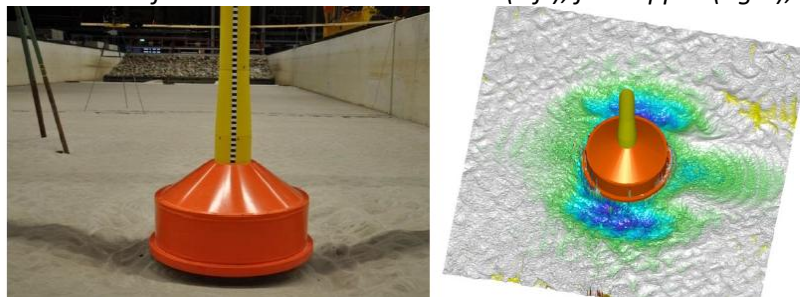


**Figure 9.2.2** Scour around foundation structure with conical transition (Deltares 2017)

Local scour can occur during placement operations (touchdown) and after placement.

Scour during placement operations can be reduced by selecting a placement window during slack tide and low wave activity or by preparing the bed with some material that prevents scour but does not impede penetration in case skirts are used.

Local scour after placement generally occurs near corner points or near individual legs (if present), but there may also be a general degradation of the bed over distances equal to several times the horizontal dimension of the structure. Square-type structures suffer the greatest scour, particularly at the corners where vortices are formed by currents and waves. Foundation structures are often equipped with skirts to prevent undermining of the structure (**Figure 9.2.2**). Scour can undermine the full depth of the skirt, particularly during storm events. Scour depth was found to be less (about 40%) for bidirectional (tidal) flow compared with unidirectional flow (May and Escarameia, 2002). A scour pit with two mild slopes is generated in biflow resulting in a more smooth flow pattern without flow separation and wake turbulence and thus less scour.

The scour extent along the flanks of the structure is of the order of 0.5 times the diameter of the structure, see **Figure 9.2.2**.

## 9.2.2 Scour near wide structures in shallow nearshore water

Emerged or submerged wall-type structures near the shore are structures oblique or parallel to the main current and wave direction. Scour near the tip of structure can be classified as *current-dominated* scour or *wave-dominated* scour. Scour is considerably enhanced, when tide-, wind- and wave-induced longshore currents with velocities exceeding 0.5 m/s are present. Wave-related scour near the shore generally is dominant in micro-tidal conditions. These scour processes are discussed in Sections 6.1 and 6.3.



### 9.2.3 Scour near wide structures in deep water

#### Laboratory, field data and empirical equations

Khalfin (1983) proposed a scour equation for full-depth structures based on based on 42 available experimental results. This equation was modified by Hoffmans and Verhey (1997), as follows:

$$d_{s,max}/b_s = 9 [(\alpha_s u_m / u_{m,cr} - 1)] [(h_s/b_s)^{1.43}] [(0.5\alpha_s u_m)^2 / (gh)]^n \quad (9.2.1)$$

$n = 0.83(h_s/b_s)^{0.34} = \text{exponent}$

with:  $b_s$  = width of structure normal to flow;  $u_m$  = depth-mean velocity;  $u_{m,cr}$  = critical depth-mean velocity;  $h_s$  = height of structure above sand bed;  $h$  = water depth;  $\alpha_s = 2$  for circular structures;  $\alpha_s = 2.3$  for rectangular structures.

Equation (9.2.1) is only valid for gravity-based structures with  $b_s/h > 1$ . It cannot be used for slender piles.

Pile example:  $h_s = h$  and  $h_s/b_s \approx 3$ ,  $h = 20$  m;  $u_m = 1$  m;  $u_{m,cr} = 0.4$  m/s leads to  $d_{s,max}/b_s \approx 0.3$  which is much too small for a slender pile,

#### Circular structures


Caisso-type foundation structures are most often circular structures in relatively deep water ( $b_s/h > 1$ ).

Whitehouse (2004) has done laboratory scale test with round foundations in currents and waves. The skirt length under each structure was 9.5 m. The basic data are given in **Table 9.2.1**. The prototype sediment is  $d_{50} = 0.34$  mm; the laboratory sand is  $d_{50} = 0.11$  mm. The geometric length scale is 1 to 40 and the corresponding velocity and time scale is 1 to 6.3. The structures were fixed in position to prevent settlement; a round skirt was attached to prevent undermining. The wave-alone and the current -alone conditions were capable of mobilising the bed sediment (live-bed conditions). The results are shown in **Figures 9.2.5** and **9.2.6**.

Whitehouse et al. (2012) have summarized scour data for two field cases with gravity-based structures (GBS), as follows:

Cover GBS:  $h = 30.5$  m;  $b_s = 10.8$  m;  $h_s = 3.55$  m;  $U_c \approx 0.9$  m/s;  $d_{50} \approx 0.2$  mm;  $d_{s,max} \approx 1.25$  m;

Small GBS:  $h = 100$  m;  $b_s = 6$  m;  $h_s = 0.6$  m;  $U_c \approx 1$  m/s;  $d_{50} \approx 0.2$  mm;  $d_{s,max} \approx 0.3$  m.

Type		Width/ Diameter (m)	Height above bed (m)	Water depth (m)	Current velocity (m/s)	Significant wave height (m) and peak period (s)	Maximum equilibrium scour depth (m)
Monopile		4.6	2	10	1.7	0	4.3 ( $d_{s,max}/b_s = 0.93$ ) (after 36 hrs)
Round; rectangular cross-section (Girder top; photo on right)		19	2	10	1.7	0	3.5 ( $d_{s,max}/b_s = 0.18$ ) (after 29 hrs)
Round; rectangular cross-section (Girder top)		19	2	10	1.5	3.9; 7.1	9.3 ( $d_{s,max}/b_s = 0.48$ ) (after 45 hrs)
Round; rectangular cross-section (Girder top)		19	2	10	0	3.9; 6.9	0.8 ( $d_{s,max}/b_s = 0.04$ ) (after 18 hrs)
Round; rectangular cross-section (concrete top; photo on left)		19	2	10	1.7	3.8; 6.9	7.5 ( $d_{s,max}/b_s = 0.39$ ) (after 38 hrs)
Round; conical cross-section (conical top; photo middle)		19	2+2=4 (halfway cone)	10	1.7	4.1; 6.9	8.5 ( $d_{s,max}/b_s = 0.45$ ) (after 28 hrs)

**Table 9.2.1** Test conditions of wide round foundations with atop monopile (Whitehouse 2004)



Similar laboratory work on various types of round foundation structures with different types of piles on top of the structure (see **Figure 9.2.3**) has been done by Simons et al. (2009) and Tavouktsoglu (2017).

Simons et al. (2009) studied scour around cylinder-type structures (diameter  $D$ ) with different heights ( $h_s$ ). The bottom of the cylinder was placed on the bed with a skirt for protection against undermining. The skirt length was varied in the range of  $0.5D$  to  $2D$ . The  $h_s/D$  ratio was in the range  $0.1$  to  $3.2$ . These results show that relative scour depth is less for small-depth foundation structures. The foundation structure was equipped with a skirt. The required minimum skirt length was found to be equal to  $1D$ . A test with a skirt length of  $0.5D$  showed severe undermining.

Tavouktsoglu (2017) studied scour around various types of round foundation structures with atop monopile. Water depths ( $h_o$ ) are in the range of  $0.35$  to  $0.55$  m. Depth-mean velocities is about  $0.25$  m/s. Sand with  $d_{50}$  of  $0.2$  mm and critical velocity of  $0.25$  m/s are used. The ratio of the depth-mean velocity and critical velocity upstream of the structure is about  $0.95$ , so close to initiation of motion. The base diameter is  $200$  mm and the stickup height (height of base plate just above bed,  $h_s$ ) is  $90$  mm. The sand bed is at the bottom of the stickup height.

The ratio of the equilibrium scour depth ( $d_{s,max}$ ) and the base diameter ( $D_{base}$ ) can be summarized by:

- monopile (uniform cylinder):  $d_{s,max}/D_{base} \cong 1.3-1.7$  for  $h_s/h_o=1$ ;  $h_s/D_{base}=1.75-2.75$
- cylindrical base:  $d_{s,max}/D_{base} \cong 0.3-0.65$  for  $h_s/h_o \cong 0.15-0.26$ ;  $h_s/D_{base}=0.45$
- conical  $45^\circ$  foundation:  $d_{s,max}/D_{base} \cong 0.4-0.7$  for  $h_s/h_o \cong 0.22-0.35$ ;  $h_s/D_{base}=0.62$
- conical  $75^\circ$  foundation:  $d_{s,max}/D_{base} \cong 0.5-0.8$  for  $h_s/h_o \cong 0.42-0.51$ ;  $h_s/D_{base}=1.15$

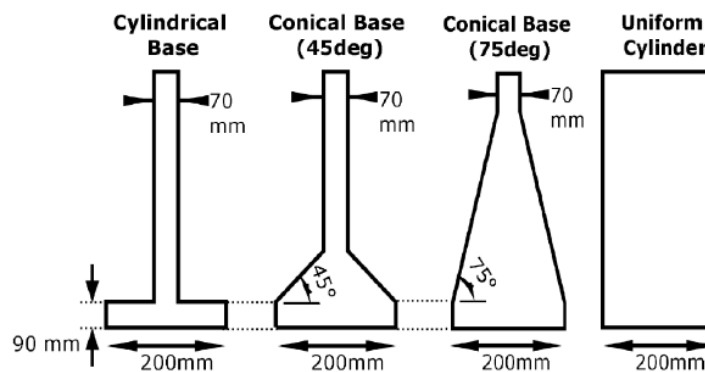


**Figure 9.2.3** Foundation structures mounted on cylinder of the same size in the bed; Tavouktsoglou (2017)

The structure height ( $h_s$ ) is herein defined at the distance between the sand bed and halfway the conical section resulting in  $h_s=90+65/2=123$  mm for conical  $45^\circ$  and  $h_s=90+280/2=230$  mm for conical  $75^\circ$ .

It can be clearly seen that the scour depth increases for increasing structure height ( $h_s/h_o$ ). Most important is the blockage area of the base foundation  $A_s = d_{base} h_s$ .

Scour along a circular caisson-type foundation structure (for a wind turbine) was studied in a scale model (1 to 35) at the university of Cantabria in Spain (2020). The data are published by Sarmiento et al. (2024). The dimensions of the gravity-based caisson are : caisson diameter=  $40$  m; caisson height=  $8.8$  m; water depth= $36$  m; depth-averaged maximum tidal velocity= $0.4$  to  $0.7$  m/s; significant wave height= $4$  to  $10$  m. peak wave period = $10$  to  $15$  s. ; prototype sand of  $0.45$  mm at bed (model sand= $0.15$  mm) ; prototype settling velocity of suspended sand  $w_s=0.04$  m/s, bed roughness  $k_s=0.03$  m.

Scour patterns are shown in **Figure 9.2.4** and **9.2.5**. The maximum scour depth along the flanks is of the order of  $3$  to  $5$  m ( $\cong 0.08-0.125 D_{base}$ ).

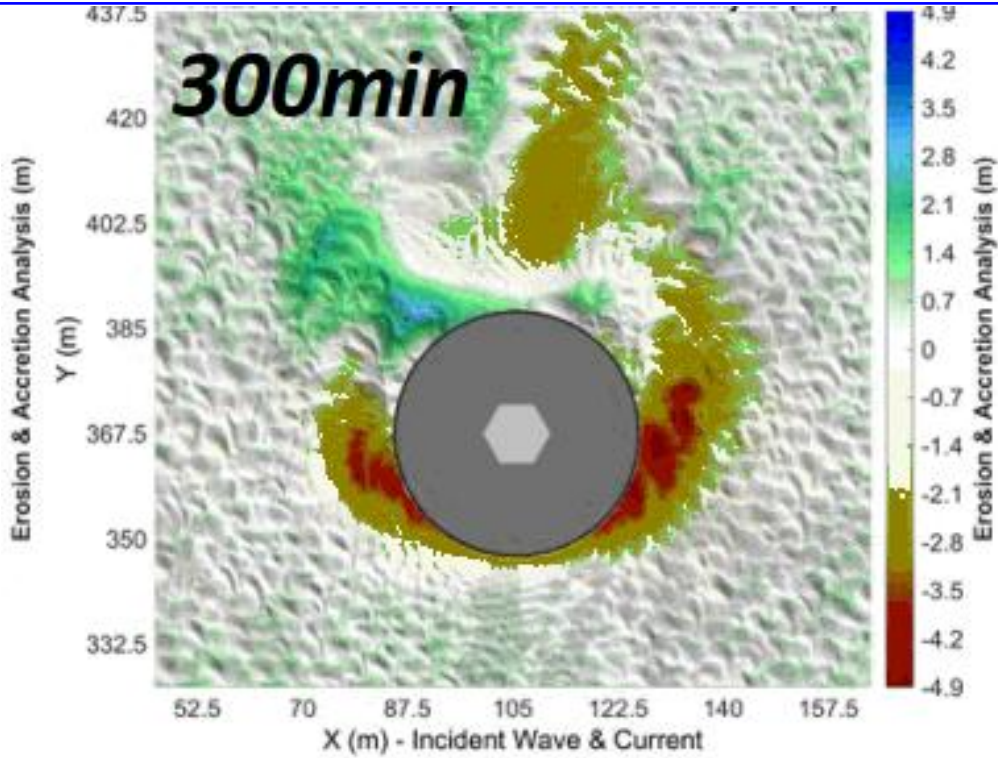


Figure 9.2.4 Scour depth around caisson-structure after 5 hours; prototype current velocity=0.4 m/s (model current=0.24 m/s)

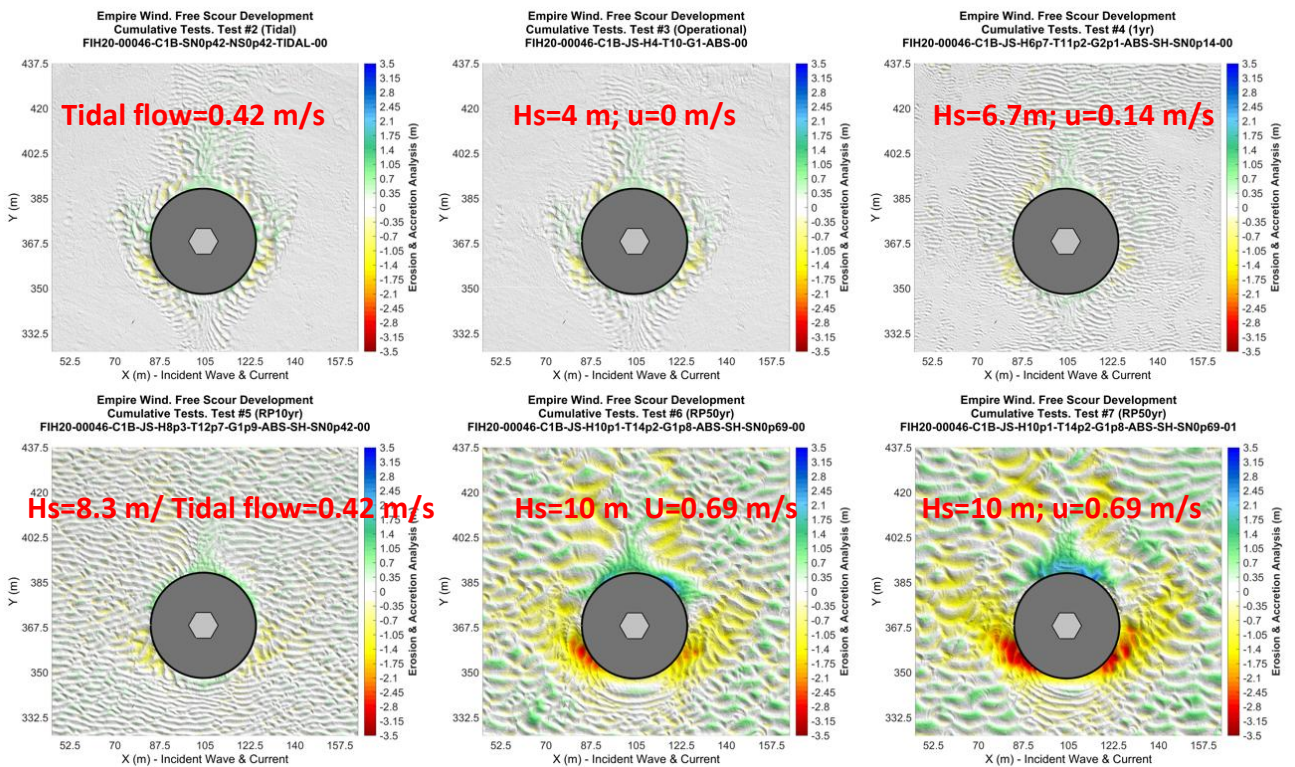


Figure 9.2.5 Scour depth around caisson-structure for different conditions



### Jacket structures

Rudolph et al. (2004) studied the scour near a jacket structure (open structure of multiple piles/legs). The structure at block L9 of the Dutch North Sea sector was installed in summer 1997. The bed level is about 24 m below LAT. The jacket structure has four legs (diameter  $D_{leg} = 1.1$  m) with a spacing of 20 m and 17 m, respectively. The support structure of the platform comprises six legs ( $D_{leg} = 1.5$  m) having spacings of 16 m and 20 m, respectively. At the seabed, all legs are connected to skirt piles. The piles resting in the seabed have a diameter of  $D_{pile} = 1.2$  m and 1.5 m, respectively. Scour protection was not applied at the jacket structures. Typical depth-averaged peak flow velocities are 0.5 m/s during spring tide and 0.35 m/s during neap tides. The estimated depth-averaged mean flow velocity is  $u = 0.25$  m/s. Metocean design conditions for a 100 year storm are:  $H_s = 8.8$  m,  $T_p = 10.1$  s and  $u = 1.2$  m/s. The actual wave conditions since installation were estimated at:  $H_s = 7.8$  m,  $T_p = 9.8$  s and  $u = 1.0$  m/s. The seabed material consists of dense fine to medium grained sand ( $d_{50} = 0.2$  mm).

Bathymetry charts showed that a wide area around the platforms was affected by scour. The extent of the far-field scour pit was in the order of 50 m in all directions. Maximum far-field scour depths were in the range of 1.5 to 5.0 m and the near-field scour near the legs/piles were in the range of 2.0 to 3.5m (about 1.5 to 2.5D). The far-field scour hole (extent of bathymetrical changes relative to the undisturbed situation) had a radius of roughly 2.5 to 3 times the pile spacing.

Bolle et al. (2012) and Baelus et al. (2018) analysed scour depth around the jacket-structure at Thornton Bank offshore windpark in the southern North Sea. The maximum scour depth was:  $d_{s,max} = 0.6D$  ( $\pm 50\%$ ).

Welzel et al. (2019) studied near and far-field scour around a jacket structure in a wave-current basin with water depth of 0.67 m (scale 1 to 30). The structure has four legs with pile diameter ( $D$ ) of 1.2 m and distance between piles ( $L_p$ ) of 16.5 m. Scour was minor for waves alone. Current velocity in range 0.1-0.4 m/s; peak orbital velocity in range 0.13-0.21 m/s. Sand bed with  $d_{50} = 0.19$  mm.

The maximum far-field scour depth within 0.5-1.5 $L_p$  from axis of structure was, as follows:

$$\begin{aligned} d_{s,max} &= 0.3D && \text{for } U_{CW} = U_c / (U_c + U_w) = 0.33; \\ d_{s,max} &= 0.5-0.7D && \text{for } U_{CW} = U_c / (U_c + U_w) = 0.55-0.75; \\ d_{s,max} &= 0.8D && \text{for } U_{CW} = U_c / (U_c + U_w) = 1. \end{aligned}$$

The maximum near-field scour depths around the least and the most exposed piles are, as follows:

$$\begin{aligned} d_{s,max} &= 0.1D; 0.2D && \text{for } U_{CW} = U_c / (U_c + U_w) = 0 \text{ (waves alone);} \\ d_{s,max} &= 0.8D; 1D && \text{for } U_{CW} = U_c / (U_c + U_w) = 0.37; \\ d_{s,max} &= 1.15D; 1.2D && \text{for } U_{CW} = U_c / (U_c + U_w) = 0.57; \\ d_{s,max} &= 1.2D; 1.65D && \text{for } U_{CW} = U_c / (U_c + U_w) = 0.76; \\ d_{s,max} &= 1.3D; 1.75D && \text{for } U_{CW} = U_c / (U_c + U_w) = 1 \text{ (current alone).} \end{aligned}$$

The dimensionless far-field scour volume within 5 $L_p$  from axis of structure was (80% with 3 $L_p$ ), as follows:

$$\begin{aligned} V_e / (nD^3) &\cong 30 && \text{for } U_{CW} = U_c / (U_c + U_w) = 0.33; \\ V_e / (nD^3) &\cong 100 && \text{for } U_{CW} = U_c / (U_c + U_w) = 0.55-0.75; \\ V_e / (nD^3) &\cong 170 && \text{for } U_{CW} = U_c / (U_c + U_w) = 1. \end{aligned}$$

The latter value yields  $V_e \cong 1500$  m<sup>3</sup> for  $D = 1.2$  m and  $n = 4$ . The scour area is about  $A_e = 2L_p \times 3L_p = 6L_p^2$  or  $6 \times 16.5 \times 16.5 = 1500$  m<sup>2</sup> and thus the average scour depth over this area is about 1 m.

### Rectangular structures

Bos et al. (2002) have studied scour and scour protection measures of a large gravity-based platform (F3) in the Dutch sector of the North Sea. Seabed consists of fine sand of 0.15 mm, see **Figure 9.2.6**.

Plan dimensions: rectangular 70x 80 m<sup>2</sup> with 3 shafts (towers) on top of the structure; height = 16 m ; water depth = 42 m.



Protection: gabion mattresses (0.5 m at corners ; 0.3 m in middle) along structure over width of 6 m from wall and attached with chains to structure on top of an under filter layer of gravel (1 m); gabion-mattresses overlain with bitumen-penetrated Sarmac-mattresses (0.4 m) pat corners.

Tests with mattresses not attached to structure showed severe undermining.

Physical model tests (scale 1 to 40) showed a maximum scour depth of 3.5 to 4 m after 10 hours at the most exposed corner (for storm with return period of 100 years), (Deltares 1992). Tests with mattresses not attached to structure showed severe undermining.

Field surveys using video-camera images showed :

- No damages to the mattresses were found since the construction in 1992. No shift of the mattresses was observed from the surveys, suggesting that the mattresses were stable. All mattresses are still located tight to the GBS. Video-images from the ROV show no gaps between the mattresses and the GBS.
- The maximum scour depth, which has been measured at the south-west corner of the F3 GBS is about 3.0 m. This scour is caused by a storm with a return period of 1/1 to 1/5 years.
- The space between mattresses and GBS was found to be acceptable. There were no large gaps between the mattresses and the GBS walls following the video.
- The mattresses are flexible and follow the seabed changes at the outer edges of the mattresses. The steepest side slope of the mattresses was about 1:2.

Maximum current: 0.65 m/s annual tides+minor storm;  
1 m/s major storm (1x 100 years) oblique to upstream wall.

Waves:  $H_s=5$  m,  $T_p=9.4$  s (annual);  $H_s=9.5$  m (1x 5 years)  $H_s=11$  m,  $T_p=14.3$  s (1x 100 years).

Maximum scour depth: 2.5 to 3.5 m at most exposed corners (during first year) based on field survey  
3.5 m based on scour test with scale of 1 to 40 (duration of 10 hours)

Maximum scour extent: about 15 to 20 m (approximately height of structure)

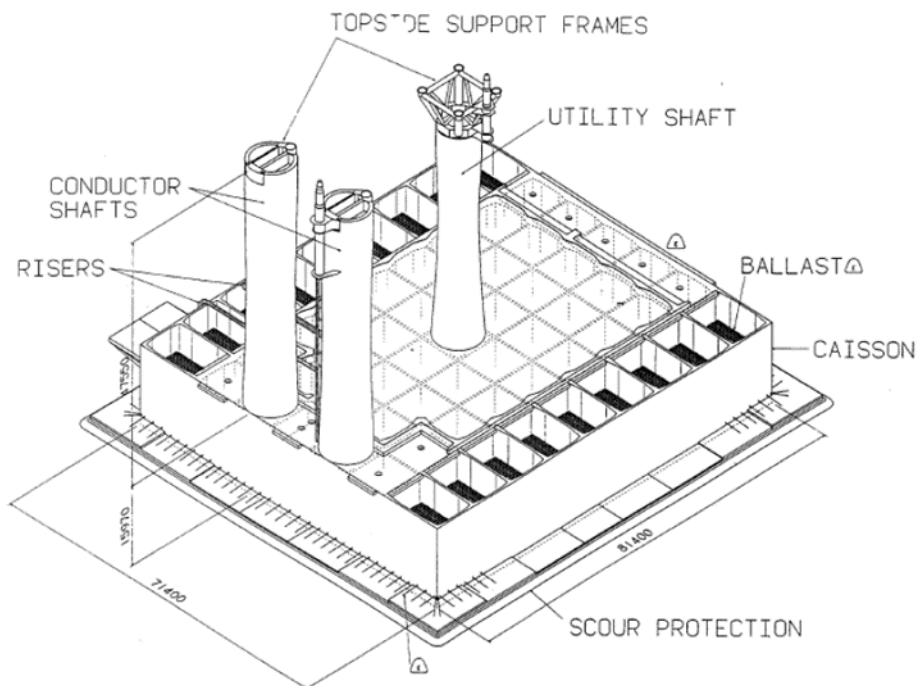


Figure 9.2.6 Caisson-type structure placed on seabed in Dutch coastal sector, 1992 (Bos et al., 2002).



Zhao et al. (2012) have studied local scour phenomena near caisson-type structures placed on the seabed. The height of the structure ( $h_s$ ) was always  $h_s < 0.5h_o$ . The length and width of the structures was in the range of 0.2 to 0.5 m;  $b_s$  is defined as the width normal to the flow direction. The height was varied in the range of 0.05 to 0.2 m. Scour measurements near the corner of the structure in a wide flume of 2 m were carried out. The horizontal shape of the caisson is rectangular and the incident direction of the flow was varied. The dominant scouring processes were found to be the velocity accelerations near the corners. Basic data are in **Table 9.2.2**. Scour contour plots are shown in **Figures 9.2.7A,E**.

Flow conditions: water depth  $h_o=0.5$  m; depth-mean velocity upstream  $U_{c,o}= 0.33$  m/s,  
 $d_{50, \text{sediment bed}}= 0.135$  mm; equilibrium scour was observed after 3 to 6 hours;  
sand ripples were generated with height of 0.02-0.04 m and lengths of 0.1 to 0.2 m.

The slopes of the scour pits are between 1 to 2 and 1 to 5. The length scale of the scour pits is of the order of the structure length in the direction of the flow. Thus:  $L_{\text{scour,nf}} \cong L_{\text{structure}}$

The morphological features can be summarized, as:

- near-field scour near the upstream corner points; the horizontal scour extent at the corners is about 0.5 times the smallest structure length;
- near-field deposition in the downstream wake region and downstream of the scour pits (most deposition takes place in far-field regions where the extra wake turbulence has decayed);
- minor far-field scour beyond the wake region.

Zhao et al. 2012 have proposed for the local scour (near-field scour) at the corner of subsea-caissons in steady currents:

$$d_{s,\text{max}}= 1.02 b_s [1-\exp\{-1.35h_s/b_s\}] \quad (9.2.2)$$

with:

$b_s$  = width of structure normal to flow;

$h_s$  = height of structure above bottom ( $h_s/h_o \leq 0.5$ ).

Test	Structure dimensions			Width normal to flow $b_s$ (m)	Scour depth $d_{s,\text{max}}$ (m)	Ratio $h_s/h_o$ (-)	Ratio $h_s/b_s$ (-)	Ratio scour $d_{s,\text{max}}/h_s$ (-)	Ratio scour $d_{s,\text{max}}/b_s$ (-)
	Length $L_s$ (m)	width $B_s$ (m)	height $h_s$ (m)						
A1	0.2	0.2	0.05	0.2	0.06	0.1	0.25	1.2	0.3
A2	0.2	0.2	0.1	0.2	0.1	0.2	0.5	1.0	0.5
A3	0.2	0.2	0.15	0.2	0.12	0.3	0.75	0.8	0.6
A4	0.2	0.2	0.2	0.2	0.14	0.4	1	0.7	0.68
B1	0.4	0.2	0.05	0.4	0.055	0.1	0.125	1.05	0.13
B2	0.4	0.2	0.1	0.4	0.11	0.2	0.25	1.05	0.26
B3	0.4	0.2	0.15	0.4	0.135	0.3	0.375	0.9	0.33
B4	0.4	0.2	0.2	0.4	0.15	0.4	0.5	0.75	0.37
C1	0.4	0.2	0.1	0.2	0.08	0.2	0.5	0.8	0.39
C2	0.4	0.2	0.2	0.2	0.13	0.4	1	0.65	0.66
D2	0.2	0.2	0.2	0.28	0.1	0.4	0.71	0.5	0.5
E2	0.4	0.2	0.2	0.42	0.12	0.4	0.48	0.6	0.3

**Table 9.2.2** Experimental data of scour near caisson-type structures (Zhao et al. 2012)

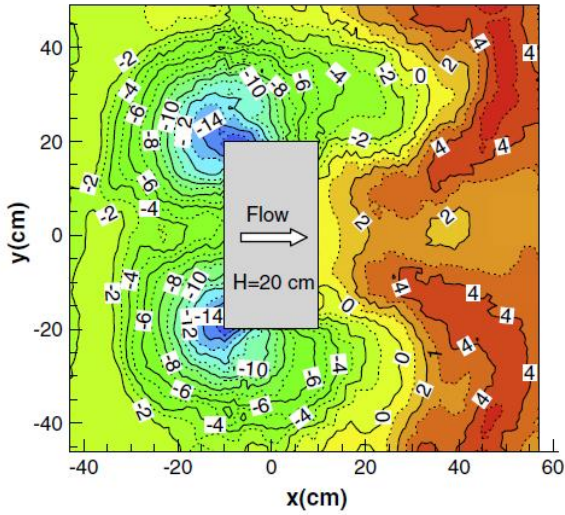


Figure 9.2.7A Equilibrium scour in test B4 (rectangular wide)

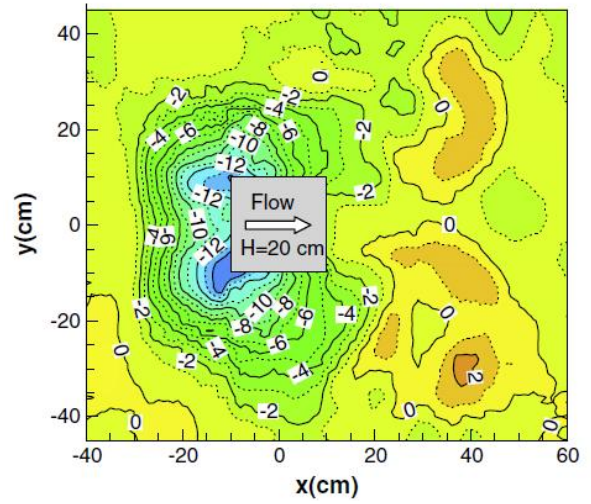


Figure 9.2.7B Equilibrium scour in test A4 (square)

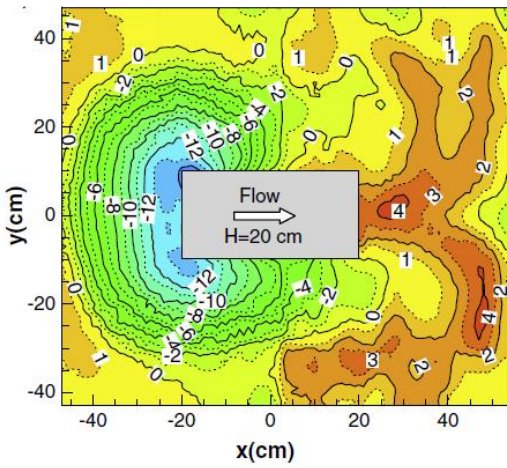


Figure 9.2.7C Equilibrium scour in test C2 (rectangular small)

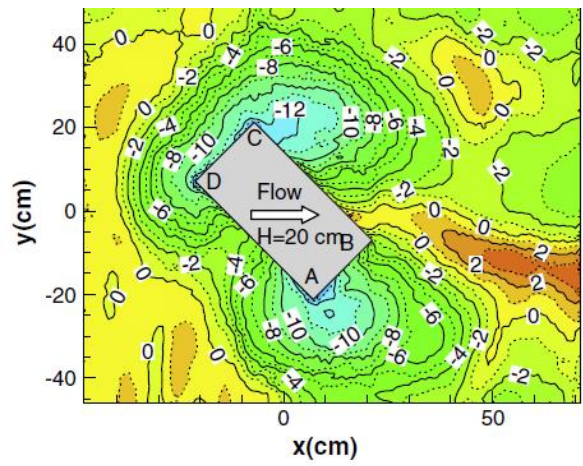


Figure 9.2.7D Equilibrium scour in test E2 (Corner into flow; rectangular)

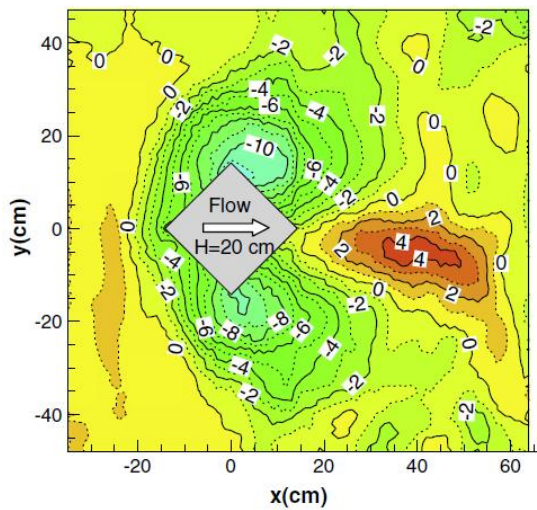


Figure 9.2.7E Equilibrium scour in test D2 (corner into flow; square)



### 9.2.4 Modelling of scour near gravity-structures

#### General

Detailed numerical modeling of fluid dynamics requires an advanced CFD-model which solves the governing non-hydrostatic flow equations (Navier-Stokes equations) using either finite-volume or finite elements. Spatial and time scales need to be very small to resolve the turbulent velocities in sufficient detail. Cell sizes close to the structure should be smaller than 0.1 m. Additional turbulence models are required for detailed modelling of turbulent velocities. Two turbulence models can be used: k-epsilon turbulence closure model or large eddy simulation turbulence model (LES). Both models need substantial calibration to obtain accurate results. **Figure 9.2.8** shows an example of numerical results with bed updating in time.

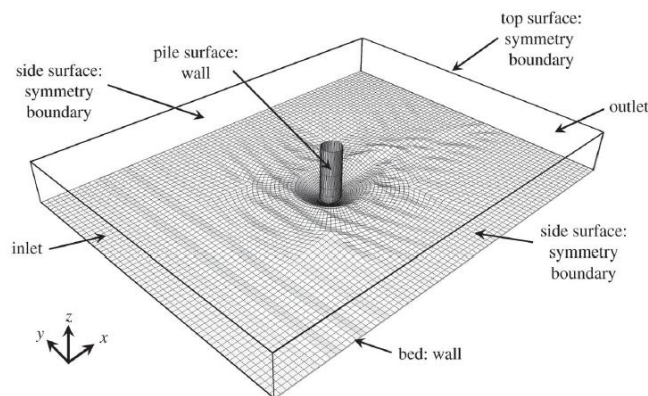


Figure 9.2.8 Numerical modelling of scour around pile structure (Van Eijk 2016)

#### SED-TUBE1D-model for scour prediction near caisson type foundation structures

The flow along the flanks of the caisson can be schematized as flow through a stream tube with varying width, as shown in **Figure 9.2.9**. A stream tube is a flow domain with constant discharge ( $Q$ ). By definition there is no flow normal to the stream tube (no inflow and outflow normal to tube). The flow velocity along the stream tube follows from the discharge and the dimensions (width and depth) of the stream tube.

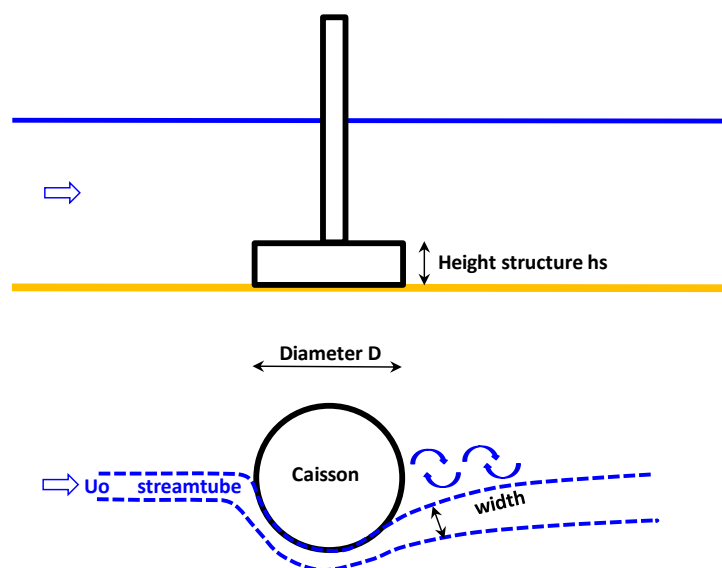


Figure 9.2.9 Stream tube along flank of caisson



When a caisson with height ( $h_{\text{caisson}}$ ) much smaller than the water depth ( $h$ ) is placed on the seabed, the flow is partly blocked by the caisson and will accelerate along the upstream flank of the caisson and decelerate along the downstream flank and in the lee region accompanied by the production of turbulence. The flow over the caisson will mainly be influenced by the smaller monopile on top of the caisson.

The 1D-SED-TUBE-model of LVRS-Consultancy can simulate the flow and sediment transport in a predefined stream tube. The dimensions of the stream tube can be derived from 3D-numerical model results or from laboratory measurements. The SED-TUBE-model computes the flow velocity, the wave parameters and the bed load and the suspended load transport along the stream tube and the associated bed level changes over time. The most basic input data of the SED-TUBE-model are:

- flow discharge  $Q$ ;
- initial water depth and flow width along stream tube;
- significant wave height and peak wave period;
- sediment parameters:  $d_{50}, d_{90}$ , settling velocity  $w_s$ , bed roughness of Nikurdse  $k_s$ ; bed porosity;
- numerical parameters: grid size, time step

The following conditions have been used for the example case of a gravity-based caisson: caisson diameter= 40 m; caisson height= 8.8 m; sand of 0.45 mm at bed; settling velocity of suspended sand  $w_s=0.04$  m/s, bed roughness  $k_s=0.03$  m. The critical velocity for initiation of motion is set to 0.42 m/s for 0.45 mm sand.

Basic assumptions for scour modelling along the caisson using the SED-TUBE-model are:

- 1) effective water depth is equal to the caisson height (8.8 m) assuming that the acceleration and deceleration of the flow mainly occur in the lower part of the water column;
- 2) maximum flow velocity along flank is equal to 1.5 times the upstream approach velocity ( $u_{\text{flank}}=1.5u_o$ ).

**Figure 9.2.10** shows the velocity increase and decrease of a steady current of  $U_o=0.4$  m/s along a caisson with diameter of 40 m and a perimeter of 126 m (4 quarters of about 31 m) as used in the SED-TUBE-model. The flow velocity increases to a value of 0.6 m/s along the upstream flank and decreases to a value of about 0.4 m/s in the lee region of the caisson.

It is noted that the assumption  $u/u_o=1.5$  remains the same during the development of the scour pit in the SED-TUBE-model, which is a conservative approach leading to overestimation of the scour depth as in reality this ratio will gradually decrease during the scouring process. The additional turbulence generated around the structure is not represented in the model leading to underestimation of the scour depth. Both effects are opposite and may thus cancel out to some extent.

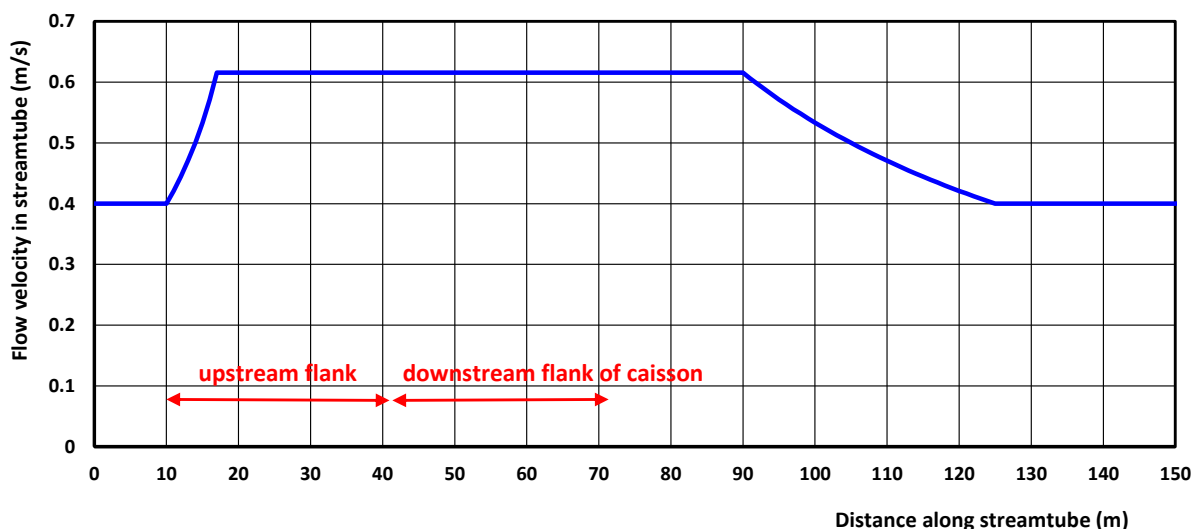


**Figure 9.2.10** Flow velocity along stream tube for approach velocity of 0.4 m/s (no waves)



Figure 9.2.11 shows the computed scour depth for a current velocity of 0.4 m/s with and without waves. The computed maximum scour depth is about 3.5 m after 1 year for an approach velocity of 0.4 m/s. The maximum scour depth can become slightly higher for a time scale > 1 year as the depth-mean flow velocity in the deepest part of the scour pit is 0.44 m/s after 1 year which is 5% higher than the critical flow velocity of 0.42 m/s for initiation of motion. The maximum scour depth is obtained when the velocity in the scour pit is equal to the critical velocity.

The development in time is shown in Figure 9.2.12. It takes about 2 to 3 years to arrive at the maximum scour depth in the case of a steady current. The scour depth is about 90% of the equilibrium scour depth after 1 year. It is noted that in a tidal current with the same peak approach velocity, the maximum scour depth will be reached after a time period which is about 3 times longer, as the peak flow conditions occur during about 30% of the time in tidal flow.

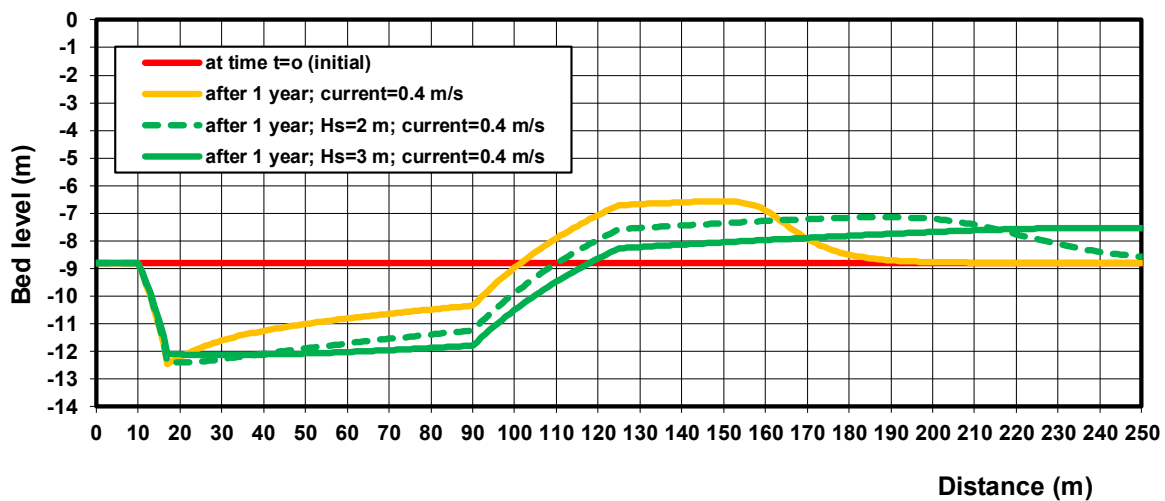


Figure 9.2.11 Scour depth after 1 year along flank of caisson; steady current=0.4 m/s and wave height of  $H_s=2$  m and 3 m,  $d_{50}=0.45$  mm

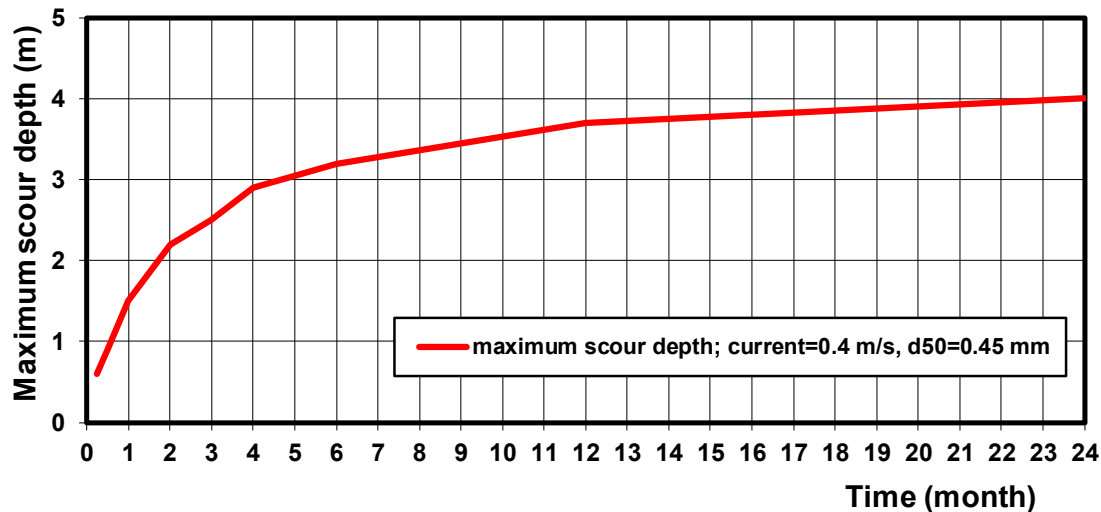


Figure 9.2.12 Maximum scour depth as function of time; steady current=0.4 m/s, no waves,  $d_{50}=0.45$  mm



Figure 9.2.13 also shows the effect of waves with a height of 2 m ( $T_p=7$  s) and 3 m ( $T_p=8$  s) on the scour depth. The near-bed orbital peak velocities are 0.1 m/s for  $H_s=2$  m and 0.25 m/s for  $H_s=3$  m in depth of 36 m. The maximum scour depth remains approximately constant, but the scour pit becomes wider and the depositional bar is flattened.

The scour depth increases slightly for finer sand with  $d_{50}=0.3$  mm or a higher bed roughness of 0.1 m in stead of 0.03 m (based on sensitivity computations).

The scour depth increases to 4.2 m for a higher approach velocity of 0.6 m/s and to 4.6 m for an approach velocity of 1 m/s.

The maximum scour depth is 4.7 m after 2 years for an approach velocity of 1 m/s.

The scour depth does not increase any more as the velocity in the deepest part of the scour pit is approximately equal to the approach velocity due to the effect of stream tube narrowing and deepening along the flank of the caisson.

When an extreme storm event with duration of 12 to 24 hours occurs ( $H_s=10.1$  m;  $T_p=14.2$  s; approach velocity=0.7 m/s; near-bed peak orbital velocity= 2 m/s ; return period= 50 years) in a situation with a flat bed in the initial situation, the maximum scour depth is about 0.25 m after 24 hours, see Figure 3.3.5.

The maximum scour depth increases to about 0.8 m when the storm lasts for 7 days. A post storm current with a velocity of 0.7 m/s without waves and a duration of 7 days produces a maximum scour depth of 0.4 m.

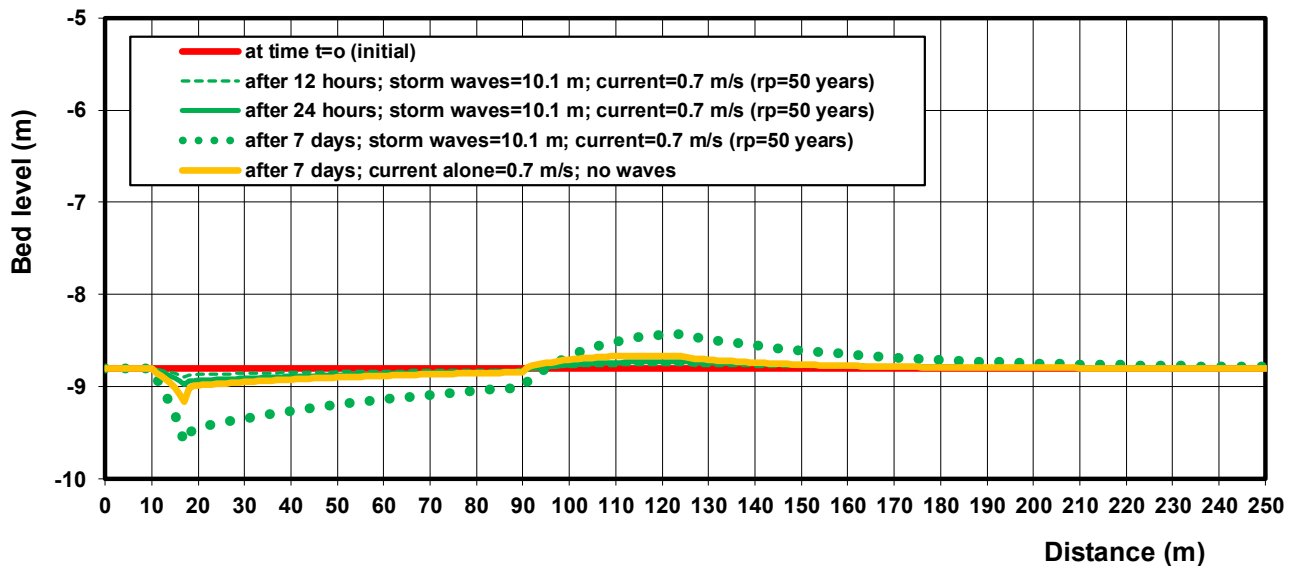


Figure 9.2.13 Scour depth after an extreme storm with wave height of 10.1 m and flow approach velocity of 0.7 m/s

The computed maximum scour depth for all results with and without waves are plotted as function of the depth-averaged current velocity in Figure 9.2.14.

All results indicate that the scour process is strongly dominated by the current velocity.

The presence of waves increases the scour depth in the case of a weak current (<0.3 m/s). In the case of stronger current (> 0.3 m/s), the scour depth is highest for a current alone without waves. The maximum scour depth is about 4.5 m. When waves are present, the relatively high suspended load coming from the upstream region causes a slight (temporary) infill of the scour pit.

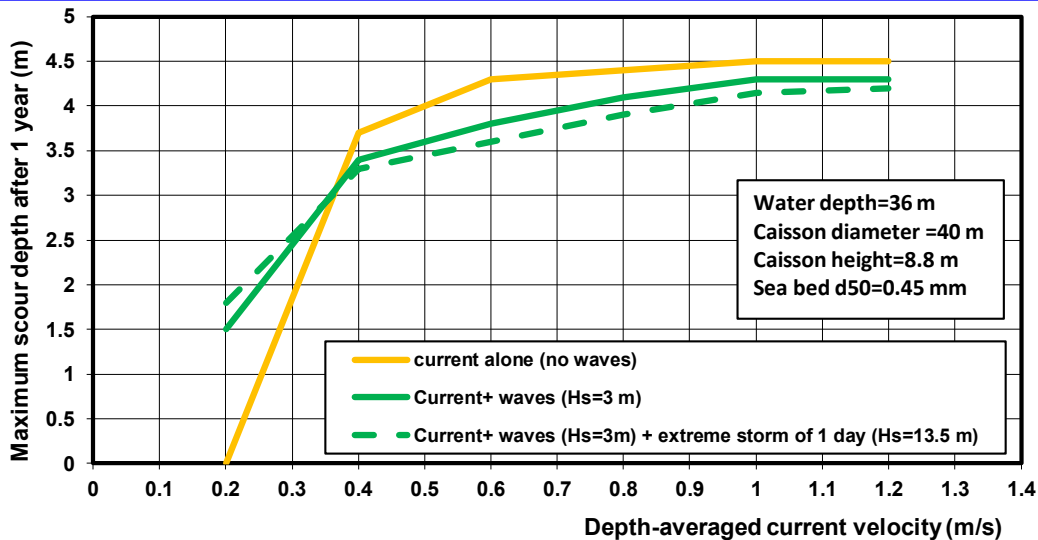


Figure 9.2.14 Maximum scour depth after 1 year for various conditions

#### SUSTIM2DV-model for scour prediction near caisson type foundation structures

The SUSTIM2DV-model can also be used to compute the sand transport in a channel (streamtube) with varying width resulting in varying flow velocities (accelerating/decelerating flow). As an example, the sand transport in accelerating and decelerating flow along a caisson structure (diameter  $D=40$  m and height  $h=10$  m) with a monopile on top of it is considered, see **Figure 9.2.9**.

The SUSTIM2DV-model has been applied to a stream tube along a wide, circular caisson-type structure placed on the seabed. The following conditions have been used: caisson diameter= 40 m; caisson height= 10 m; water depth= 10 m; seabed consisting of sand.

Basic assumptions for the flow around a caisson-type of structure placed on the seabed are:

- width of streamtube is constant in time, which is a conservative assumption leading to overestimation of the maximum scour depth;
- maximum flow velocity along flank is equal to 1.7 times the upstream approach velocity ( $u_{\text{flank}} \cong 1.7u_o$ ; minimum width streamtube  $\cong 0.6$  width at entrance,  $b_{\text{minimum}} \cong 0.6b_o$ ).

The basic input data are:

- water depth upstream of trench:  $h= 10$  m to MSL;
- tidal current with tidal period of 12 hours; maximum depth-averaged current:  $u_{c,\text{max}}= 1$  m/s and 0.7 m/s at  $t=3$  and  $t=9$  hours; no phase shift between water levels and current velocities;
- tidal amplitude=1 m;
- approach angle= $90^\circ$  (for flood and ebb flow);
- sand  $d_{50}=0.4$  mm;  $d_{90}=1$  mm; fall velocity=0.03,  $\beta=1.5$ ;
- sand  $d_{50}=0.25$  mm;  $d_{90}=0.5$  mm; fall velocity=0.02,  $\beta=1$ ;
- bed roughness  $k_{s,c}=k_{s,w}=k_a=0.1$  m;
- scaling coefficient bed reference concentration  $\alpha_c=1$ ;  $a$ =reference level=0.05 m;
- thickness wave-related mixing layer  $\delta_b=0.2$  m; wave-related mixing coefficient  $\gamma_3=0.5$ ,  $\gamma_4=0.5$ ;
- density:  $\rho_s= 2650$  kg/m<sup>3</sup>,  $\rho_w= 1025$  kg/m<sup>3</sup>,  $\nu= 0.000001$  m<sup>2</sup>/s,
- porosity=0.4;
- computation period=90 days; timestep =8 s, NZ=25.

The following cases are considered :

- Case A :  $u_{c,\text{max}}= 1$  m/s; sand  $d_{50}=0.4$  mm;  $d_{90}=1$  mm; fall velocity suspended sand  $w_s=0.03$  m/s;
- Case B :  $u_{c,\text{max}}= 0.7$  m/s; sand  $d_{50}=0.4$  mm;  $d_{90}=1$  mm; fall velocity suspended sand  $w_s=0.03$  m/s;
- Case C :  $u_{c,\text{max}}= 0.7$  m/s; sand  $d_{50}=0.25$  mm;  $d_{90}=0.5$  mm; fall velocity suspended sand  $w_s=0.02$  m/s.



The width is schematized as follows (caisson perimeter between  $x=330$  and  $390$  m ; center at  $x=360$  m):

- $x= 0, 300, 320, 340, 360, 380, 400, 420, 720$  m;
- $w= 1, 1, 0.8, 0.7, 0.6, 0.7, 0.8, 1. 1$  m.

The wave order over the computation period of 90 days is as follows :

- wave height  $H_s= 0, 3, 4, 3, 0$  m ;
- peak wave period  $T_p = 0, 10, 12, 10, 0$  s ;
- duration  $t_{dur}=40, 4, 2, 4, 40$  days.

### Case A

Figure 9.2.15 shows for the velocity variation along the streamtube at the flank of the caisson at  $t=3$  hours (maximum flow conditions). The maximum depth-averaged velocity upstream of the caisson is 1 m/s. The caisson has a diameter of 40 m and a perimeter of 126 m (4 quarters of about 31 m); the maximum flow velocity increases to a value of 1.65 m/s along the upstream flank and decreases to a value of about 1 m/s in the lee region of the caisson.

The maximum scour depth is about 4.5 m after 40 days (no waves between  $t=0$  and 40 days).

The maximum scour depth decreases to 4 m after 50 days due to deposition during the storm period ( $t=40$  to 50 days with waves between  $H_s=3$  and 4 m).

The maximum scour depth increases to 5 m after 90 days (no waves between  $t=50$  and 90 days).

The maximum scour depth after 90 days is almost the same (5 m) in conditions without a storm period.

The eroded sediment is deposited on both sides of the caisson. The bed on left side of the scour hole is slightly eroded during the storm period of 10 days due to the ebb flow with smaller water depths (stronger wave effect).

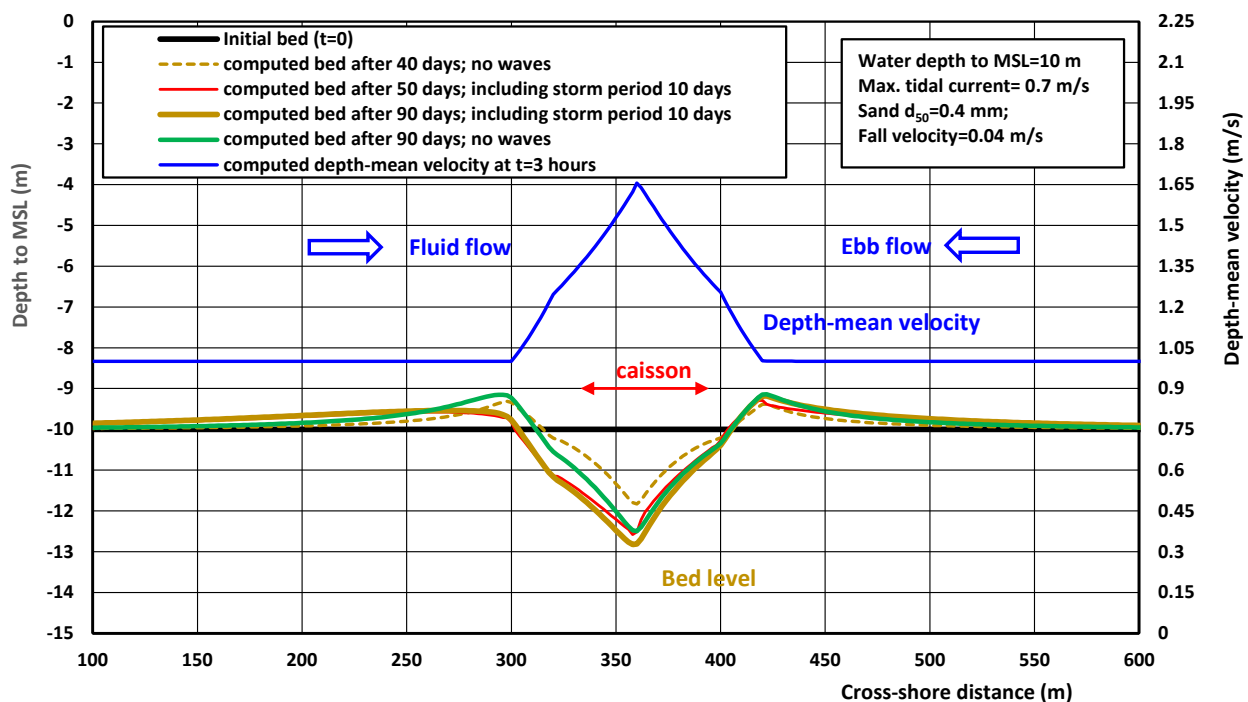


Figure 9.2.15 Case A; Flow velocity and scour along caisson-structure; maximum approach velocity 1 m/s;  $d_{50}=0.4$  mm (short traject)



Figure 9.2.16 shows results of the same computation for a longer trajectory with boundary conditions farther away (500 m extra on both sides) from the scour hole. The effect of a longer trajectory on the computed scour depth is marginal.

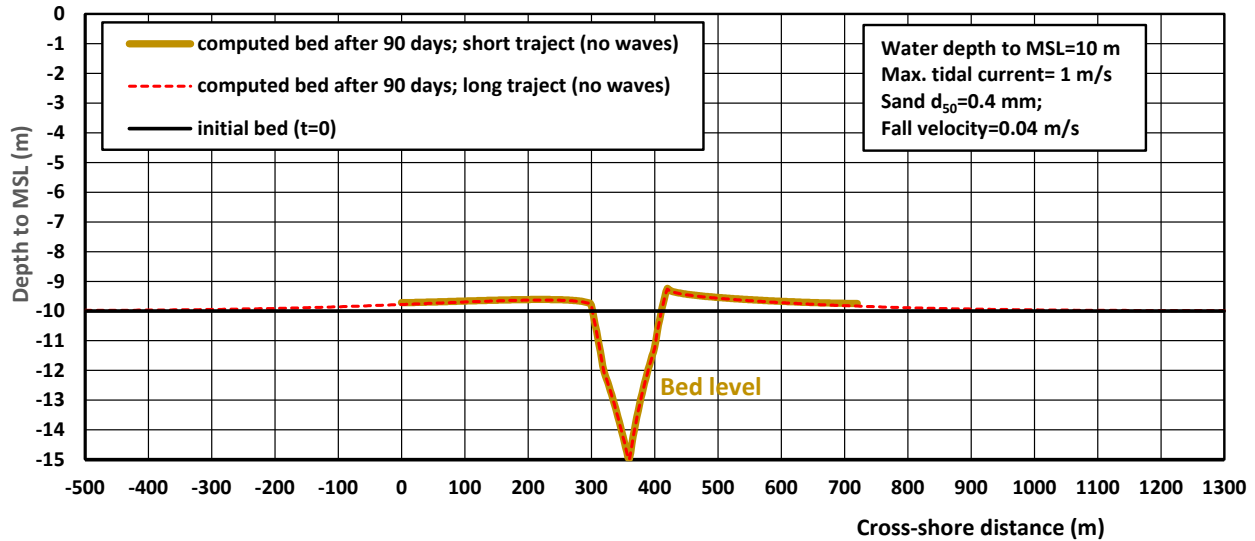


Figure 9.2.16 Case A; Flow velocity and scour along stream tube for maximum approach velocity 1 m/s;  $d_{50}=0.4$  mm (long trajectory)

### Case B

Figure 9.2.17 shows the computed scour hole over 90 days for a lower peak tidal flow velocity of 0.7 m/s (in stead of 1 m/s; Case A) resulting in a lower sand transport value at peak tidal flow conditions. The maximum scour depth is about 1.8 m after 40 days (tidal flow without waves), which increases to about 2.6 m after 50 days for tidal flow and a storm period of 10 days ( $t=40$  to 50 days) with  $H_s$  between 3 and 4 m. The maximum scour depth increases to about 2.8 m after 90 days (no waves between  $t=50$  and 90 days). The maximum scour depth after 90 days is slightly smaller (2.5 m) in conditions without a storm period. The scour on the left slope is lower and the deposition on the left side is somewhat higher.

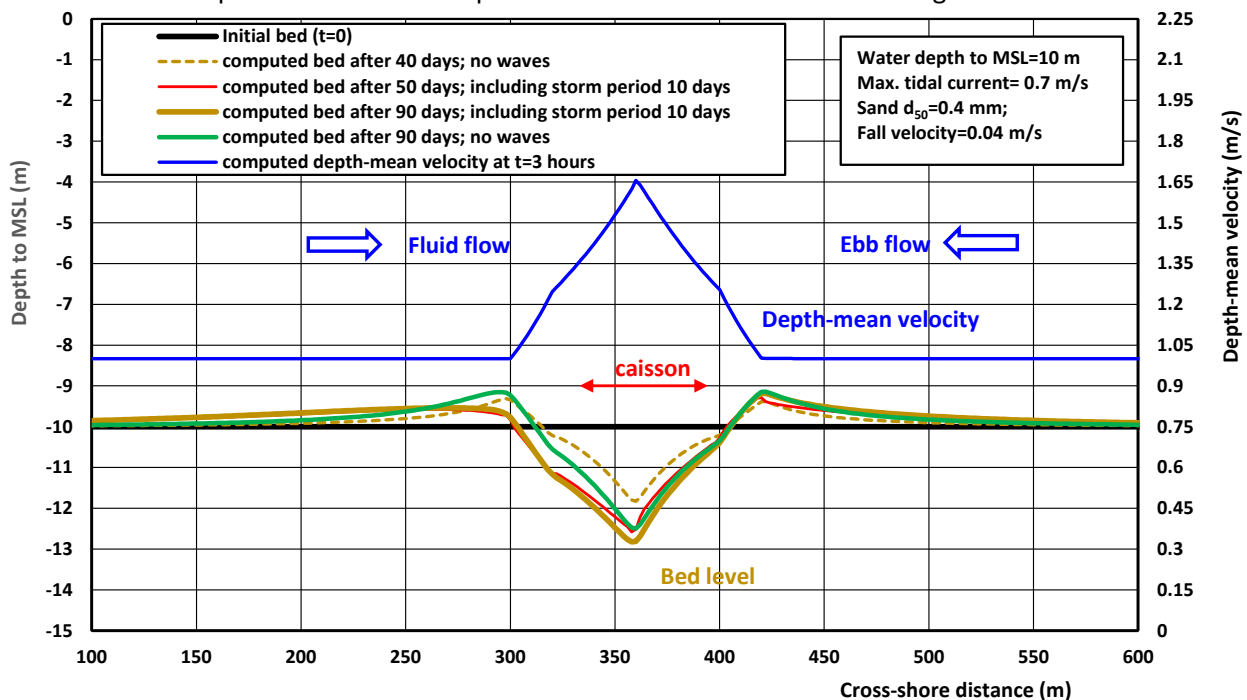


Figure 9.2.17 Case B; Flow velocity and scour along stream tube ; maximum velocity= 0.7 m/s ;  $d_{50}=0.4$  mm



**Case C**

Figure 9.2.18 shows the effect of a storm period of 10 days with  $H_s$  between 3 and 4 m on the deposition in a deep scour hole with maximum depth of 5 m in a sand bed of  $d_{50}=0.25$  mm. The flow velocity in the deepest part of the scour hole increases due to flow contraction (decrease of width), but decreases due to flow expansion (larger water depth in scour hole). The maximum depth-mean velocity at  $t=3$  hours (peak tidal flow) is about 0.8 m/s. Deposition of sand occurs in the storm period, mostly at the right slope due to higher sand transport during ebb flow when the water depth is smallest. Erosion occurs on the left slope.

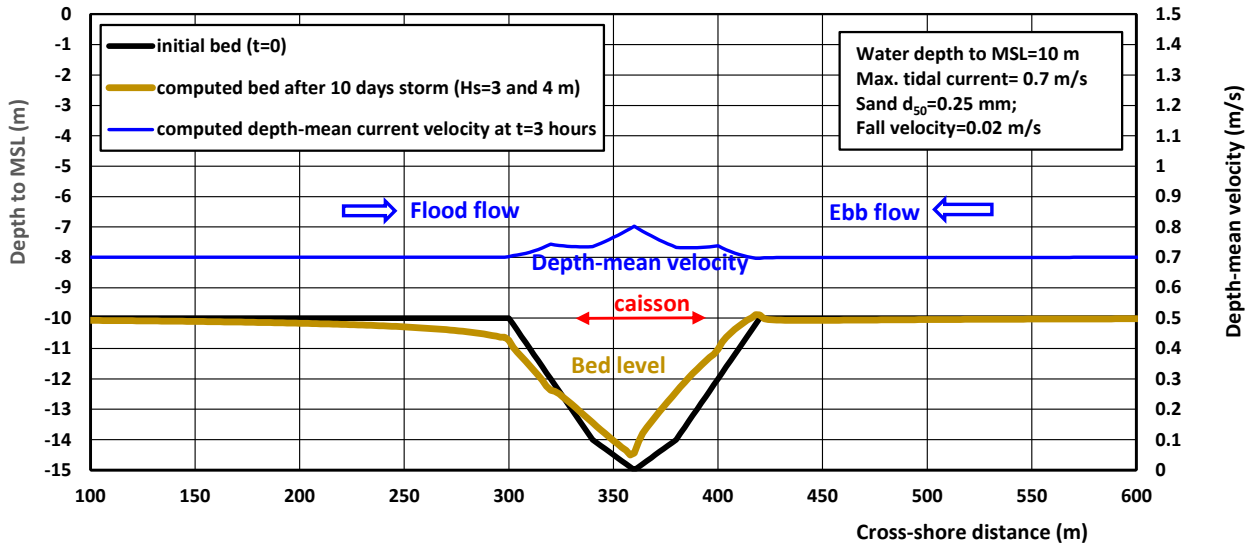


Figure 9.2.18 Case C; Flow velocity and scour along stream tube ; maximum velocity= 0.7 m/s ;  $d_{50}=0.25$  mm

**DELFT3D-model for scour prediction near caisson type foundation structures**

The DELFT3D-model in depth-averaged mode has been used to compute the scour depth along a caisson (GBS) with diameter of 40 m and height of 8.8 m resting on a sand bed of 0.45 mm.

Figure 9.2.19 shows the computed scour after one year for approach velocity of 0.4 m/s. Note that negative values (blue-colored) correspond to erosion, whereas positive values (brown-colored) correspond to sedimentation. The black circle denotes the approximate location of the GBS.

The most important results are:

- computed scour depths amount to less than 1.0 m in the upstream half of the perimeter (near-field scour), with local-maximum near-field scour depths of about 1.6 m; deposition occurs in the downstream half of the perimeter;
- scour further away from the structure (far-field scour in lee region) does not occur as the flow velocities are close or below the values for initiation of motion.
- computed scour hole develops fastest in the first few months and slows down afterwards, but is not fully in equilibrium after one year.

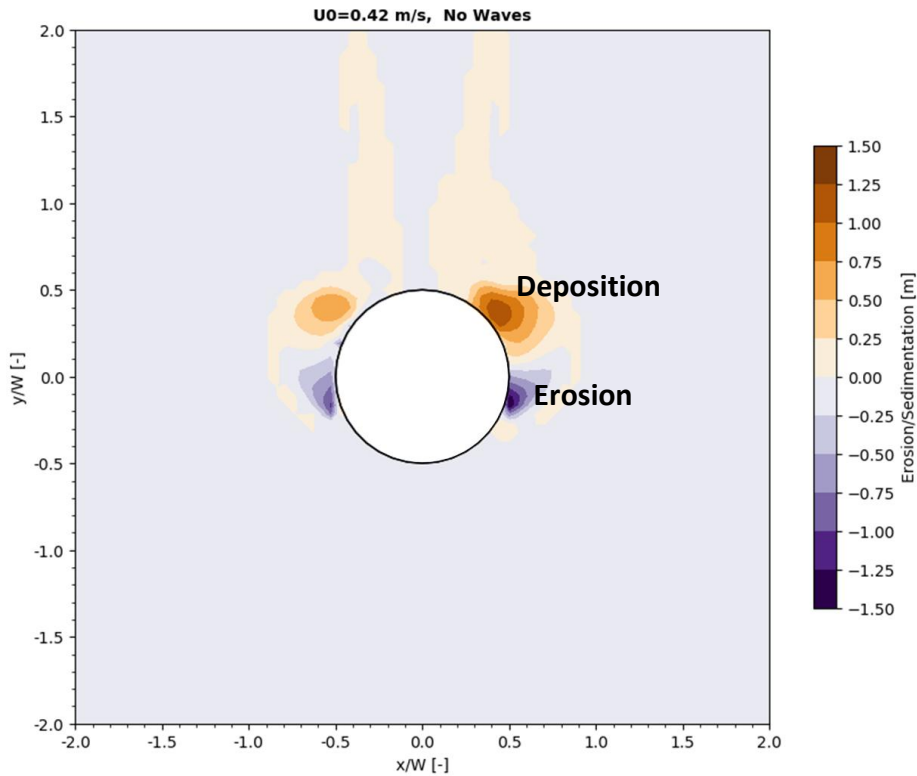


Figure 9.2.19 Computed bed level changes after 1 year based on DELFT3D-model; current only  $U_0=0.42$  m/s

Figure 9.2.20 shows the results for an approach velocity of 0.7 m/s:

- computed near-field scour depths is between 0.5 and 2.5 m for a region of about the size of the GBS at either flank along the caisson;
- maximum local scour is about 3.0 to 3.5 m which is computed along the flanks of the caisson, in the downstream half of the GBS region.
- deposition occurs in the upstream area, which in reality will not be present due to the downward flow (underestimated by the model), some scour is also expected upstream the GBS;
- deposition in the form of a ridge occurs in the middle of the lee region which is realistic; most likely far-field scour will be generated on both sides of the ridge which is not computed by the model (underestimation of wake velocities and related turbulence).

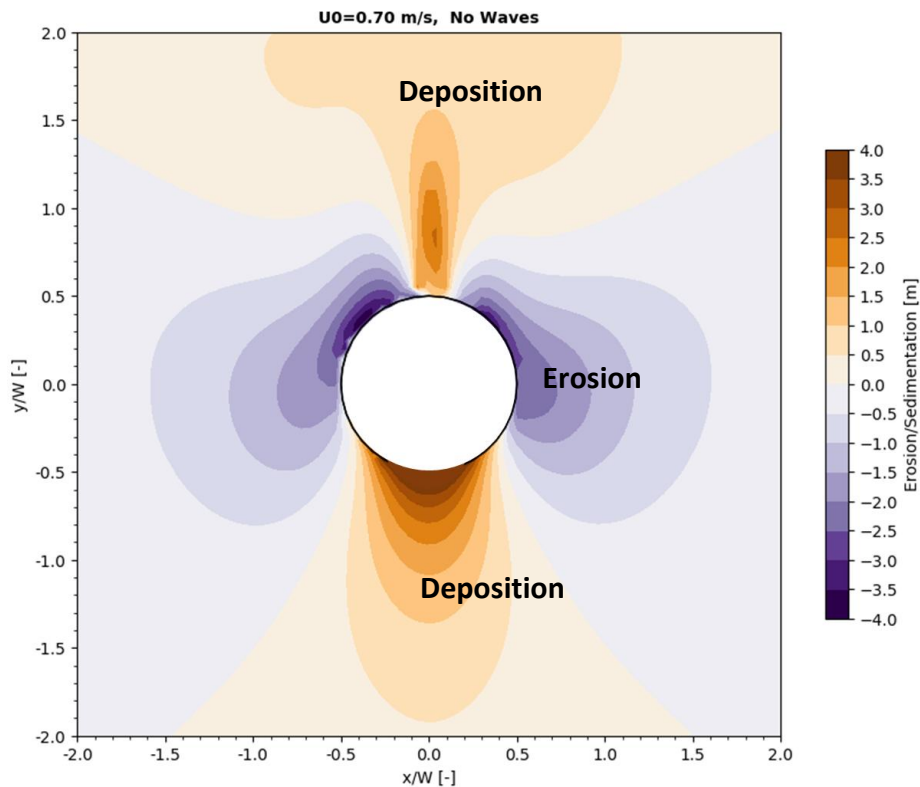


Figure 9.2.20 Computed bed level changes after 1 year based on DELFT3D-model; current only  $U_o=0.7$  m/s

Figure 9.2.21 shows the computed scour field for a case with combined current and waves. The incoming waves of a storm event with  $H_s=8.3$  m and  $T_p=12.7$  s (duration of 48 hours) are perpendicular to the approaching current. Wave height variations are computed by the SWAN-model.

The main results are:

- scour is limited to the up-wave flank (area A) of the GBS where the interaction of the current and incident waves is most intense and amounts to about 1.0 to 1.5 m;
- the overall morphological pattern in areas B, C and D is characterized by deposition of about 1.0 to 2.0 m, while for some regions massive deposition is computed, even exceeding half the GBS height (approx. 4.5 m).

In combined current and wave conditions, the incoming sediment load is much higher than in conditions with a current of 0.42 m/s only (no waves). This may easily lead to infill in potential scour areas with velocity increase, as follows:

- area A: velocity increase (acceleration area) producing erosion; waves are not much affected (same as up-wave); overall erosion (scour);
- area B: velocity decrease (deceleration area) producing deposition; waves are not much affected (same as up-wave); overall deposition (scour);
- area C: velocity decrease producing deposition; waves are slightly higher than up-wave giving slightly more erosion; overall, deposition wins;
- area D: velocity increase (acceleration area) giving erosion; waves are smaller smaller in lee of caisson leading to deposition; overall, deposition wins.

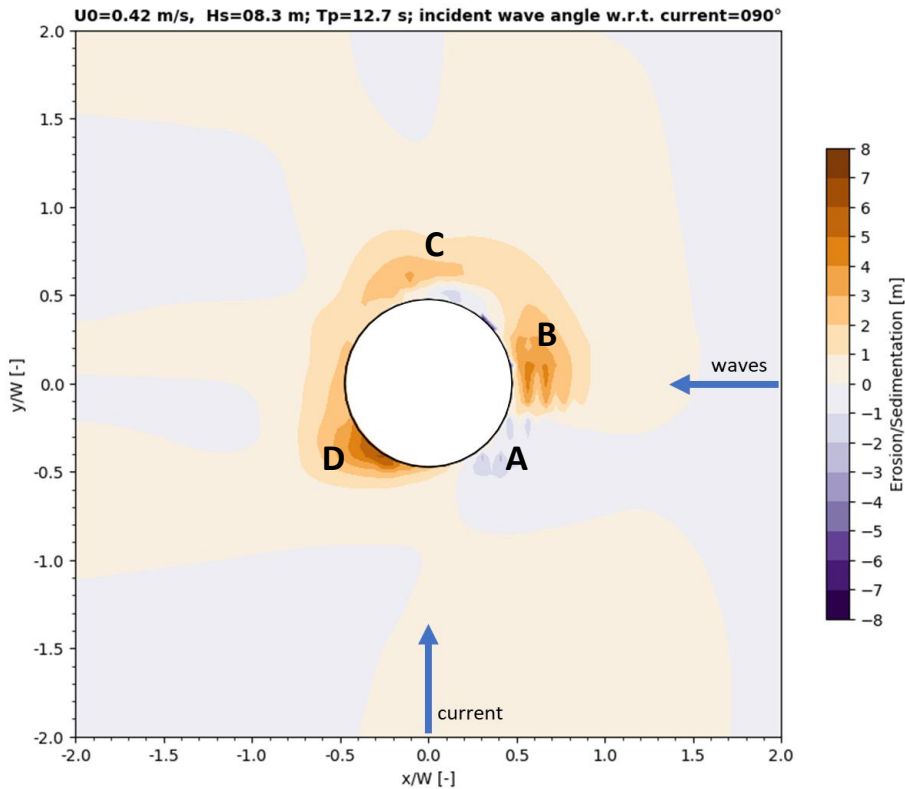


**Figure 9.2.21** Computed bed level changes after 1 year based on DELFT3D-model; combined currents and waves  $U_0=0.42$  m/s;  $H_s=8.3$  m

### 9.2.5 Synthesis of results; design graphs

**Figures 9.2.22 to 9.2.24** are summary plots with the scour data of Zhao et al. (2012), Whitehouse (2004) and Tavouktsoglou (2017).

**Figure 9.2.22** shows the ratio of scour depth and structure width ( $d_{s,max}/b_s$ ) as function of the ratio of structure height and width ( $h_s/b_s$ ). It can be seen that the relative scour is smaller for wide, low structures compared with the high, small (slender) structures). The latter produce much larger horseshoe type of vortices. The results of Whitehouse (2004), Zhao et al. (2012) and Tavouktsoglou (2017) are in fairly good agreement.

The results for GBS-structures (wide and low structures) can be crudely represented by:

$$d_{s,max}/b_s = 0.4 (b_s/h)^{0.5} (h_s/b_s)^{0.5} (V_{par})^{0.5} \quad (9.2.3)$$

with:

$b_s$  = width (diameter) of structure normal to flow;

$h$ = water depth;  $h_s$ = height of structure above bottom ( $h_s/h_o \leq 0.5$ );

$V_{par} = [ \{ (\alpha_s U_c)^2 + (0.7 U_w)^2 \}^{0.5} - U_{cr} ] / U_{cr}$  = dimensionless velocity parameter,

$U_w$ = near bed peak orbital velocity of annual-mean wave height (range 1 to 2 m/s);

$U_c$ = maximum flow velocity upstream due to tide+wind;

$U_{cr}$ = critical velocity for initiation of motion;

$\alpha_s$  = velocity increase and turbulence factor (1.1 to 1.3 for circular structures and rectangular structure with corner into flow direction; 1.2 to 1.5 for rectangular structures).



In the case of a current without waves, the scour depth is zero for  $V_{par}=0$  or  $= [\alpha_s U_c - U_{cr}]/U_{cr}=0$  or  $U_c = U_{cr}/\alpha_s$ .

Equation (9.2.3) is plotted in **Figure 9.2.22** for three values of  $V_{par}=0.5, 1, 1.5$  and  $b_s/h=1$ .

Example caisson:  $U_c = 1$  m/s;  $U_{cr} = 0.4$  m/s;  $\alpha_s = 1.1$ ;  $b_s = 20$  m;  $h_s = 5$  m;  $h = 20$  m yields:  
 $b_s/h = 20/20 = 1$ ;  $h_s/b_s = 5/20 = 0.25$ ;  $V_{par} = (1.1 \times 1 - 0.4)/0.4 = 1.75$ ;  
 $d_{s,max}/b_s = 0.4 \times (1)^{0.5} \times (0.25)^{0.5} \times 1.75^{0.5} = 0.26$  or  $d_{s,max} = 0.26 \times 20 = 5.2$  m.

Example F3-GBS North Sea:  $U_c = 1$  m/s;  $U_{cr} = 0.4$  m/s;  $\alpha_s = 1.1$ ;  $b_s = 70$  m;  $h_s = 16$  m;  $h = 42$  m yields:  
 $b_s/h = 70/42 = 1.67$ ;  $V_{par} = 1.75$  and  
 $d_{s,max}/b_s \cong 0.4 \times (1.67)^{0.5} \times (16/42)^{0.5} \times (1.75)^{0.5} = 0.42$  or  $d_{s,max} = 0.42 \times 16 = 6.7$  m  
(observed 2.5 to 3.5 m)

Example Cover GBS:  $U_c = 1$  m/s;  $U_{cr} = 0.4$  m/s;  $\alpha_s = 1.1$ ;  $b_s = 10.8$  m;  $h_s = 3.55$  m;  $h = 30.5$  m yields:  
 $V_{par} = 1.75$  and  $d_{s,max}/b_s \cong 0.4 \times (10.8/30.5)^{0.5} \times (3.55/10.8)^{0.5} \times (1.75)^{0.5} = 0.18$  or  
 $d_{s,max} = 0.18 \times 3.55 = 0.65$  m (observed 1.25 m)

The far-field (edge) scour is of the order of  $d_{s,max,ff} \cong 0.2-0.3h_s$  and  $L_{scour,ff} \cong L_{structure}$

The horizontal extent of the scour with respect to the axis of the structure derived from available laboratory tests and field data, is given by:

- near-field (local scour) extent of  $1L_s$  with  $L_s = (b_s h_s)^{0.5}$  for round caisson-type structure; most of the scour occurs along the flanks of the structure where the flow velocity increase is maximum;
- near-field extent  $1L_s$  to  $1.5L_s$  for square caisson-type structure;
- near-field extent  $1L_s$  to  $1.5L_s$  for round caisson-type structure and conical transition section;
- far-field scour extent of  $3L_s$  to  $5L_s$  for round structures due to wake effects.

**Figure 9.2.23** shows the ratio of scour depth and structure height ( $d_{s,max}/b_s$ ) as function of the ratio of structure height and water depth ( $h_s/h_o$ ). The relative scour decreases for relatively low structures.

**Figure 9.2.24** shows the ratio of scour depth and structure height ( $d_{s,max}/h_s$ ) as function of the ratio of structure height and water depth ( $h_s/h_o$ ). The ratio  $d_{s,max}/h_s$  is relatively large if  $h_s/h_o$  is relatively small, because most of the flow goes over the structure and the scouring processes are dominated by relatively strong vortices. The ratio  $d_{s,max}/h_s$  is relatively small if  $h_s/h_o$  is relatively large, because the scouring processes are dominated by the velocity accelerations around the corners.

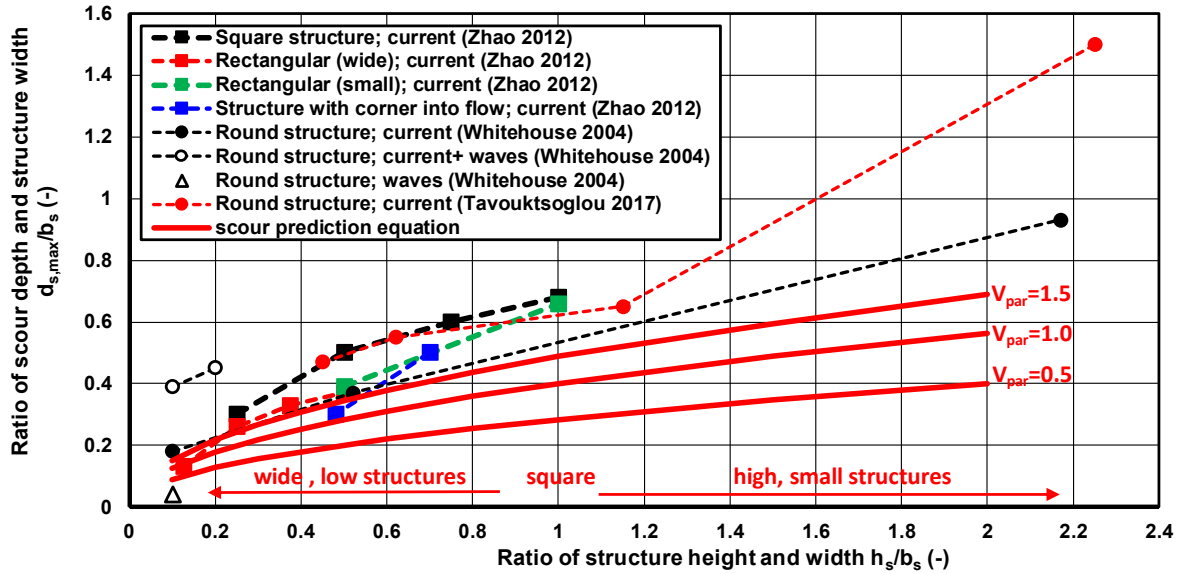


Figure 9.2.22 Ratio of scour depth and structure width as function of structure height and structure width

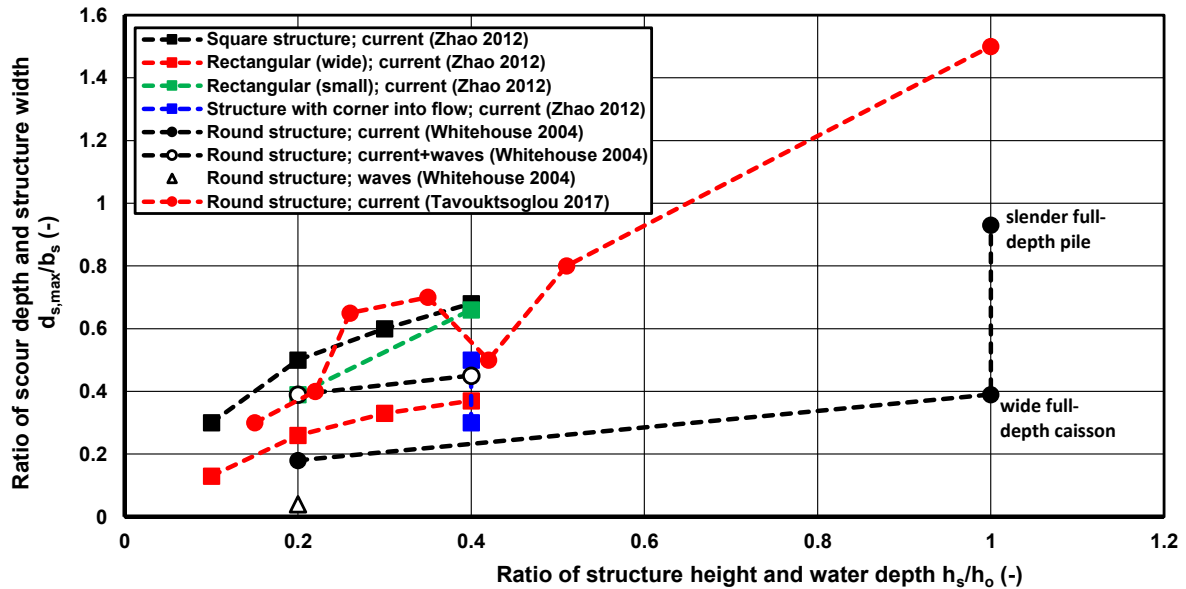


Figure 9.2.23 Ratio of scour depth and structure width as function of structure height and water depth

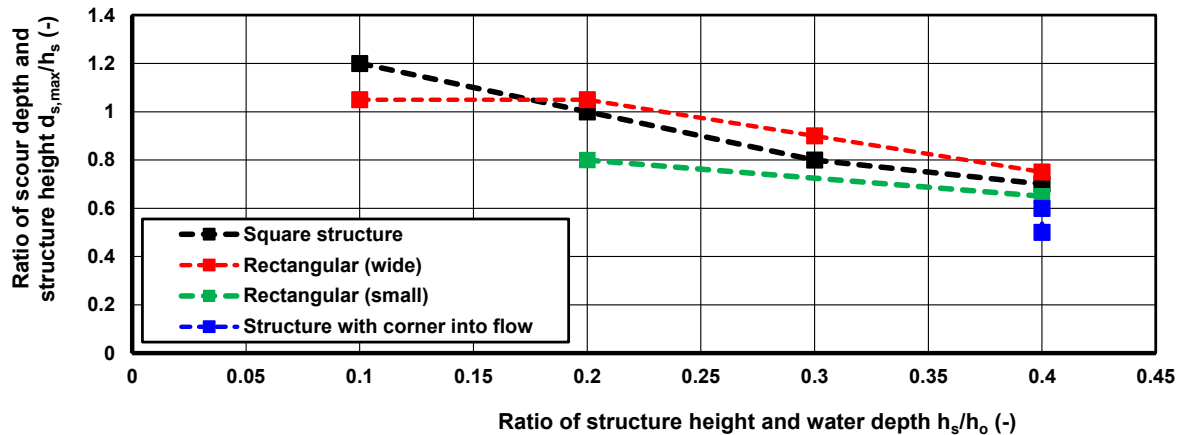


Figure 9.2.24 Ratio of scour depth and structure height as function of structure height and water depth



### 9.3 Scour mitigation measures

If a gravity-based structure is placed on a seabed consisting of mobile sediments, severe scour and undermining may occur depending on the shape and dimensions of the structure and the hydrodynamic conditions.

Scour mitigation measures are :

- bed protection over some distance from the wall of the structure, particularly near the corners; most often rock material with appropriate grading to prevent loss of soil from between the rock armour is used (double layer of rock of maximum 0.8 m on top of a filter layer of 0.7 m); gabion-type mattresses may also be used;
- vertical skirts penetrating into the bed (over at least 3 m); skirt length should be longer than predicted scour depth, otherwise the structure may be undermined and may sink into the bed; additional bed protection is required in severe scour conditions;
- placement of structure in a predredged pit/trench (with depth of 2 to 5 m).

The scour protection should be placed on a geotextile, otherwise the rocks/stones will partly sink into the bed ( $\cong 0.2-0.3D$ ) due to erosion of particles through the pores of the protection layer (Nielsen, 2011).

The horizontal extent of the scour protection can be smaller than the scour extent, as some edge scour beyond the scour protection can be accepted. Generally, it is sufficient to protect the bed over a distance of  $0.3b_s$  to  $0.5b_s$  with  $b_s$ =width of structure normal to the main flow direction.

Edge scour can be reduced by placing the scour protection material in predredged pit/trench.

Often, additional protection measures are required to repair damage due to major storm events. This can be done by removing the upper layer over a depth of 1 to 1.5 m around the structure by dredging and placement of granular backfill material of graded rock (0.8 m) on top of a filter layer (0.7 m).

Often, edge scour occurs on the downstream side of a scour protection. The edge scour depth is in the range of  $0.6-1.2D$  and depends on the current strength, the wave height, the local water depth and the thickness of the protection layer.

The scour depth can be substantially reduced by placing the protection layer in a trench around the monopile so that the top of the protection layer is flush with the surrounding seabed. This requires the dredging of a trench around the monopile.

The scour length in the direction of the main current is of the order of  $5D$ .

The scour length normal to the main current direction is of the order of  $3D$ .



## 10. Scour near bed due to ship propeller

The jet produced by a ship propeller can seriously impact the seabed. The propeller jet can scour the bed for a distance of several propeller diameters from the propeller. Near such an intense jet flow, seabed material can easily be entrained and severe erosion can occur on the bed or bank of navigation channels and around harbor structures. The impingement of propeller or thruster jets is more serious where large ships navigate in shallow water with a minimum keel clearance. Furthermore, modern ships have bow and stern thrusters. Hong et al. 2013 have carried out experimental research to determine the dimensions of the scour hole, see **Figure 10.1**. The scour depth at time  $t$  is given by:

$$d_{s,t} = K_1 \gamma_s D [-K_2 + \log(U_p t/D)]^{K_3} \quad (10.1)$$

with:

- $d_{s,t}$  = scour depth at time  $t$ ,
- $\gamma_s$  = safety factor,
- $U_c$  = flow velocity,  $U_p$  = velocity produced by propeller,
- $D$  = propeller diameter,
- $y_o$  = distance of centre of propeller to bed,
- $d_{50}$  = median sediment size of bed,
- $M_p = U_p / [(s-1)gd_{50}]^{0.5}$ ,
- $M_F = (U_c + U_p) / [(s-1)gd_{50}]^{0.5}$ ,
- $s = \rho_s / \rho$ ,  $\rho_s$  = sediment density,
- $\rho$  = fluid density,  $\alpha_w = U_w / U_{cr}$  with  $\alpha_w = 1$  if  $U_w < U_{cr}$ ,
- $U_w$  = peak orbital velocity near bed,  $U_{cr}$  = critical velocity initiation of motion,  $t$  = time.

$$K_1 = 0.014 M_p^{1.12} (y_o/D)^{-1.74} (y_o/d_{50})^{-0.17}$$

$$K_2 = 1.88 M_p^{-0.009} (y_o/D)^{2.3} (y_o/d_{50})^{-0.44}$$

$$K_3 = 2.48 M_p^{-0.073} (y_o/D)^{0.53} (y_o/d_{50})^{-0.045}$$

The maximum (equilibrium) scour depth is given by:

$$d_{s,max} = 0.265 \gamma_s D (M_F - 4.11 (y_o/D))^{0.95} (y_o/D)^{-0.022} \quad \text{for } y_o/D > 0.5 \quad (10.2)$$

$$d_{s,max} = 0.2 \gamma_s D M_F \quad \text{for } y_o/D < 0.5$$

Van Rijn uses:

$$d_{s,max} = 0.2 \gamma_s D (y_o/D) (\alpha_w)^{0.25} M_F \quad \text{for } y_o/D > 0.5 \quad (10.3)$$

$$d_{s,max} = 0.2 \gamma_s D (\alpha_w)^{0.25} M_F \quad \text{for } y_o/D < 0.5$$

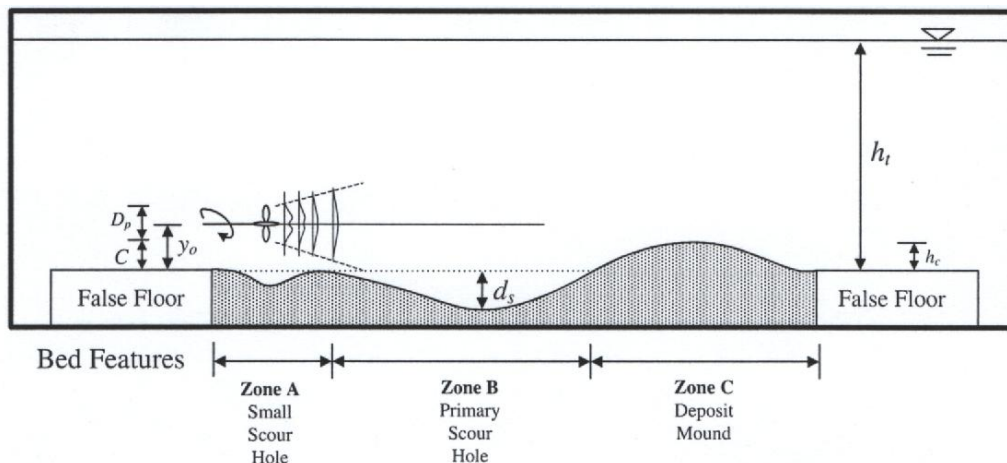


**Figure 10.1** Scour due to propeller jet



## 11. Scour near ship wrecks

### Scour processes

Erosion (scour) around an obstacle/structure on the seabed will occur when loose sediments (mud, sand or gravel) are eroded in response to forcing by waves and/or currents (wind-, tide- and wave-related currents). Scour processes can ultimately lead to the (partial) burial of an object (pipeline, wreck) lying on the seabed or the complete collapse of a structure resting on the seabed (foundation legs). Scour signatures at the seabed have been widely observed in marine conditions. The placement of an object on the seabed leads to a local increase in both flow velocity for reasons of continuity and turbulence intensity due to the generation of vortices (vortex shedding), see **Figure 11.1**. Typical hydrodynamic phenomena near submerged and emerged objects/structures are: flow contraction, formation of horse vortex (flow rotation) in front of the object, formation of lee wake vortices behind the object (turbulence production), wave reflection and wave breaking against the object, wave diffraction around the object.

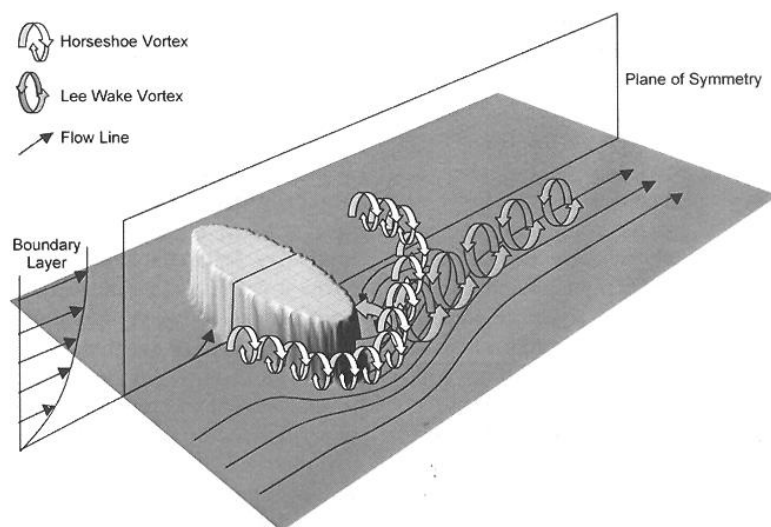


**Figure 11.1** Flow patterns and vortex generation around submerged object (Quinn 2006)

When the seabed consists of loose, movable sediments, the local sediment transport capacity will increase due to the presence of an obstacle resulting in the lowering (scouring) of the local seabed with respect to the surrounding (original) bed. Commonly, the eroded sediments are deposited somewhat further away from the object resulting in local deposition (accretion). Liquefaction of the sediment bed may occur temporarily (intermittently) under the object, which basically is a re-arrangement of the grain skeleton due to overpressure of the pore fluid and reduction of grain skeleton forces. This may occur under highly dynamic loading (forcing) conditions and as a result the object may sink slowly into the bed.

Scour is broadly classified as local scour near the object (near-field scour) and dishpan scour further away from the object (shallow wide depressions; far-field scour).

Scour around an object on the seabed depends on many factors, as follows:

- dimensions, shape (streamlined or not) and state (submerged or partly emerged) of the object;
- orientation (parallel, perpendicular or oblique) of the object to the direction of the waves and the currents;
- strength of the currents (weak current 0.1 to 0.5 m/s, mild current 0.5 to 1.0 m/s, or strong currents of about 1 -2 m/s);
- water depth and wave heights (low, medium or high waves; shoaling or breaking waves);
- sediment composition and sizes.



### Scour in strong currents

Quinn (2006) has analysed scour data of various wrecks. The most detailed data refer to scour around various wrecks in the Outer Thames Estuary (UK) with strong tidal currents. The following scour marks were observed:

- average scour length of 275 m with flow-parallel scour features up to 1 km (parallel to the peak tidal flows);
- single and double scour marks; small wrecks (average width less than 13 m across the current) produce single scour marks with lengths up to 130 m ( $\cong 10 b_s$  with  $b_s$  = width of structure/object normal to the flow); large wrecks (width greater than 60 m across the current) produce double scour marks with lengths up to 400 m;
- the shortest and narrowest scour marks were found near wrecks aligned with their longest axis parallel to the peak tidal currents (streamlined condition);
- the majority of scour depths in the Thames Estuary was 1.5 to 2 m below the surrounding bed;
- wreck marks on a sand floor generally are broad, shallow and longitudinally extensive whereas those on gravel floors are relatively narrower, deeper and less extensive.

Quinn (2006) has presented idealised qualitative scour marks around submerged wrecks in strong tidal flows, see **Figure 11.2**. Longer scour marks are formed in the direction of the stronger flood- or ebb currents. In rotary tidal currents the far-field scour marks are weaker or absent and near-field local scour is dominant causing gradual sinking of the wreck into the subsoil. Some wrecks (City of Bristol off the north coast of Ireland) are completely buried into the scour hole formed under rotary tidal flow.

Quinn has analysed a partly buried wreck of 44x16.5 m resting in a water depth of about 13 m on the flank of Arklow Bank approximately 11 km off the east coast of Ireland. The wreck stands proud of the seabed by up to 2 m at mid vessels, with the wreck aligned about 60° to the dominant flow direction. The tidal range is about 2 m and the tidal flows are strong with velocities up to 1.5 m/s. The maximum scour depth is about 3 m at about 20 m from the wreck (lee zone), see **Figure 11.3**. The length of the scour mark is about 50 m (about the length of the wreck). This scour mark is generated by strong tidal flow over a large-scale submerged object with a maximum height of about 2 m above the seabed. Deposition is present on the port (left) side of the wreck.

### Scour due to high waves

In marine environments with high waves and weak tidal currents the wave-induced shear stresses exerted on the bed are relatively large. Hence, the scouring processes around wrecks in the nearshore zone are quite intensive. Based on laboratory data of submerged cylindrical objects, Quinn (2006) has also presented idealised scour marks for submerged wrecks under wave conditions, see **Figure 11.4**.

At scour initiation, a triple-scour mark is formed, approximately parallel to the main wave direction. A central single-scour mark forms near the centre and two shorter single-scour marks form at the tips (bow and stern). With time, small sand waves develop at the bow and stern, decaying with distance from the wreck. Under storm events, the scour marks transform into an expanded scour regime with a semi-elliptical scour area. The scour area may grow out to the size of the wreck resulting in (partial) burial of the wreck. This may proceed rather quickly at very exposed coasts.

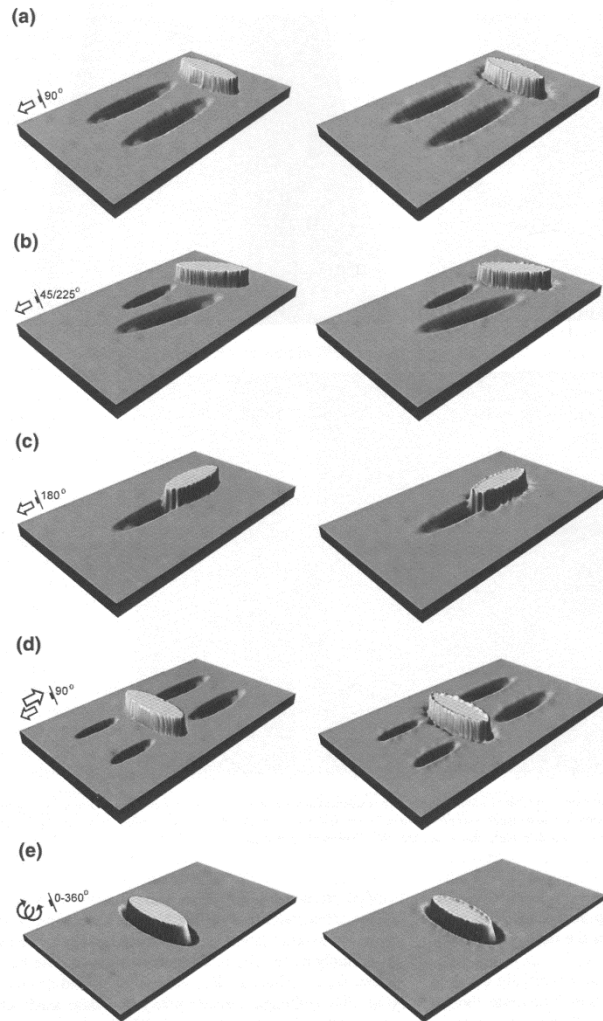


**Figure 11.2** Idealised scour marks of submerged wrecks under various angles to strong flows based on Quinn (2006); near-field and far-field scour; depositional marks are left out  
a, b, c= steady flow,  
d= tidal bi-directional flow,  
e= rotary tidal flow.

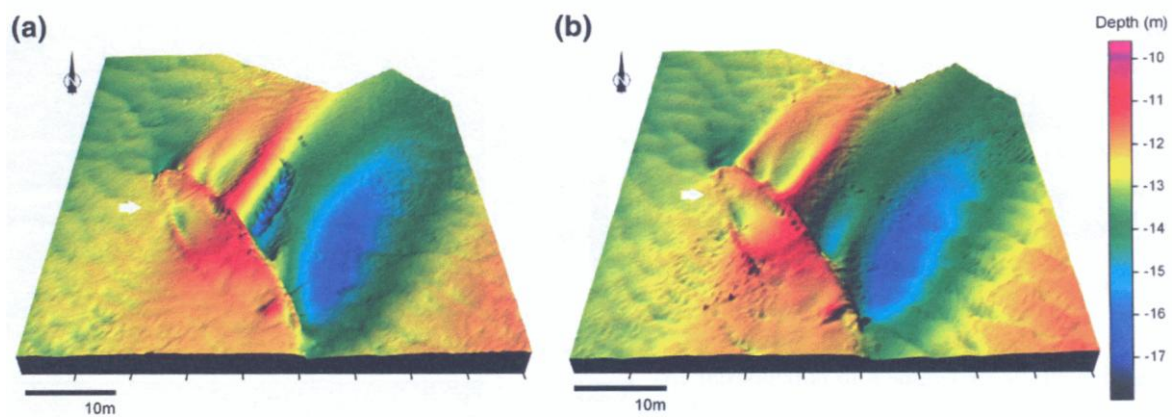
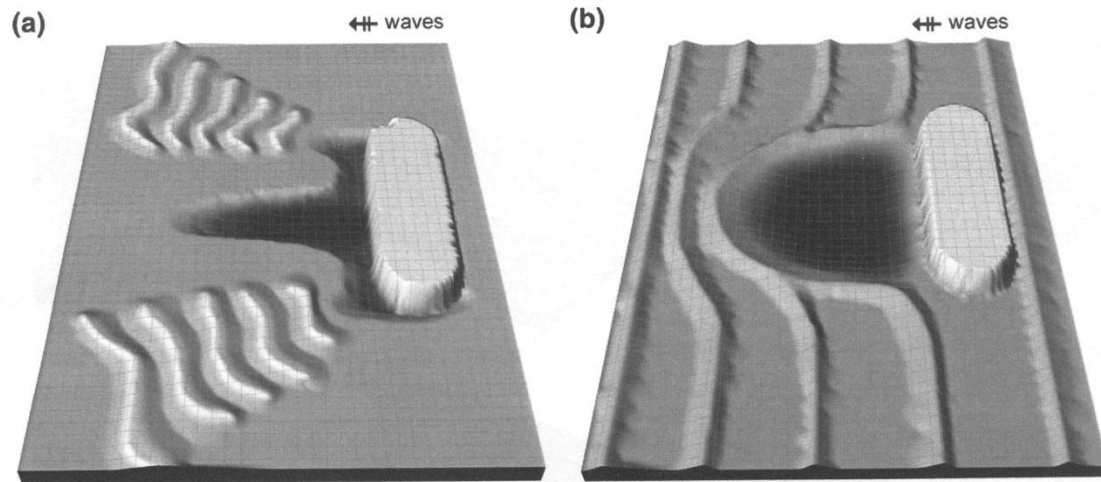


**Figure 11.3** Scour near wreck Arklow Bank (wreck indicated by white arrow, Quinn 2006);  
a= data of 12 August 2003, b= data of 23 August 2003



**Figur 11.4** *Idealised scour marks of submerged wrecks under wave conditions (Quinn 2006);  
Left= initial scour; Right= expanded scour after various storm events*



## 12. References

- Baelus, L., Bolle, A. and Szengel, V., 2018 Long term scour monitoring around offshore jacket foundations on a sandy seabed. In *Proceedings of the Ninth International Conference on Scour and Erosion, ICSE 9, Taipei, Taiwan, 5–8 November 2018*.
- Bolle, A., de Winter, J., Goossens, W., Haerens, P. and Dewaele, G., 2012. Scour monitoring around offshore jackets and gravity based foundations. In *Proceedings of the Sixth International Conference on Scour and Erosion, ICSE 6, Paris, France, 27–31 August 2012*.
- Bos, K.J., Chen, Z., Verheij, H.J., Onderwater, M. and Visser, M. 2002. Local scour and scour protection of F3 offshore GBS platform. Paper 28127 *Proceedings OMAE'02 21st International Conference on Ocean, Offshore and Arctic Engineering, June 23-28, 2002, Oslo, Norway*.
- Breusers, H.N.C., 1967. Two-dimensional scour in loose sediments. Publ. 64, Delft Hydraulics, Delft, The Netherlands.
- Breusers, H.N.C., Nicollet, G. and Shen, H.W., 1977. Local scour around cylindrical piers,, p. 211-252. *Journal Hydraulic Res., Vol. 15*
- Cefas, 2006. Scroby sands offshore wind farm; coastal processes monitoring. Cefas Lowestoft Laboratory, UK
- Cevik, E. and Yüksel, Y., 1999. Scour under submarine pipelines in waves in shoaling conditions, p. 9-19. *Journal of Waterway, Port, Coastal and Ocean Engineering, Vol. 125, No. 1*
- Coleman, S.E. and Melville, B.W., 2001. Case study: New Zealand bridge scour experiences, p. 535-546. *Journal of Hydraulic Engineering, Vol. 127, No. 7*
- Coleman, S.E., Lauchlan, C.S. and Melville, B.W., 2003. Clear-water scour development at bridge abutments, p. 521-531. *Journal of Hydraulic Research, Vol. 41, No. 5*
- De Bruyn, C.A., 1988. Scour near platform pier due to current and breaking waves (in Dutch). Dept. of Coastal Eng., Delft Univ. Technology, Delft, The Netherlands.
- Dean, R.G., 1986. Coastal armoring: effects, principles and mitigation, p. 1843-1857. 20<sup>th</sup> ICCE, Taipei
- Delft Hydraulics, 1985. St. George Harbor, Alaska. Report M2102, Delft, The Netherlands
- Delft Hydraulics, 1988. Scour near harbour of IJmuiden (in Dutch). Report H 460, Delft, The Netherlands
- Deltares, 2017. Scour and scour mitigation. Report WOZ2170029, Delft, The Netherlands
- Deltares 2020. Scour and scour mitigation for Hollandse Kust (West) wind farm zone. Project 11204811, Delft, The Netherlands
- Deltares (Rudolph, D and Bos, K.J.), 2006. Scour around a monopile under combined wave-current conditions and low KC-numbers. *Third International Conference Scour and erosion, Amsterdam, The Netherlands*
- Deltares (Raaijmakers, T. and Bos, K.J.), 2008 Time dependent scour development under combined current and wave conditions. Delft, The Netherlands
- Dietz, J.W., 1969. Kolkbildung in feinen oder leichten sohlmaterialien bei strömendem abfluss, *Mitteilungen Heft 155, p.1-121, T.U. Hannover, Germany*
- Dudill, A., Vasquez, J. and Mclean, D., 2018. Scouring due to submerged sills. *E3S Web of Conferences 40, 03021. Doi: 10.1051/e3sconf/20184003021*
- Eadie, R.W. and Herbich, J.B., 1986. Scour around a single, cylindrical pile due to combined random waves and a current, p. 1858-1870. 20<sup>th</sup> ICCE, Taipei, Taiwan
- Fowler, J.E., 1992. Scour problems and methods for prediction of maximum scour at vertical seawalls. T.R. CERC 92-16. U.S.W.E.S., Vicksburg, USA
- Fredsøe, J. and Sumer, B.M., 1997. Scour at the round head of a rubble-mound breakwater. p. 231-263. *Coastal Engineering, Vol. 29, No. 3-4*
- Garcia, K., Jordan, C., Melling, G., Schendel, A., Welzel, M. and Schlurmann, T., 2025. Scour variability across offshore wind farms (owfs): identifying site-specific scour drivers as a step towards assessing potential impacts on the marine environment. *Wind Energ. Sci., 10, 2189–2216, 2025. Doi: 10.5194/wes-10-2189-2025*
- Griggs, G.B., Tait, J.F. and Scott, K., 1990. The impact of shoreline protection structures on beaches along Monterey Bay, California, p. 2810-2823. 22<sup>nd</sup> ICCE, Delft, The Netherlands
- Griggs, B. et al., 1994. The interaction of seawalls and beaches: seven years of of monitoring, Monterey Bay, California, p. 21-28, *Shore and Beach, July*



- Guan, D., Melville, B.W., and Friedrich, H., 2015. *Live-bed scour at submerged weirs. Journal Hydraulic Engineering* Vol. 141 (2), 0401471
- Guan, D., Melville, B.W., and Friedrich, H., 2016. *Local scour at submerged weirs in sand-bed channels. Journal Hydraulic Research* Vol. 54 (2), 172-184
- Herbich, J.B., 1991. *Scour around pipelines, piles and seawalls*, p. 867-958. In: *Handbook of Coastal and Ocean Engineering*, Gulf Publishing Company, Houston, USA
- Herbich, J.B. et al., 1965. *Scour of flat sand beaches due to wave action in front of seawalls. Coastal Engineering, Santa Barbara Specialty Conference, ASCE.*
- Hjorth, P., 1975. *Studies on the nature of local scour. Inst. for Teknisk Vattenresurslara, Lunds Tekniska Hogskola, Lunds University, Sweden*
- Hoffmans, G. J.C.M., 1990. *Concentration and flow velocity measurements in a local scour hole. Report 4-90. Department of Civil Engineering, Delft University of Technology, Delft, The Netherlands*
- Hoffmans, G. J.C.M. and Verheij, H.J., 1997, *Scour manual, Balkema, The Netherlands*
- Høgedal, M. and Hald, T., 2005. *Scour assessment and design for scour for monopile foundations for offshore wind turbines. Copenhagen offshore wind 2005*
- Hong, J.H., Chiew, Y.M., and Cheng, N.S., 2013. *Scour caused by a propeller jet. Journal of Hydraulic Engineering, Vol. 139, No. 9, 1003-1012*
- Hotta, S. and Marui, N., 1976. *Local scour and current around a porous breakwater, p. 1590-1604. 15<sup>th</sup> ICCE, Honolulu, Hawai, USA*
- Hughes, S.A. and Kamphuis, J.W., 1996. *Scour at coastal inlet structures, p. 2258. 25<sup>th</sup> ICCE, Orlando, USA*
- Ichikawa, T., 1967. *Scouring damages at vertical wall breakwaters of Tagonoura port, p. 95-108. Coastal Engineering in Japan, Vol. 10*
- Irie, I. and Nadaoka, K., 1984. *Laboratory reproduction of seabed scour in front of breakwaters, p. 1715-1731. 19<sup>th</sup> ICCE, Houston, USA*
- Irie, I. et al., 1986. *Study on scour in front of breakwaters by standing waves and protection methods, p. 4-86. Port and Harbour Research Institute, Vol. 25, No. 1, Japan*
- Katayama, T. et al., 1974. *Performance of offshore breakwaters of the Niigata coast, p. 129-139. Coastal Engineering in Japan, Vol. 17*
- Khalfin, I.S., 1983. *Local scour around ice-resistant structures caused by wave and current effect. 7<sup>th</sup> Int. Conf. Port and Ocean Engineering under arctic conditions. Vol. 2, 992-1002, Helsinki, Finland,*
- Kiziloz, B. et al., 2013. *Scour below submarine pipelines under irregular wave attack. Coastal Engineering, Vol. 79, 1-8*
- Kjeldsen, S.P. et al., 1973. *Local scour near offshore pipelines. p. 308-331. Sec. Int. Conf. Port and Ocean Eng., Reykjavik Univ. of Iceland*
- Komar, P.D. and McDougal, W.G., 1988. *Coastal erosion and engineering structures: The Oregon experience, p.79-94. Journal of Coastal Research, SI 4*
- Kothyari, U.C. et al., 1992. *Live-bed scour around cylindrical bridge piers. Journal of Hydraulic Research, IAHR, Vol. 30, No. 5*
- Kothyari, U.C. and Ranga Raju, K.G., 2001. *Scour around spur dikes and abutments, p. 367-374. Journal of Hydraulic Research, Vol. 39, No. 4*
- Kraus, N.C., 1988. *The effects of seawalls on the beach: a literature review, p. 1-29. Journal of Coastal Research, SI 4*
- Kraus, N.C. and McDougal, W.G., 1996. *The effects of seawalls on the beach: Part I and Part II, p. 691-701 and p. 702-713. Journal of Coastal Research, Vol. 12, No. 3*
- Lillycrop, W.J. and Hughes, S.A., 1993. *Scour hole problems experienced by the Corps of Engineers. Miscellaneous papers. CERC-93-2. USWES, Vicksberg, USA*
- Lim, S.Y., 1997. *Equilibrium clear-water scour around an abutment. Journal of Hydraulic Engineering, Vol. 123, No. 3*
- Losada, M.A. and Gimenez-Curto, L.A., 1981. *Flow characteristics on rough permeable slopes under wave action. p. 187-206. Journal of Coastal Engineering, Vol. 4*
- May, R.W.P. and Ecaramaia, M., 2002. *Local scour around structure in tidal flows. First Int. Conf. on scour of foundations. ISCF-1., eds Chen et al., Texal A&M University, College Station, Texas, USA, 320-336*



- Melville, B.W., 1988.** *Scour at bridge sites.*, p. 327-362. Technomic Publishing Company, USA, Civil Engineering Practice, 2
- Melville, B.W., 1997.** *Pier and abutment scour: integrated approach.* Journal of Hydraulic Engineering, Vol. 123, No. 2
- Melville, B.W. and Sutherland, A.J., 1988.** *Design method for local scour at bridge piers.* Journal of Hydraulic Engineering, ASCE, Vol. 114, No. 10.
- Melville, B.W. and Coleman, S.E., 2000.** *Bridge scour.* Water resources Publications. Littleton, Colorado, USA
- Miles, J., Martin, T., and Goddard, L., 2017.** *Current and wave effects around wind farm monopile foundations.* Coastal Engineering 121, 167-178
- Munoz-Peres, J.J., et al. 2015.** *Sinking of concrete modules into a sandy seabed: a case study.* Coastal Engineering, Vol. 99, 26-37
- Myrhaug, D. and Rue, H., 2003.** *Scour below pipelines and around vertical piles in random waves,* p. 227-242. Coastal Engineering, Vol. 48
- Nelson, R.C., 1983.** *Wave heights in depth-limited conditions.* 6<sup>th</sup> Australian Conf. on Coastal and Ocean Engineering.
- Nielsen, A.W., 2011.** *Scour protection of offshore wind farm.* Doctoral Thesis, Department of Mechanical Engineering, Technical University of Denmark
- Oumeraci, H., 1994a.** *Review and analysis of vertical breakwater failures: lessons learned,* p. 3-29. Coastal Engineering, Vol. 22
- Oumeraci, H., 1994b.** *Scour in front of vertical breakwaters: review of problems.* Proc. Int. Workshop on wave barriers in deep water, p. 281-307. Port and Harbour Research Inst., Yokosuka, Japan
- Petersen, T.U., Mutlu Sumer, B., Fredsøe, J., Raaijmakers, T.C. and Schouten, J.J. 2015.** *Edge scour at scour protections around piles in the marine environment; Laboratory and field investigation.* Coastal Engineering 106, 42-72
- Pilkey, O.H. and Wright, H.L., 1988.** *Seawalls versus beaches,* p. 41-66. Journal of Coastal Research, SI 4
- Powell, K.A., 1987.** *Toe scour at seawalls subject to wave action.* Report SR 119, HR Wallingford, England
- Quinn, R., 2006.** *The role of scour in vesselwreck site formation processes and the preservation of wreck-associated scour signatures in the sedimentary record - evidence from seabed and sub-surface data.* Journal of Archaeological Sciences 33, 1419-1432.
- Raaijmakers, T.C., Joon, T., Segeren, M.L.A. and Meijers, P. 2013.** *Scour: to protect or not to protect, that's the question!; feasibility of omitting scour protection.* Proc. EWEA Offshore, Frankfurt, Germany
- Raaijmakers, T.C., Van Velzen, G. and Riezbos, H.J., 2014.** *Dynamic scour prediction for offshore monopiles.* Proceedings of 7<sup>th</sup> Int. Conf. Scour and Erosion. 2-4 December 2014, Perth, Australia.
- Rahman, M.M. and Haque, M.A., 2003.** *Local scour estimation at bridge pier site: modification and application of Lacey formula.* International Journal of Sediment Research, Vol. 18, No. 4, p. 333-339
- Rance, P.J., 1980.** *The potential for scour around large objects,* p.41-53. Scour prevention seminar, London, Soc. for Underwater Technology
- Richardson, E.V. et al., 1988.** *Highways in the river environment.* Federal Highway Administration, US Dept. of Transportation, Ft. Collins, Colorado, USA
- Rijkswaterstaat, 1996.** *Morphologic evaluation of dam Eierland, The Netherlands (in Dutch).* Dir. Noord-Holland, Haarlem, The Netherlands
- Rudolph, R., Bos, K.J., Luijendijk, A.P., Rietema, K. and Out, J.M.M., 2004.** *Scour around offshore structures; analysis of field measurements, Deltares, Delft, The Netherlands*
- Rudolph, D., Raaijmakers, T. and Stam, C.J., 2008.** *Time-dependent scour development under combined current and wave conditions; hindcast of field measurements.* Fourth International Conference on scour and erosion, Tokyo.
- Sato, S. et al., 1968.** *Study on scouring at the foot of coastal structures,* p. 579-598. 11<sup>th</sup> ICCE, London, England
- Sarmiento, J., Guancho, R., Losada, I.J. and Serna, J. 2024.** *Experimental analysis of scour around an offshore wind gravity base foundation.* Ocean Engineering Vol. 308, Doi.org/10.1016/j.oceaneng.2024.118330
- Schoppman, B. 1972.** *Strömungs- und transportmechanismen einer fortschreitenden Auskolkung.* Thesis, University of Karlsruhe, Germany.



- Sheppard, D.M., 2003.** *Large scale and live bed local pier scour experiments (phase 1). Final Report Florida Department of Transportation FDOT Contract BB-473*
- Sheppard, D.M. and Albada, E., 1999.** *Local scour under tidal flow conditions. In: Stream stability and scour at highway bridges, Compendium of papers ASCE. Water Res. Eng. Confs. 1991 to 1998, edited by Richardson, E.V. and Lagasse, P.F., ASCE, New York; 767-773*
- Sheppard, D.M. and Miller, W., 2006.** *Live-Bed local pier scour experiments. Journal of Hydraulic Engineering, ASCE, Vol. 132, No.7 , 635-642*
- Shore protection manual, 1984.** *Volume I and II, Coastal Engineering Research Center, Dep. of the Army, Waterways Exp. Station, Vicksburg, Mississippi, USA*
- Silvester, R., 1991.** *Scour around breakwaters and submerged structures, p. 959-996. In: Handbook of Coastal and Ocean Engineering, Gulf Publishing Company, Houston, USA*
- Simons, R.R., Weller, J. and Whitehouse, R.J.S. 2009.** *Scour development around truncated cylindrical structures. Coastal Structures 2007, Proceedings of the 5th Coastal Structures International Conference, CSt07, Venice, Italy, 2-4 July 2007, (Eds) Franco, L., Tomasicchio, G.R. and Lamberti, A., 1881-1891. World Scientific.*
- Steezel, H., 1988.** *Scour holes near seawalls (in Dutch), Report H298 part 4, Delft Hydraulics, Delft, The Netherlands*
- Sumer, B.M. and Fredsøe, J., 1990.** *Scour below pipelines in waves, p. 307-323. Journal of Waterways, Port, Coastal and Ocean Engineering, ASCE, Vol.116, No.3.*
- Sumer, B.M, et al., 1992.** *Scour around vertical pile in waves, p. 15-31. Journal of Waterways, Port, Coastal and Ocean Engineering, ASCE, Vol.118, No.1.*
- Sumer, B.M, et al., 1993.** *Influence of cross-section on wave scour around piles, p. 477-495. Journal of Waterways, Port, Coastal and Ocean Engineering, ASCE, Vol.119, No.5.*
- Sumer, B.M. and Fredsøe, J., 1997.** *Scour at the head of a vertical-wall breakwater, p. 201-230. Coastal Engineering, Vol. 29, No. 3-4*
- Sumer, B.M. and Fredsøe, J. 1998.** *Wave scour around group of vertical piles, p. 248-256. Journal of Waterway, Port, Coastal and Ocean Engineering, Vol. 124, No. 5*
- Sumer, B.M. and Fredsøe, J. 2000.** *Experimental study of 2D scour and its protection at a rubble-mound breakwater, p. 59-87. Coastal Engineering, 40*
- Sumer, B.M. and Fredsøe, J. 2001.** *Wave scour around a large vertical circular cylinder, p. 125-134. Journal of Waterway, Port, Coastal and Ocean Engineering, Vol. 127, No. 3*
- Sumer, B.M. and Fredsøe, J. 2001.** *Scour around pile in combined waves and current, p. 403-411. Journal of Waterway, Port, Coastal and Ocean Engineering, Vol. 127, No. 5*
- Sumer, B.M. and Fredsøe, J. 2000.** *The mechanics of scour in the marine environment. World Scientific, Singapore*
- Sumer, B.M. , Whitehouse, R.J.S. and Tørum, A., 2001.** *Scour around coastal structures: a summary of recent research, p. 153-190. Coastal Engineering, Vol 44*
- Sumer, B.M. , Truelsen, C., Sichman, T. and Fredsøe, J. 2001.** *Onset of scour below pipelines and self-burial, p. 313-335. Coastal Engineering, Vol. 42*
- Sumer, B.M., et al., 2005.** *Local scour at roundhead and along the trunk of low crested structures. Coastal Engineering, Vol. 52, 995-1025*
- Tavouktsoglu, N.S., 2017.** *Scour and scour protection around offshore gravity-based foundations. Doctoral Thesis, University College, London, UK.*
- Uda, T. and Noguchi, K., 1993.** *Beach changes caused by elongation of breakwater of Kashiwazaki Port, p. 229-244. Coastal Engineering in Japan, Vol. 36, No. 2*
- University of Cantabria, 2020.** *Experimental modelling of ELISA gravity base foundation. Instituto de Hidraulica Ambiental, Spain*
- Üşenti, B., 2019.** *Scour hole formation for lateral non-uniform flow in non-cohesive sediments. MSc. Thesis, Delft University of Technology, Delft, The Netherlands.*
- Van Eijk, T.F.A., 2016.** *Gravity-based foundation; scour and design optimisation. MSc. Thesis, Department of Civil Engineering. Delft University of Technology, Delft, The Netherlands*



- Van der Meulen, T. and Vinjé, J.J., 1975.** *Three-dimensional local scour in non-cohesive sediments. 15<sup>th</sup> Congress IAHR, Sao Paulo, Vol. 2, Paper B33*
- Van Rijn, L.C., 1984a.** *Sediment Transport, Part I: Bed Load Transport. Journal of Hydraulic Engineering, ASCE, Vol. 110, No. 10.*
- Van Rijn, L.C., 1984b.** *Sediment Transport, Part II: Suspended Load Transport. Journal of Hydraulic Engineering, ASCE, Vol. 110, No. 11.*
- Van Rijn, L.C., 1984c.** *Sediment Transport, Part III: Bed Forms and Alluvial Roughness. Journal of Hydraulic Engineering, ASCE, Vol. 110, No. 12.*
- Van Rijn, L.C., 1993, 2012.** *Principles of sediment transport in rivers, estuaries and coastal seas. Aqua Publications, Amsterdam, The Netherlands ([WWW.AQUAPUBLICATIONS.NL](http://WWW.AQUAPUBLICATIONS.NL))*
- Van Rijn, L.C., 2007a.** *Unified view of sediment transport by currents and waves, I: Initiation of motion, bed roughness, and bed-load transport. Journal of Hydraulic Engineering, 133(6), p 649-667.*
- Van Rijn, L.C., 2007b.** *Unified view of sediment transport by currents and waves, II: Suspended transport. Journal of Hydraulic Engineering, 133(6), p 668-389.*
- Van Rijn, L.C., 2006, 2012.** *Principles of sedimentation and erosion engineering in rivers, estuaries and coastal seas. Aqua Publications, The Netherlands ([www.aquapublications.nl](http://www.aquapublications.nl))*
- Van Rijn, L.C. et al., 2018.** *Sediment pickup function. Journal of Hydraulic Engineering, ASCE.*
- Welzel, M., Schendel, A., Schlurmann, T. and Hildebrandt, A., 2019.** *Volume-based assessment of erosion patterns around a hydrodynamic transparent offshore structure. Energies, 12. Doi: 10.3390/en12163089*
- Whitehouse, R.S.J., 1998.** *Scour at marine structures. Pub. Thomas Telford Ltd*
- Whitehouse, R.S.J., 2004.** *Marine scour at large foundations. Second International Conference on Scour and Erosion, Singapore*
- Whitehouse, R., Harris, J., Sutherland, J. and Rees, J., 2008.** *An assessment of field data for scour at offshore wind turbine foundations. Fourth International Conference on scour and erosion, Tokyo.*
- Whitehouse, R.J.S, Harris, Mundon, T.R., and Sutherland, J., 2010.** *Scour at offshore structures. Proc. 5<sup>th</sup> Int. Conf. Scour and Erosion, ISCE-5, ASCE, San Francisco, California, USA*
- Whitehouse, R., Harris, J. and Sutherland, J., 2012.** *Evaluating scour at marine gravity structures. HR Wallingford; ICE-Maritime Engineering, 164, 143-157*
- Whitehouse, R., Harris, J., Sutherland, J. and Rees, J., 2008.** *An assessment of field data for scour at offshore wind turbine foundations. Fourth International Conference on scour and erosion, Tokyo.*
- Xiang, Q., Wei, K., Qiu, F, Yao, C and Li, Y., 2020.** *Experimental study of local scour around caissons under unidirectional and tidal currents. Water, 12, Doi: 10.3390/w12030640*
- Xie, S.L., 1981.** *Scouring patterns in front of vertical breakwaters and their influence on the stability of the foundations of the breakwaters. Coastal Eng. Dep. Civil Engineering, Delft Univ. of Technology, Delft, The Netherlands.*
- Yeow, K. and Cheng, L., 2004.** *Local scour around a vertical pile with a caisson foundation. Proc. Asian and Pacific Coasts 2003, eds. Goda et al., World Scientific*
- Yokoyama, Y. et al. 2002.** *A quantitative evaluation of scour depth near coastal structures, p. 1830-1841. 28<sup>th</sup> ICCE, Cardiff, UK*
- Zhao, M., Zhu, X., Cheng, L. and Teng, B., 2012.** *Experimental study of local scour around subsea caissons in steady currents. Coastal Engineering, Vol. 60, 30-40*